8-7-2008

Simulation of Combustion and Thermal-flow Inside a Pyroscrubber

Lei Zhao
University of New Orleans

Simulation of Combustion and Thermal-flow Inside a Pyroscrubber

A Thesis

Submitted to the Graduate Faculty of the
University of New Orleans
in partial fulfillment of the
requirements for the degree of

Master of Science
in
Mechanical Engineering

by

Lei Zhao

B.S. University of Science and Technology of China, 2005

August, 2008

ACKNOWLEDGMENT

I would like to show my deep thankfulness to my advisor Dr. Ting Wang for his sincere, patient and thoughtful guidance throughout my two years of study and research with him so far. Without his innovative ideas and hard work, there will not be this thesis. It is great honor and luck of mine to have him as my advisor.

I would like to show appreciation to CII Carbon, L.L.C. for their trust, support and funding on this research as well as the funding from the Industrial Ties Research Subprogram (ITRS) administered by the Louisiana Board of Regents.

I would also like to thank my colleague students and researchers from Energy Conversion and Conservation Center (ECCC), Armin Silaen, Jobaidur Khan, Day Benjamin, Zhang Zexuan, Dr. Dhanasekaran, Dr. Li Xianchang and so many others for their kind help and beneficial discussions.

In the last I would like to thank my friends and family for their supports and understanding.

TABLE OF CONTENTS

LIST OF FIGURES

LIST OF TABLES

NOMENCLATURE

c	Concentration (mass/volume, moles/volume)
c_p, c_v	Specific heat at constant pressure, volume (J/kg-K, Btu/lbm-°F)
Dij	Mass diffusion coefficient (m^2/s, ft^2/s)
E	Total energy, activation energy (J, Btu)
f	Mixture fraction (dimensionless)
g	Gravitational acceleration (m/s^2 , ft/s^2)
H	Total enthalpy (energy/mass, energy/mole)
h	Heat transfer coefficient (W/m^2-K, Btu/ft^2-hr-°F)
h	Species enthalpy (energy/mass, energy/mole)
h_0	Standard state enthalpy of formation (energy/mass, energy/mole)
J	Mass flux; diffusion flux (kg/m^2-s, lbm/ft^2-s)
K	Equilibrium constant = forward rate constant/backward rate constant (units vary)
k	Kinetic energy per unit mass (J/kg, Btu/lbm)
k	Reaction rate constant, e.g., k1, k-1, $k_{f;r}$, $k_{b;r}$ (units vary)
k	Thermal conductivity (W/m-K, Btu/ft-hr-°F)
k_B	Boltzmann constant ($1.38x10^{-23}$ J/mole-K, $7.27x10^{-27}$ Btu/mole-°R)
k,kc	Mass transfer coefficient (units vary)
m	Mass (kg, lbm)
M_w	Molecular weight (kg/kgmol)
Nu	Nusselt number = hL/k (dimensionless)
P	Pressure (Pa, atm, mm Hg, lbf/ft^2)
Pr	Prandtl number = α/ν (dimensionless)
q"	Heat flux (W/m^2 , Btu/ft^2-hr)
R	Gas-law constant ($8.31447x10^3$ J/kgmol-K, 1.98588 Btu/lbmol-°F)
R	Reaction rate (units vary)
Re	Reynolds number ≡ UL/ν (dimensionless)
S	Total entropy (J/K, J/kgmol-K, Btu/lbmol-°F)
s	Specific entropy
s_0	standard state entropy (J/kgmol-K, Btu/lbmol-°F)
Sc	Schmidt number = ν/D (dimensionless)
S_{ij}	Mean rate-of-strain tensor (s^{-1})
T	Temperature (K, °C, °R, °F)
t	Time (s)
t	thickness (m, ft)
U	Free-stream velocity (m/s, ft/s)
u; v; w	Velocity components (m/s, ft/s);

V	Volume (m^3, ft^3)
X	Mole fraction (dimensionless)
Y	Mass fraction (dimensionless)

Greek Letter

α	Permeability, or flux per unit pressure difference (L/m^2-hr-atm, ft^3/ft^2-hr-(lbf/ft^2))
α	Thermal diffusivity (m^2/s, ft^2/s)
α	Volume fraction (dimensionless)
β	Coefficient of thermal expansion (K-1)
γ	Specific heat ratio, c_p/c_v (dimensionless)
Δ	Change in variable, final – initial (e.g., .p, .t, .H, .S, .T)
ε	Emissivity (dimensionless)
ε	Turbulent dissipation rate (m^2/s^3, ft^2/s^3)
η',η''	Rate exponents for reactants, products (dimensionless)
ν	Dynamic viscosity (Pa-s, lbm/ft-s)
μ	Kinematic viscosity (m^2/s, ft^2/s)
ν',ν''	Stoichiometric coefficients for reactants, products (dimensionless)
ρ	Density (kg/m^3, lbm/ft^3)
σ	Stefan-Boltzmann constant (5.67×10^{-8} W/m^2-K^4, 1.71×10^{-9} Btu/hr-ft^2-°R^4)
σ_s	Scattering coefficient (m^{-1})
$\bar{\bar{\tau}}$	Stress tensor (Pa, lbf/ft^2)
τ	Shear stress (Pa, lbf/ft^2)
τ	Time scale, e.g., τ_c, τ_p (s)
Φ	Equivalence ratio (dimensionless)

ABSTRACT

The main function of a pyroscrubber in petroleum coke calcining process is to oxidize the carbonaceous contents, including hydrocarbon volatiles, of the exhaust gas from the calcination kiln, so as to leave no more than small traces of unburned volatiles, solid carbon, ashes, or emissions (e.g. CO, NO_x and SO_x) in the flue gas finally discharged.

To maximize the energy recovery and reduce pollutant emission from the pyroscrubber, 3-D computational models are developed using FLUENT to simulate the combustion and thermal-flow phenomena inside the pyroscrubber.

The results show the 3-D behavior of the flow, the reaction inside the pyroscrubber, effect of different amounts of air injection with respect to combustion efficiency, energy output and NO_x emission. A multistage burning strategy is introduced and studied and results show it successfully cuts emission without compromising energy output. A particle combustion model with the homogeneous gas combustion model is also developed and incorporated to investigate CO emission.

Keywords: Calcination, Pyroscrubber, Combustion, Multistage Burning, coke fine combustion, NO_x,

CHAPTER ONE

INTRODUCTION

1.1 Background

Petroleum coke is usually calcined in a gas-fired rotary kiln or rotary hearth at high temperatures, around 1,200 to 1,350 °C, to remove moisture, drive off volatile matters, increase the density of the coke structure, increase physical strength, and increase the electrical conductivity of the material. The product is hard, dense carbon (calcined petroleum coke) with low hydrogen content and good electrical conductivity. These properties along with the low metals and ash contents make calcined petroleum coke the best material currently available for making carbon anodes for smelting of alumina to aluminum [Bagdoyan and Gootzait, 1985].

The schematic of the entire calcining processes for petroleum coke is shown in Figure 1.1. The calcination operation as mentioned above is carried out in an inclined rotary kiln where green coke is fed near the upper end. Air for combustion of volatiles is supplied at one or more locations, and burners are located at the bottom end of the kiln to provide heat at start-up and to provide supplementary heat to control the material structure and quality of the final product. Calcined coke, issuing from the lower end of the kiln, enters a rotary cooler, typically at a temperature of 1,200 ^{o}C. The coke is cooled by spraying water to quench the coke. The resultant steam, together with air drawn in through the inlet end of the cooler is drawn off through a surrounding manifold by means of a suction fan.

The pyroscrubber receives the exhaust gases from the feedstock feeding end of the kiln, typically between 500 ^{o}C and 1,000 ^{o}C, having a substantial content of unburned volatiles and entrained solid carbon particles and somewhat dusty air/water vapor mixture. The solids and volatiles are burned during passage through the pyroscrubber by means of further air injection by blowers. The product gases from the pyroscrubber, now essentially free from abrasive coke particles, is passed at a high temperature, typically 1200 ^{o}C, to a waste heat boiler for recovery of the thermal energy of the gas，and then to steam turbines for power generation.

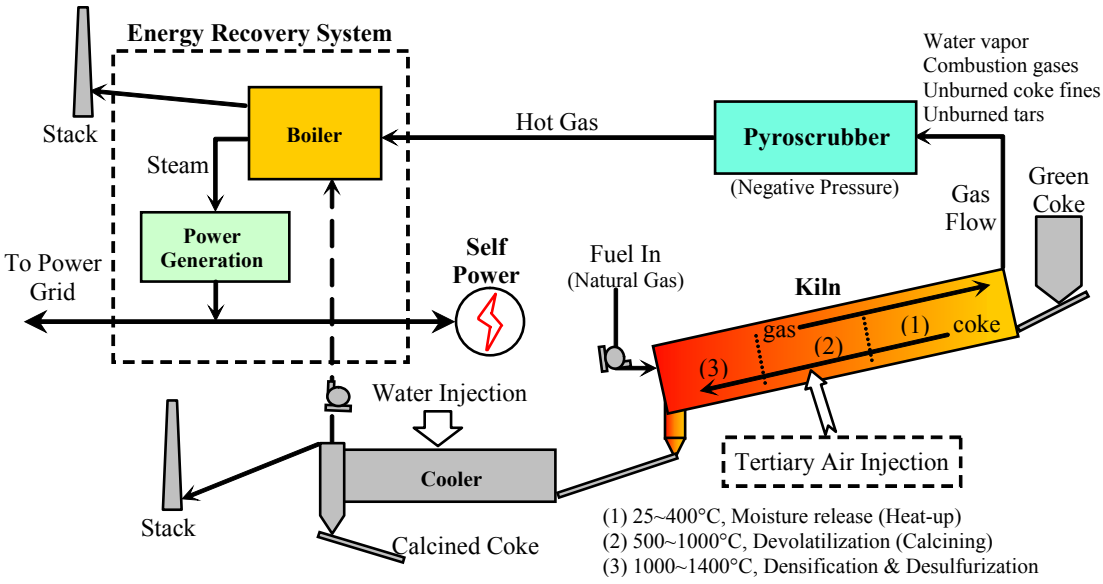

Figure 1.1 Schematic of the calcining process for petroleum coke

1.2 Objectives

To maximize the energy recovery and reduce pollutant emission from the pyroscrubber, more detailed information and a better understanding of thermal-flow and combustion process inside the pyroscrubber are needed. The **objective** of this study is to employ computational fluid dynamics (CFD) technique with the appropriate combustion model to better understand the combustion and thermal-flow phenomena inside the pyroscrubber, and investigate further the potential means to improve combustion performance and reduce emissions. The specific goals are:

1. Develop a numerical model of the pyroscrubber that simulates the thermal-flow, combustion processes. Special attention will be paid to the modeling of coke fines, combustion gases burning, and pollutant emissions.
2. Investigate flow pattern, temperature distribution, combustion process, and emission information inside the pyroscrubber.
3. Study the effect of different amounts of air injection with respect to combustion efficiency, energy output and NO_x emission.

4. Simulate and study the effect of introducing a multistage burning strategy on emission control and energy output.
5. Develop and incorporate a heterogeneous particle combustion model with the homogeneous gas combustion model and investigate CO emission.

CHAPTER TWO

LITERATURE SURVEY

The literature survey focuses on introducing types, functions, fundamental mechanisms of combustion and emissions in pyroscrubbers.

2.1 Pyroscrubber

A pyroscrubber is namely a furnace burning carbon particles in a stream of waste gas, particularly from a petroleum coke calcination kiln or hearth. The combusted hot gases are ducted through a boiler to produce steam that is used to generate electricity through steam turbines. A pyroscrubber typically comprises of a U-shaped combustion chamber having a first passage arranged parallel with (preferably above) a second passage, so there is a reversal in gas flow direction between the two passages. The combustion chamber has an inlet to receive exhaust gases from the calcining kiln and an array of air injection inlets at the inlet end of the first passage. A gas outlet preferably leads laterally out of the side of the structure at the outlet end of the second passage to secure an abrupt change in the direction of gas flow. The main function of the pyroscrubber is to oxidize the carbonaceous contents, including hydrocarbon volatiles in the exhaust gas from the calcination kiln, so as to leave no more than small traces of unburned volatiles, solid carbon, ashes, or emissions (e.g. CO, NO_x and SO_x) in the flue gas finally discharged. Where incandescent carbon particles are carried in an oxygen-containing gas stream, the products of its own combustion tend to increase in its immediate surroundings and reduce its rate of oxidation. This can be counter-acted by increasing turbulence in the gas stream and by increasing "slip" between the particles and the gas. When the gas moves at a different

speed from the entrained particles, there is "slip" or relative movement of the particles to the gas.

The reversed-flow two-passage design in the pyroscrubber construction has the advantage because the gases passing through the combustion chamber turn through 180^{o} in passing from the first passage to the second passage, leading to an increase in turbulence in the gas stream and in the slip between the gas and the entrained particles. This leads to increased speed of combustion by separating the coke particles from their own combustion products.

Pyroscrubbers of different designs have been employed worldwide to compete for more efficient and cleaner combustion of exhaust gases from coke calcination kilns or hearths. Known pyroscrubbers have comprised of a long, straight combustion chamber with a large cross section to permit passage of the large volume of gases flying through with dense carbon particles. They rely on normal flue draught for drawing in air at various locations in the combustion chamber. Supplementary air is drawn into the combustion chamber at a substantial distance from the inlet end of the combustion chamber, which results in a delay of thorough mixing of the air and the waste gas stream to ensure a complete combustion of solid carbon particles. Consequently, the dimensions of the combustion chamber of known pyroscrubbers are rather large. Since the function of pyroscrubber-steam generator assembly is similar to the conventional coal-fired boiler assembly, the literature search will start with boiler review.

2.2 Combustion

Combustion or burning is a complicated sequence of chemical reactions between a fuel and an oxidant accompanied by the production of heat or both heat and light in the form of either a glow or flames. In a complete combustion reaction, a compound reacts with an oxidizing element at the maximum percentage, and the products are compounds of each element in the fuel with the oxidizing element. The complete combustion reaction of carbon with oxygen is:

$$C + O_2 \rightarrow CO_2 + \text{Heat} \quad \text{(Eq.2.1)}$$

In reality, combustion processes are never perfect or complete. In flue gases from combustion of carbon (Eq.2.2) or carbon compounds (as in combustion of hydrocarbons, wood etc.) both unburned carbon (known as soot) and carbon compounds (CO (Eq.2.3) and others) will be present.

$$C + \tfrac{1}{2}O_2 \rightarrow CO + \text{Heat} \quad \text{(Eq.2.2)}$$

$$CO + \tfrac{1}{2}O_2 \rightarrow CO_2 + \text{Heat} \quad \text{(Eq.2.3)}$$

Also, when air is the oxidant, some nitrogen will be oxidized to various, mostly harmful, nitrogen oxides (NO_x). The effectiveness of combustion can be determined by analyzing the flue gas and the amount of soot.

There are three types of fuel present in the calcining process, methane (as natural gas), solid carbon (as petroleum coke), and volatile matters (as hydrocarbons).

The complete combustion of methane and volatile matters can be presented as:

$$CH_4 + 2O_2 \rightarrow CO_2 + 2H_2O + \text{Heat} \quad \text{(Eq.2.4)}$$

$$C_xH_yO_z + \left(x + \tfrac{y}{4} - \tfrac{z}{2}\right)O_2 \rightarrow xCO_2 + \tfrac{y}{2}H_2O + \text{Heat} \quad \text{(Eq.2.5)}$$

2.3 NO_x

Control of NO_x emission is a major factor in the design of a modern combustion system. NO_x emissions cause serious health issues, ranging from bronchitis to altered immune system function. Currently, 8.5 million Americans live in countries with NO_x levels higher than EPA's health standards prescribed. NO_x also contributes significantly to environmental problems such as acid rain and ozone depletion.

NO_x emission consists of mostly nitric oxide (NO). It also contains nitrogen oxide (NO_2)

and nitrous oxide (N_2O). The quantity of NO_x formed depends on the three T's: Temperature, Time, and Turbulence.

Oxides of Nitrogen Formation:

In every circumstance where combustion occurs, the formations of nitrogen oxides (NO_x) are inevitable. From a home open fire to a coal fired power plant, NO_x is formed as an undesired product and a contributor to air pollution.

NO_x is used to refer to NO and NO_2. NO is the primary form in combustion products (typically 95 percent of total NO_x). NO is subsequently oxidized to NO_2 in the atmosphere.

Nitrogen Oxide formation occurs through three reaction paths, each having unique characteristics which are responsible for the formation of NO_x during combustion processes:

(1) Thermal NO_x: formed by the combination of atmospheric nitrogen and oxygen at high temperatures

(2) Fuel NO_x: formed from the oxidation of fuel-bound nitrogen

(3) Prompt NO_x: formed by the reaction of fuel-derived hydrocarbon fragments with atmospheric nitrogen in an early phase of the flame front

NO_x emissions do not form in significant amounts until flame temperatures reach 1810.93 K (2800^{o}F). Once that threshold is passed, any further rise in temperature causes a rapid increase in the rate of NO_x formation. Lower excess air levels (fuel rich) starve the reaction for oxygen, and higher excess air levels (lean burn) drive down the flame temperature, slowing the rate of reaction, hence reducing thermal NO_x formation.

In the combustion of fuels that contain no nitrogen, nitric oxide is formed by three chemical mechanisms:

1. The Thermal or Zeldovich Mechanism

2. The Prompt or Fenimore Mechanism
3. The N_2O Intermediate Mechanism

Thermal NO_x Formation

Thermally produced NO_x is the largest contributor to these types of emissions. Thermal NO_x is produced during the combustion process when nitrogen and oxygen are present at elevated temperatures. The two elements combine to form NO or NO_2. NO_x is generated by many combustion processes. It combines with other pollutants in the atmosphere and creates O_3, a substance known as ground level ozone.

The formation of thermal mechanism dominates in high-temperature combustion over a fairly wide range of equivalence ratios. Equivalence ratio is defined as the ratio of actual fuel/air ratio over the theoretical fuel/air ratio. The formation of thermal NO_x is determined by a set of highly temperature-dependent chemical reactions known as the extended Zeldovich mechanism. The principal reactions governing the formation of thermal NO_x from molecular nitrogen are as follows:

$$O + N_2 \Leftrightarrow NO + N \quad \text{(Eq.2.6)}$$

$$N + O_2 \Leftrightarrow NO + O \quad \text{(Eq.2.7)}$$

A third reaction, particularly at near-stoichiometric conditions and in fuel-rich mixtures, contributing to the mechanism is

$$N + OH \Leftrightarrow NO + H \quad \text{(Eq.2.8)}$$

The activation energy for first reaction (Eq.2.6) is relatively large, 319,050 kJ/kmol. Therefore, this reaction has very strong temperature dependence. The thermal mechanism is

unimportant at temperatures below 1800 K (2780^{o}F). Compared with the time scales of fuel oxidation processes, NO is formed rather slowly by thermal mechanism; therefore, thermal NO is generally considered to be formed in post flame gases.

Fuel NO_x Formation

Fuel NO_x formation is a more complex process involving local concentration of oxygen and nitrogen and is reduced by minimizing the availability of oxygen during various stages of the combustion process. Fuel-bound NO_x is generated from nitrogen compounds present in the fuel itself. Gaseous fuels, such as natural gas or propane, are free of nitrogen compounds. However, fuel oils and coal can contain significant amounts of fuel-bound nitrogen. During combustion, the conversion rate of fuel-bound nitrogen to NO_x varies widely over a range of 20 to 70%.

During the combustion process, nitrogen-containing organic compounds present in liquid or solid fossil fuel contributes to the total NO_x formed. The fuel nitrogen is a particularly important source of nitrogen oxide emissions for residual duel oil, coke, and coal, which typically contain 0.3-2% nitrogen by weight. The fuel-bound NO_x contribution depends on the amount of nitrogen that is chemically bound in the fuel. The fuel NO_x formation is generally important in non-premixed combustion. The fuel NO_x formation is not important in premixed combustion applications since most fuels used in premixed combustion contain little or no bound nitrogen.

Under the reducing conditions surrounding the burning droplets or particles, the fuel-bound nitrogen is converted to fixed nitrogen species such as HCN and NH_3. These, in turn, are readily oxidized to form NO if they reach the lean zone of the flame. Between 20 and 80

percent of the bound nitrogen is typically converted to NO_x, depending on the design of the combustion equipment. With prolonged exposure (order of 100 ms) to high temperature and reducing conditions, however, these fixed nitrogen species can be converted to molecular nitrogen and avoid the NO formation path. The fuel NO_x mechanism is shown in Figure 2.2.

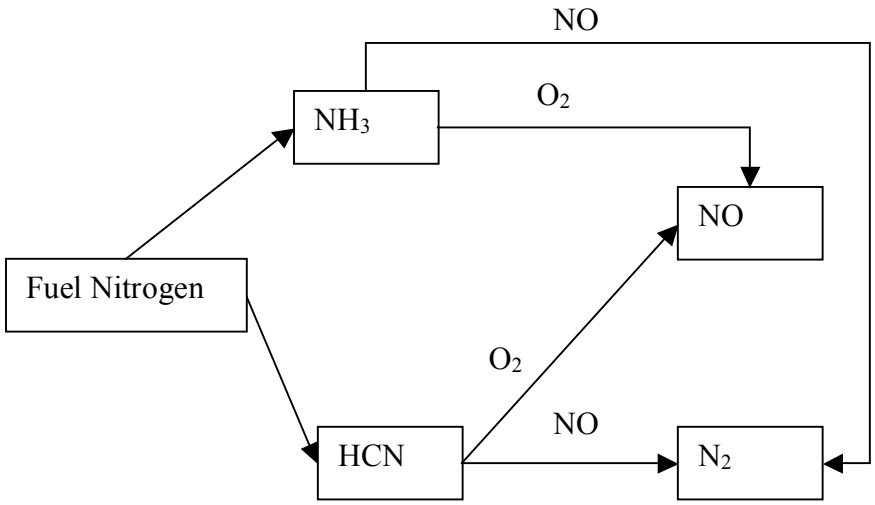

Figure 2.1 Fuel NO_x mechanism

Prompt NO_x Formation

Prompt NO_x is the third and least significant NO_x formation mechanism. In this mechanism, nitrogen from combustion air reacts with hydrocarbon radicals from the fuel to form a hydrogen cyanide intermediate. The hydrogen cyanide then reacts with oxygen and nitrogen in combustion air to form nitrogen oxide.

Hydrocarbon fragments (such as C, CH, CH_2) may react with atmospheric nitrogen under fuel-rich conditions to yield fixed nitrogen species such as NH, HCN, H_2CN, and CN. These in turn can be oxidized to NO in the lean zone of the flame. In most flames, especially those from

nitrogen-containing fuels, the prompt mechanism is responsible for only a small fraction of the total NO_x. Its control is important only when attempting to reach the lowest possible emissions.

The formation of prompt NO_x is governed by a set of equations known as Fenimore mechanism. These equations show that hydrocarbon radicals react with molecular nitrogen to form amines or cyano compounds. The amines and cyano compounds are then converted to inverted compounds that ultimately form NO. Fenimore mechanism is given as:

$$CH + N_2 \Leftrightarrow HCN + N \quad \text{(Eq.2.9)}$$

$$C + N_2 \Leftrightarrow CN + N \quad \text{(Eq.2.10)}$$

$$N + O_2 \Leftrightarrow NO + O \quad \text{(Eq.2.11)}$$

$$HCN + OH \Leftrightarrow CN + H_2O \quad \text{(Eq.2.12)}$$

$$N + OH \Leftrightarrow NO + H \quad \text{(Eq.2.13)}$$

In the atmosphere, nitric oxide ultimately oxidizes to form nitrogen oxides, which contribute to production of acid rain and photochemical smog. Production of NO associated with the Fenimore prompt mechanism is shown in Figure. 2.3.

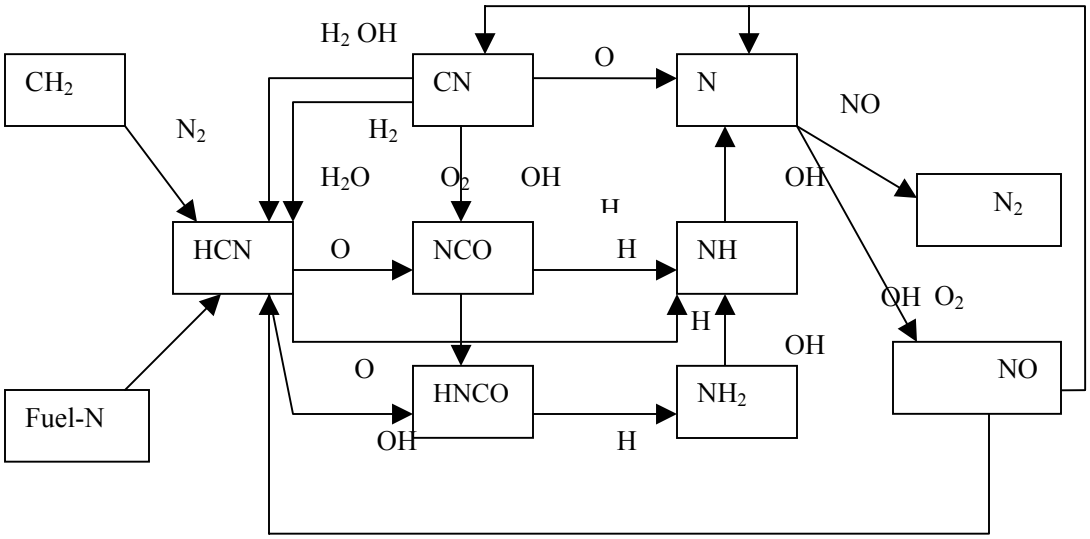

Figure 2.2 NO production associated with Fenimore prompt mechanism

Prompt NO_x formation is proportional to the number of carbon atoms present per unit volume and is independent of the parent hydrocarbon identity. The quantity of HCN formed increases with the concentration of hydrocarbon radicals, which in turn increases with equivalence ratio. As the equivalence ratio increases, prompt NO_x production increases, passes a peak, and finally decreases due to deficiency in oxygen.

NO_x Formation From Reburning

In reburning NO mechanism, NO reacts with hydrocarbons and is subsequently reduced. In general the mechanism is given as

$$CH_i + NO \longrightarrow HCN + \text{products} \qquad \text{(Eq.2.14)}$$

Three reburn reactions for temperature range $1600 \leq T \leq 2100$ K are

$$CH + NO \xrightarrow{K1} HCN + O \qquad \text{(Eq.2.15)}$$

$$CH_2 + NO \xrightarrow{K2} HCN + OH \quad \text{(Eq.2.16)}$$

$$CH_3 + NO \xrightarrow{K3} HCN + H_2O \quad \text{(Eq.2.17)}$$

Where K1, K2 and K3 are rate constants for the above reactions

$K_1 = 1 * 10^8$ [m^3 / gmol-s]

$K_2 = 1.4 * 10^6 * e^{-550/T}$ [m^3 / gmol-s]

$K_3 = 2 * 10^5$ [m^3 / gmol-s]

NO_x Control

NO_x control technologies currently used within the industry can be grouped into two categories i.e. combustion modifications and post-combustion NO_x control technologies. The first addresses reduced production of NO_x by making changes in the combustion process or the fuel stream. The second involves mitigating the NO_x that has been produced by the application of post-combustion technology through the use of chemical reagents. For coal-fired applications, combustion system modifications are generally less costly and may independently result in emissions levels that satisfy regulatory requirements. Several methods are available to effectively limit NO_x formation during combustion. The optimum combustion system redesign may blend several of these, including selected on the basis of unit capacity, fuels to be fired,and applicable NO_x reduction requirements.

For processes dominated by thermal NO_x formation, time, temperature, and oxygen availability are the primary variables affecting NO_x yields. Production of thermal NO_x can be controlled by reducing the thermal loading to the combustion zone. NO_x mechanisms include (1) increasing the size of the combustion zone for a given thermal input, (2) reducing the rate of combustion and peak flame temperatures with specially designed burners, and (3) addition of

recirculated flue gas to the combustion air to depress flame temperature and increase residence time.

Fuel NO_x formation can be reduced by switching to, or co-firing with, fuel with lower nitrogen content and/or by limiting oxygen availability during the early stages of combustion. Oxygen reduction mechanisms include reducing excess air, reducing burner stoichiometry by removing a portion of the combustion air from the burner zone and introducing this air later through NO_x or overfire air (OFA) ports (i.e. air staging), and limiting the rate that air is introduced to the fuel during the early stages of combustion with specially designed burners.

Combustion Modifications for NOx control

Low Excess Air ---- Reducing the air supplied in the furnace lowers NO_x production. Thermal NOx emissions peak at leaner than stoichiometric equivalence ratios. The NO_x creation rate typically peaks at excess oxygen levels of 5-7% where the combination of high combustion temperatures and the higher oxygen concentration act together. At both lower and higher air/fuel ratios, NO_x production falls off due to lower flame temperature at high excess air levels and lower oxygen at low air levels. Low air is achieved by changes in operating procedures, system controls or both. The NO_x reduction technique involves reducing the air supplied. Only limited NO_x reductions are possible when low air level is supplied because excessive reduction in air can be accompanied by significant increases in CO.

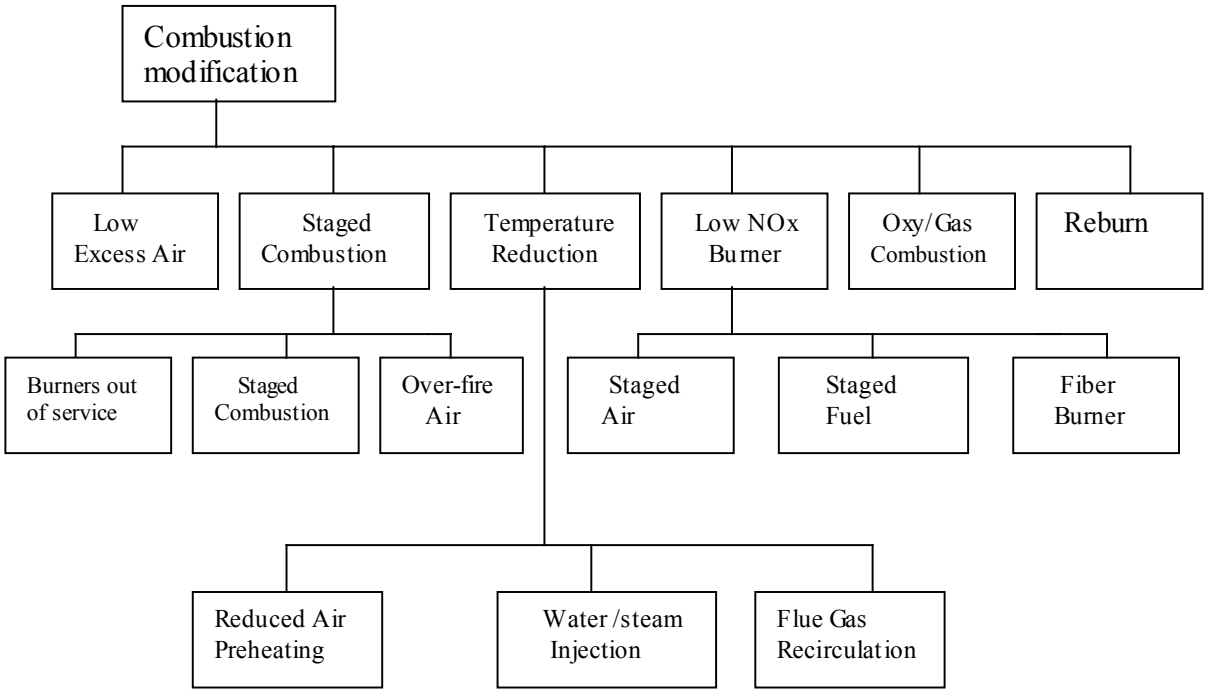

Figure 2.3 Combustion modification technologies for NO_x control

Staged Combustion — Staged combustion processes significantly reduce NO_x emissions. In the initial stage of combustion, the air supplied to the burners is less than the amount required to completely burn the fuel. During this stage, fuel-bound nitrogen is released but cannot be oxidized, so it forms stable molecules of harmless molecular nitrogen (N2). Other components of the fuel are also released without being fully oxidized. These include carbon particles and carbon monoxide. By adding a second stage, in the air-fuel mixture, the carbon and carbon monoxide can be burned, converting them to carbon dioxide.

Over-fire Air — Over-fire air is the air that is injected into the furnace above the normal combustion zone. Generally when Over-fire air is employed, the burners are operated at a lower than normal air-to-fuel ratio, which reduces NO_x formation. Over-fire air, which is frequently used in conjunction with low NO_x burners, completes the combustion process at a lower

temperature. Figure 2.4 shows a typical over-fire air boiler.

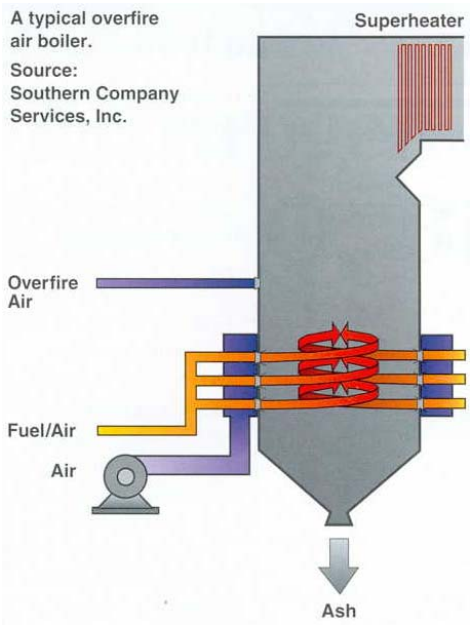

Figure 2.4 Example of a typical over-fire air boiler (Source: Southern Company Services, Inc.)

Flue Gas Recirculation — Flue Gas Recirculation, in which part of the flue gas is recirculated to the furnace, can be used to modify conditions in the combustion zone (lowering the temperature and reducing the oxygen concentration) to reduce NO_x formation. Flue Gas Recirculation is also used as a carrier to inject fuel into a reburn zone to increase penetration and mixing.

Operational Modifications — Changing certain boiler operational parameters can create conditions in the furnace that will lower NO_x production. Examples include burners-out-of-service (BOOS), low excess air (LEA), and biased firing (BF). In BOOS, selected burners are removed from service by stopping fuel flow, but airflow is maintained to create staged combustion in the furnace. LEA involves operating at the lowest possible excess air level without interfering with good combustion, and BF involves injecting more fuel to some burners

(typically the lower burners) while reducing fuel to other burners (typically the upper burners) to create staged combustion conditions in the furnace.

Low NO_x Burners (LNB) — Low NO_x Burners are burners designed to control the mixing of fuel and air to achieve what amounts to staged combustion. This staged combustion reduces both flame temperature and oxygen concentration during some phases of combustion, in turn, reduces both thermal NO_x and fuel NO_x production. An example of LNB is shown in Figure 2.5 The most common LNB types achieve lower NO_x emissions by "staging" the injection of either air or fuel in the burner region. Low NO_x burners are classified as either a staged air or a staged fuel burner. Air staging is more common. As the name implies, the staged air burner gradually introduces combustion air to the fuel at various regions along the flame front. These regions are typically referred to as the primary, secondary and tertiary (staged) air zones. The division of combustion air reduces the oxygen concentration in the primary burner combustion zone, lowering the amount of NO formed there and increasing the amount of NO-reducing agents formed in an oxygen deficient combustion zone. Secondary and tertiary air injections complete the combustion downstream of the primary zone, lowering the peak temperature and reducing thermal NO_x formation. Aside from the basic staged air burner, there are other variations of staged air burners that incorporate internal recirculation of combustion products to aid in NO_x reduction. Low NO_x burners are often coupled with over fire (secondary) air (OFA) injection to assure complete combustion. Low NO_x burner employing air staging and fuel staging is shown in Figure 2.6.

Reburning — In the Reburning process, part of the boiler fuel input (typically 10-25%) is added in a separate reburn zone. The fuel-rich reducing conditions in this zone lead to the reduction of

NO_x formed in the normal combustion zone. OFA is injected above the reburn zone to complete combustion. Thus with reburn, there are three zones in the furnace: (1) a combustion zone with an approximately normal air-to-fuel ratio, (2) a reburn zone where added fuel results in a fuel-rich condition, and (3) a burnout zone where OFA completes the combustion. Coal, oil, or gas can be used as the reburn fuel.

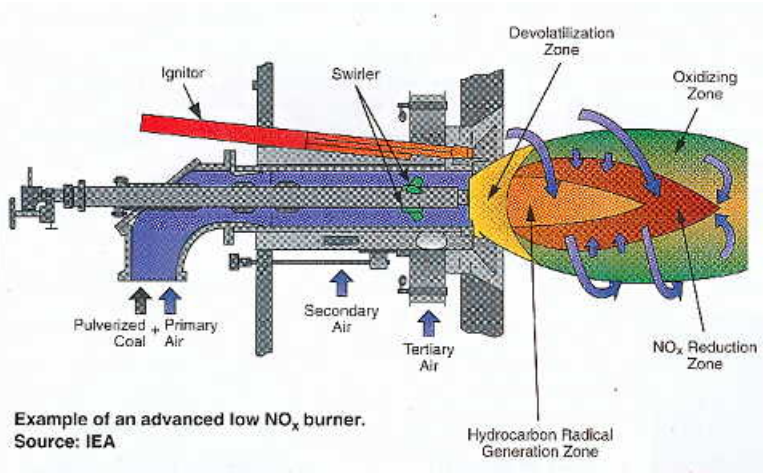

Figure 2.5 Example of Low NOx Burner (Source: the International Energy Agency)

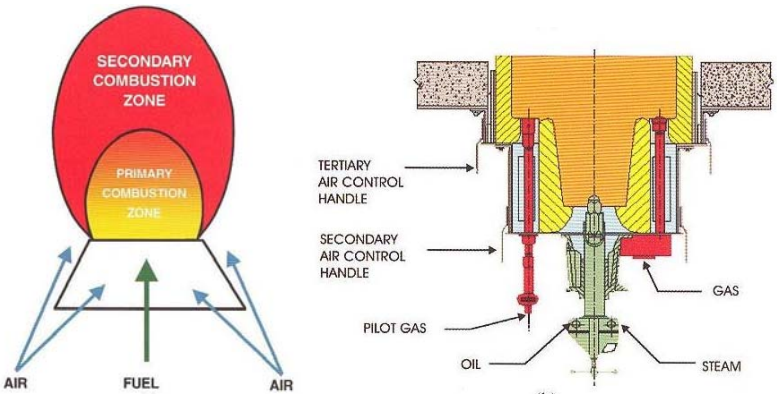

(a)

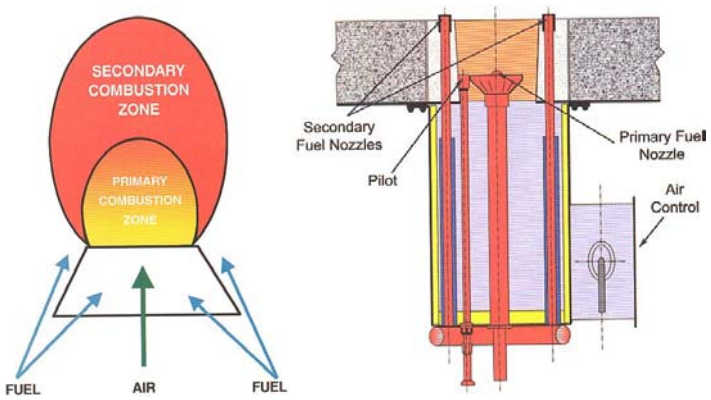

(b)

Figure 2.6 (a) Low NOx burner employing air staging (above)

(b) Low NOx burner employing fuel staging

(Source: The John Zink Combustion Handbook)

Post-Combustion controls for NO_x reduction

Post-combustion controls can be achieved by using selective non-catalytic reduction (SNCR) and selective catalytic reduction (SCR) as shown in Figure 2.7

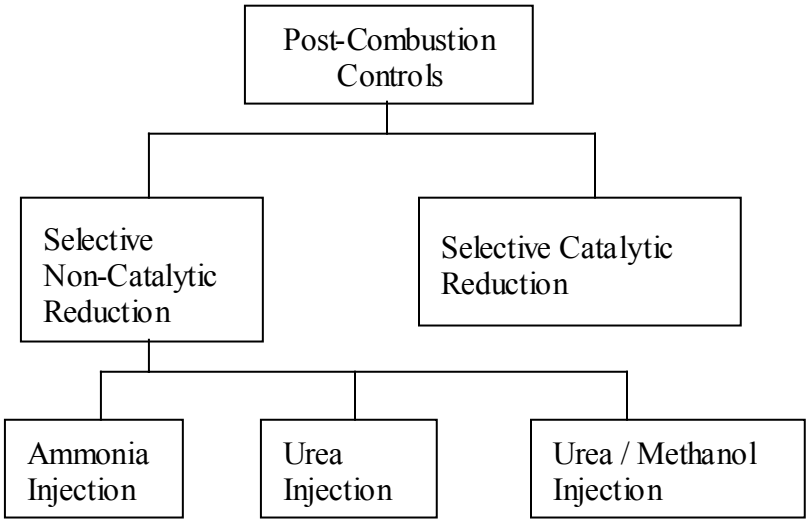

Figure 2.7 Post-combustion control technologies for NOx reduction

Selective Non-Catalytic Reduction (SNCR) — In this post control technique, a nitrogen containing additive, ether ammonia, urea, or cyanuric acid, is injected and mixed with flue gases to affect chemical reduction of NO to N_2 without the aid of catalyst. Temperature is a critical variable, and operation within a relatively narrow range of temperatures is required to achieve large NO_x reductions.

Selective Catalytic Reduction (SCR) — In this technique, a catalyst is used in conjunction with ammonia injection to reduce NO to N_2. Effective reduction depends on the temperature range and is about 480 K to 780 K. Greater NO_x reductions are possible, but the cost of NO_x removal is generally the highest of all NO_x control techniques because of both the initial cost and the operating costs associated with catalyst replacement.

CHAPTER THREE

MODELING AND METHODOLEGY

The pyroscrubber studied in this thesis is shown in Figure 3.1. Geometric information of the pyroscrubber is obtained through the blueprints of the CII Carbon Norco Plant in Louisiana. Assumptions and simplifications are made for effective modeling and simulation. The modeled domain includes part of the calcining kiln, settling chamber, inlet duct, which connects the settling chamber with the main chamber, air injection section, main chamber, and outlet duct,connecting the main chamber to the boiler. Details of the air injectors and the burner are shown in Figure 3.2.

The inlet of the pyroscrubber receives exhaust gases from the exit of the calcining kiln. After completion of the calcining process inside the kiln, combustion product gases, together with unburned volatiles and coke fines are fed into the pyroscrubber through the settling chamber and the inlet duct. Air is injected into the main chamber through two air injection sections. The first air injection section consists of 28 air injection tubes shooting at 45^{o} from the vertical direction (Y direction). Not only is the second air-injection section, located at the burner slots on the east wall of the main chamber, used to inject natural gas as the start-up fuel, but they also blow air into the main chamber after the ignition and start-up process. Hot product gases exit the pyroscrubber main chamber through the outlet duct and are fed into the steam boiler to generate electricity.

The major characteristics and general assumptions are listed below:

1. The flow inside the pyroscrubber is three dimensional, incompressible, and turbulent.
2. Gas species involved in this study are Newtonian fluids with variable properties as functions of temperature.
3. Buoyancy and radiation effects are considered.
4. Non-slip and adiabatic wall conditions are assumed.

CFD commercial software FLUENT (version 6.2.16) is employed to complete the calculation process of the modeling. The simulation uses the segregated solver, which employs an implicit pressure-correction scheme. The SIMPLE algorithm is used to couple the pressure and velocity. Second order upwind scheme is selected for spatial discretization of the convective terms and species. Lagrangian trajectory calculations are employed to model the dispersed phase of particles. The impact of particles on the continuous phase is considered as source terms to the governing equations. After obtaining an approximate flow field of the continuous phase (gas flow in this study), particles are injected and their trajectories are calculated. At the same time, drag, heat and mass transfer between the droplets and the airflow is calculated.

Iteration proceeds alternatively between the continuous and discrete phases. Twenty iterations in the continuous phase are conducted between two iterations in the discrete phase. Converged results are obtained after the specified residuals are met. A converged result renders mass residual of 10^{-4}, energy residual of 10^{-6}, and momentum and turbulence kinetic energy residuals of 10^{-5}. These residuals are the summation of the imbalance for each cell, scaled by a

representative of the flow rate. Typically, 8000 to 12000 iterations are needed to obtain a converged result, which takes about 15~20 hours on a 10-node computer cluster of parallel computation with each node a 2.8 GHz Pentium personal computer.

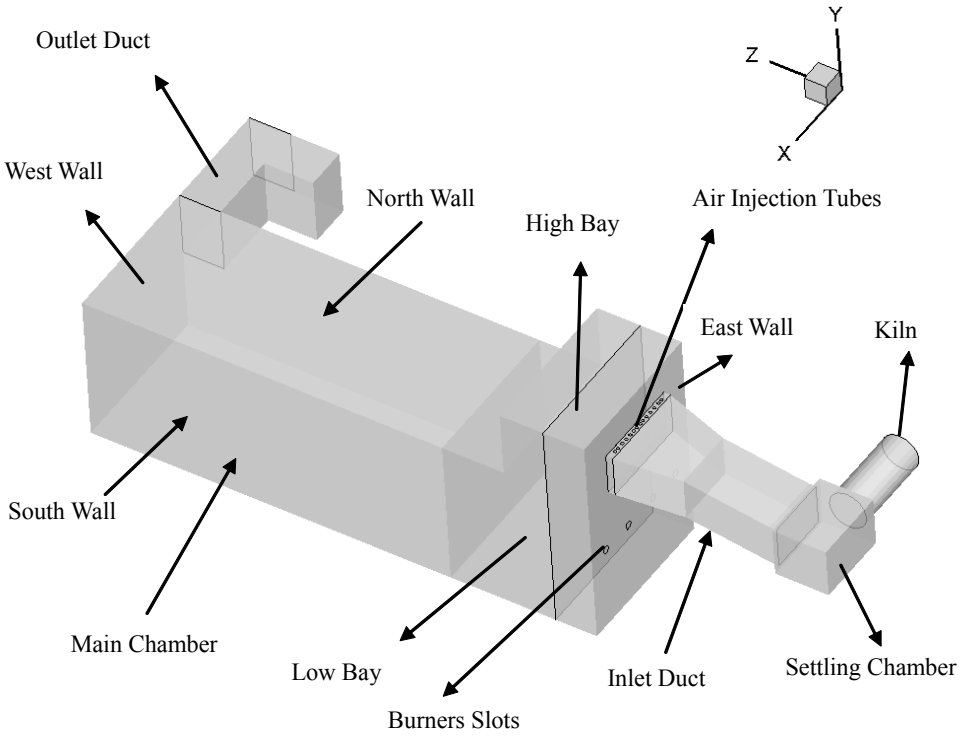

Figure 3.1 A 3-D view of the pyroscrubber

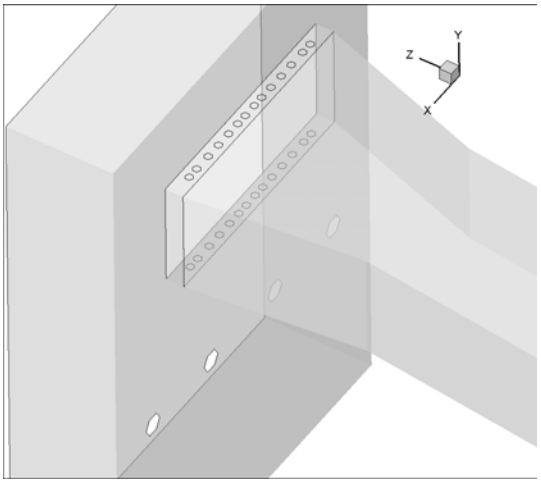

Figure 3.2 Detailed air injections and burners

3.1 Governing Equations

The conservation equations for mass, momentum and energy in general forms are shown below.

$$\frac{\partial \rho}{\partial t} + \nabla \bullet \left(\rho \vec{v}\right) = 0 \qquad \text{(Eq.3.1)}$$

$$\frac{\partial}{\partial t}\left(\rho \vec{v}\right) + \nabla \bullet \left(\rho \vec{v}\vec{v}\right) = -\nabla p + \nabla \bullet \left(\overline{\overline{\tau}}\right) + \rho \vec{g} + \vec{F} \qquad \text{(Eq.3.2)}$$

$$\frac{\partial}{\partial t}\left(\rho E\right) + \nabla \bullet \left(\vec{V}\left(\rho E + p\right)\right) = \nabla \bullet \left(k_{eff} \nabla T - \sum_j h_j \vec{J}_j + \left(\overline{\overline{\tau}}_{eff} \bullet \vec{v}\right)\right) + S_h \qquad \text{(Eq.3.3)}$$

The momentum equations are solved with the complete three-dimensional Navier-Stokes equations, so, $\overline{\overline{\tau}}$, the stress tensor is given by

$$\overline{\overline{\tau}} = \mu\left[\left(\nabla \vec{v} + \nabla \vec{v}^{T}\right) - \frac{2}{3}\nabla \bullet \vec{v} \bullet I\right] \qquad \text{(Eq.3.4)}$$

where I is the unit tensor.

In the energy equation, E is given as

$$E = h - \frac{p}{\rho} + \frac{v^2}{2} \qquad \text{(Eq.3.5)}$$

"h" is the sensible enthalpy and for incompressible flow and it is given as

$$h = \sum_j Y_j h_j + \frac{p}{\rho} \qquad \text{(Eq.3.6)}$$

$$h_j = \int_{T_{ref}}^{T} c_{p,j} dT \qquad \text{(Eq.3.7)}$$

T_{ref} is the reference temperature, taken as 298.15 K

S_h in the energy equation is the source term and is provided by the net enthalpy formation rates

from the species transport reactions.

3.2 Meshes

The mesh used in this study is generated using GAMBIT (version 2.2.30). Structured grids are employed in meshing the kiln, part of the main chamber, and the outlet duct; unstructured grids are employed for all the other parts, namely the settling chamber, inlet duct, and part of the main chamber. All together there are 70,729 nodes, 708,418 faces and 340,800 cells. Meshes of each part are shown in detail in Figure 3.3.

Grid Sensitivity Study

A grid sensitivity study of two different mesh numbers (325,431 and 968,235) has been performed and investigated. The computational time for the low mesh number case is about 20 hours and for the high mesh number case is about 60 hours. The temperature variation within the whole domain lies within 50k to 150k (2.6%-7.9%). At the exit, the difference of mass weighted temperature is about 90 K (4.7%). Although the grid independency has not been achieved, for the purpose of current study, 10 % of computational uncertainty is acceptable. Therefore the mesh number around 340,000 is used for this study to save 66% of the computational time.

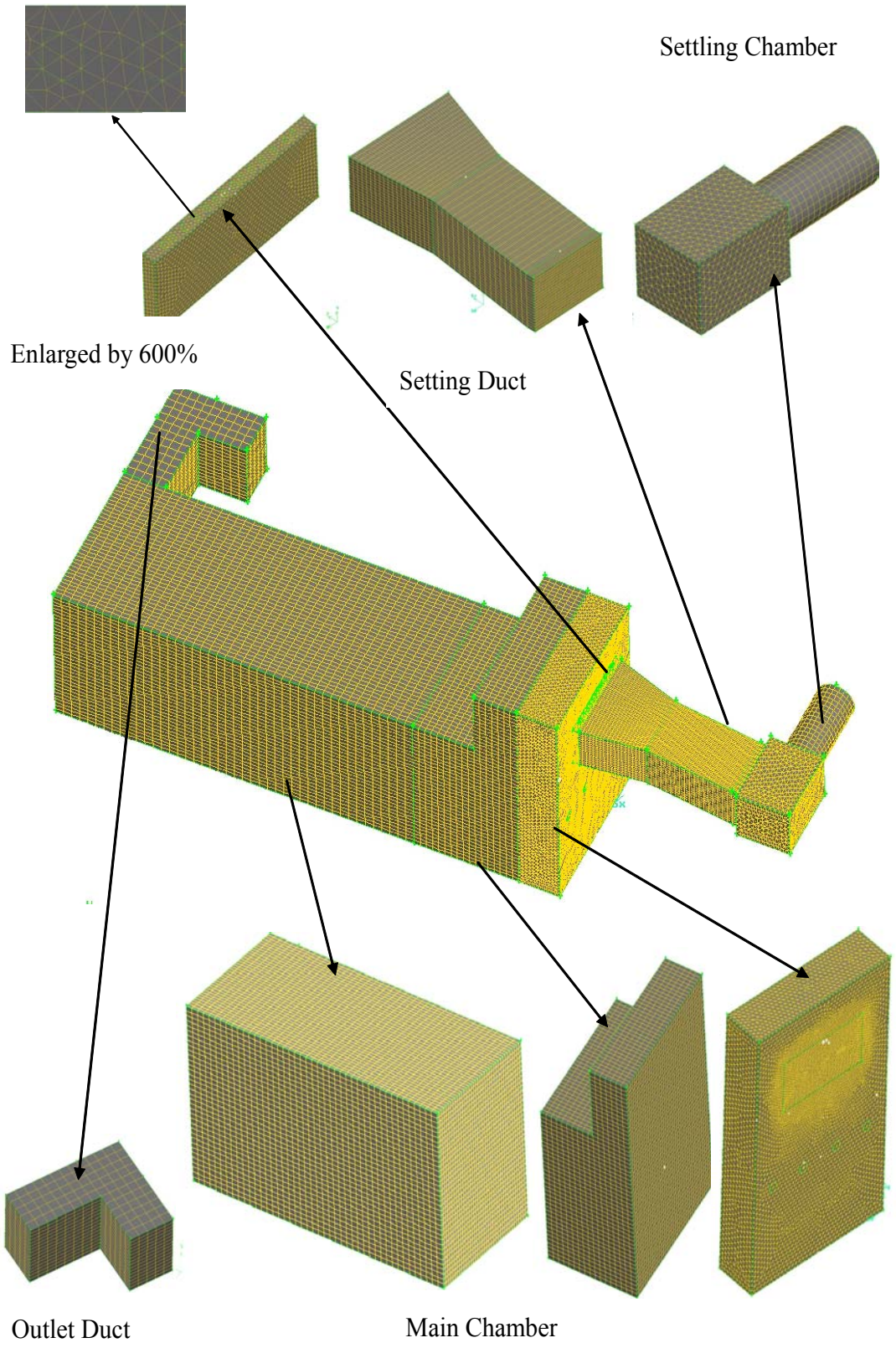

Figure 3.3 Meshes of different parts of the pyroscrubber

3.3 Inlet Condition

The composition of the pyroscrubber inlet species is complex due to the calcining and combustion process inside the kiln. Since their quantities are not subject to measurement yet, the inlet condition is prone to uncertainty. Therefore, a sound estimate of the inlet species is critical for conducting an appropriate simulation. The inlet condition of the pyroscrubber is based on information from three sources: (a) the electric power output from the steam power plant, (b) the computational simulation results of the rotary kiln from a previous report (Sean Zhang and Wang 2007), and (c) the model from a previous Canadian report. Detailed information from each of the three resources is provided below:

(a) According to the operation data of the steam power plant, the hot gases coming out of the pyroscrubber supply the energy for the steam power plant to generate a power output of 15MW. The overall efficiency for the steam power plant is 29.75% (85% boiler efficiency and 35% steam turbine efficiency).

(b) From a previous report (Sean Zhang and Wang 2007), which simulates the calcining process inside the kiln, the exit species composition from the kiln is shown in Table 3.1.

(c) From the Canadian report, the kiln feeding information is:

Green coke feed rate: 9.3 kg/s (16.74 ton/hr, here 1short ton = 2000 lbs)

5.2 % moisture

0.15 % impurities

10.2 % volatile matters (4.09 % burned in kiln and 6.11 % unburned goes into pyroscrubber)

3.72 % coke burned in kiln

9.12 % coke goes into pyroscrubber

Yield: 71.61 % (mass)

To appropriately set up the inlet condition, the information from these three resources needs to be re-examined, cross-checked, and verified. The following observations are made based upon the information from these three sources.

1. All three sources suggest natural gas is burned out inside the kiln, and it is not an important energy source in the pyroscrubber.

2. The energy released and used for the power generation comes from two main sources: coke fines and unburned volatile matters.

3. From Table 3.1, it is noticed that the total energy generated from source (b) is not enough to sustain a 15 MW power output through the current steam power plant because coke fines entrainment from the kiln into the pyroscrubber are not considered in the calculation of source (b). The energy deficiency between (a) and (b) is supplied by combustion of coke fines.

4. Table 3.2 shows the necessary mass flow rate of using only carbon or volatiles as the fuel to supply the 15MW power output. Based on the calculation, it can be concluded that the majority of energy is from the coke fines rather than the volatile.

Based on the above information, the following assumptions are made in this study:

1. The green coke feed rate is 9.3 kg/s, of which 6% is moisture. After the moisture is driven off, 8% (7.52 % of total green coke mass) is volatiles. So the total volatiles

feed rate of the kiln is $9.3\,\text{kg/s} \times 0.94 \times 0.08 = 0.6994\,\text{kg/s}$, of which 40% (0.28 kg/s) is burned in the kiln and 60% (0.42 kg/s) goes into the pyroscrubber.

2. Coke fines are entrained into the pyroscrubber at the rate of 1.54kg/s.

3. All the other gas species feeding rates into the pyroscrubber follow the results given by report (Sean Zhang and Wang 2007).

Table 3.1 Kiln exit species composition summary from Zhang and Wang (2007)

species	mass fraction	mass flow rate(kg/s)	standard state enthalpy (J/kgmol)	energy released through complete combustion (J/kg-fuel)	total energy released(MW)
N_2	0.709	9.091	0	-	-
CH_4	0.000	0.000	-7.49E+07	-	-
C	0.001	0.017	-101.268	3.28E+07	0.554
H_20	0.075	0.964	-2.42E+08	-	-
CO_2	0.197	2.520	-3.94E+08	-	-
O_2	0.010	0.127	0	-	-
volatile	0.008	0.099	-5.60E+07	4.12E+07	4.100
total	1.000	12.818	-	-	4.654

Table 3.2 Energy release by complete combustion

fuel	energy released through complete combustion(kJ/kg fuel)	mass flow needed for 15MW power generation(kg/s)
C	3.28E+04	1.537
volatile	4.12E+04	1.224

Table 3.3 Inlet species composition summary for 3 cases

inlet species	mass flow(kg/s)	mass fraction	Stoichiometric air needed (kg/s)	80% air (kg/s)	150% air (kg/s)
N_2	9.070	0.622	0.000	same as inlet condition in stoichiometric case	
CH_4	0.000	0.000	0.000		
C	1.537	0.105	17.669		
H_20	1.154	0.079	0.000		
CO_2	2.159	0.148	0.000		
O_2	0.237	0.016	-1.021		
volatile	0.419	0.029	5.719		
total	14.577	0.999	22.366		
burner air injection	11.483	0.513	11.483	9.186	17.224
air injection-up	5.442	0.243	5.442	4.353	8.163
air-injection-down	5.442	0.243	5.442	4.353	8.163

The species composition and feeding rate at the main inlet, air injection tubes and burner slots are summarized in Table 3.3. The amount of stoichiometric air needed for each combustible fuel component (C and volatiles) is calculated and listed. The negative value associated with

O_2 indicates the amount of air which can be reduced due to oxygen contained in the incoming fuel. In the Other boundary conditions of different surfaces are listed as following:

1. Inlet temperature:
    a Main inlet gases: 500 K (440.33 °F).
    b Injection tubes air: 300 K (80.33 °F)
    c Burner slots air: 300 K (80.33 °F)
2. Pressure outlet -- The outlet is defined as the constant pressure outlet. The pressure, temperature, and species mass fraction of the mixture of the potential reverse flow are specified as follows:
    a. Gas outlet: Constant pressure outlet condition, P = 1 atm
    b. Temperature condition, T_{outlet} = 1000 K (1340.33 °F)
    c. Mass fraction:
        i. $O_2 = 0.23$
        ii. $N_2 = 0.77$
3. Wall -- The walls are treated as adiabatic with no-slip velocity condition:
    a. Adiabatic wall condition, heat flux = 0
    b. No slip condition at the walls, u = 0, v = 0, w = 0

3.4 Turbulence Model

The standard k - ε model is employed in this study to simulate the turbulent flow due to its suitability for a wide range of wall-bounded and free-shear flows. The standard k - ε model is the simplest of turbulence two-equation model in which the solution of two separate transport equation allows the turbulent velocity and length scales, to be independently determined. The k -

ε model is a semi-empirical model with several constants, which were obtained from experiments.

All the three k - ε models have similar forms with major differences in the method of calculating the turbulent viscosity: the turbulent Prandtl numbers and the generation and destruction terms in the k - ε equations.

The standard k - ε model is a semi-empirical model based on model transport equations for the turbulence kinetic energy (k) and its dissipation rate (ε). The model transport equation for (k) is derived from the exact equation; while the model transport equation for (ε) is obtained using physical reasoning and bears little resemblance to its mathematically exact counterpart.

The turbulence kinetic energy (k), and its rate of dissipation (ε), are obtained from the following transport equations:

$$\frac{\partial}{\partial t}(\rho k)+\frac{\partial}{\partial x_i}(\rho k u_i)=\frac{\partial}{\partial x_j}\left[\left(\mu+\frac{\mu_t}{\sigma_k}\right)\frac{\partial k}{\partial x_j}\right]+G_k+G_b-\rho\varepsilon-Y_M+S_k \qquad \text{(Eq.3.8)}$$

$$\frac{\partial}{\partial t}(\rho \varepsilon)+\frac{\partial}{\partial x_i}(\rho \varepsilon u_i)=\frac{\partial}{\partial x_j}\left[\left(\mu+\frac{\mu_t}{\sigma_\varepsilon}\right)\frac{\partial \varepsilon}{\partial x_j}\right]+C_{1\varepsilon}\frac{\varepsilon}{k}(G_k+C_{3\varepsilon}G_b)-C_{2\varepsilon}\rho\frac{\varepsilon^2}{k}+S_\varepsilon \qquad \text{(Eq.3.9)}$$

In these equations, G_k represents the generation of turbulence kinetic energy due to the mean velocity gradients and the Reynolds stress, calculated as

$$G_k=-\overline{\rho u_i' u_j'}\frac{\partial u_j}{\partial x_i} \qquad \text{(Eq.3.10)}$$

G_b represents the generation of turbulence kinetic energy due to buoyancy, calculated as

$$G_b=\beta g_i\frac{\mu_t}{Pr_t}\frac{\partial T}{\partial x_i} \qquad \text{(Eq.3.11)}$$

where Pr_t is the turbulent Prandtl number and g_i is the component of the gravitational vector in the i-th direction. For standard k - ε model the value for Pr_t is set to be 0.85 in this study.

β is the coefficient of thermal expansion and is given as

$$\beta = -\frac{1}{\rho}\left(\frac{\partial \rho}{\partial T}\right)_P \qquad \text{(Eq.3.12)}$$

Y_M represents the contribution of the fluctuating dilatation in compressible turbulence to the overall dissipation rate, and is given as

$$Y_M = 2\rho\varepsilon M_t^2 \qquad \text{(Eq.3.13)}$$

where M_t is the turbulent Mach number, given as

$$M_t = \sqrt{\frac{k}{a^2}} \qquad \text{(Eq.3.14)}$$

where $a = (\gamma RT)^{0.5}$ is the speed of sound.

The turbulent (or eddy) viscosity, μ_t, is computed by combining k and ε as

$$\mu_t = \rho C_\mu \frac{k^2}{\varepsilon} \qquad \text{(Eq.3.15)}$$

$C_{1\varepsilon}$, $C_{2\varepsilon}$, C_μ, σ_k and σ_t are constants and have the following values

$C_{1\varepsilon} = 1.44$, $C_{2\varepsilon} = 1.92$, $C_\mu = 0.09$, $\sigma_k = 1.0$, and $\sigma_t = 1.3$

These constant values have been determined from experiments using air and water for fundamental turbulent shear flows including homogeneous shear flows and decaying isotropic grid turbulence. They have been found to work fairly well for a wide range of wall- bounded and free-shear flows. The initial value for k and ε at the inlets and outlets are set as 1 m^2/s^2 and 1 m^2/s^3 respectively.

In general, turbulent flows are significantly affected by the presence of walls. Very close to the wall, viscous damping reduces the tangential velocity fluctuations. While kinematic blocking reduces the normal fluctuations, away from the wall, the turbulence is increased by the production of turbulence kinetic energy. In the near-wall region, the solution variables have large

gradients, and the momentum and other scalar transports occur strongly. Therefore, accurate representation of the flow in the near-wall region is required for successful predictions of wall-bounded turbulent flows.

The k - ε turbulence model used in this study is primarily valid for turbulent core flows (i.e., the flow in the regions somewhat far from walls). Wall functions are used to make this turbulence model suitable for wall-bounded flows. Wall functions are a collection of semi-empirical formulas and functions that link the solution variables at the near-wall cells and the corresponding quantities on the wall. The wall functions consist of the following:

1. Laws of the wall for mean velocity and temperature and other scalars
2. Equations for near-wall turbulent quantities.

The law-of-the-wall for mean velocity gives

$$U^+ = \frac{1}{\kappa}\ln\left(Ey^+\right) \qquad \text{(Eq.3.16)}$$

$$\text{where} \quad U^+ \equiv \frac{U_P C_\mu^{0.25} k_P^{0.5}}{\frac{\tau_w}{\rho}} \qquad \text{(Eq.3.17)}$$

$$y^+ \equiv \frac{\rho C_\mu^{0.25} k_P^{0.5} y_P}{\mu} \qquad \text{(Eq.3.18)}$$

κ = von Karman constant (= 0.42)

E = empirical constant (= 9.793)

U_P = mean velocity of the fluid at point P

k_P = turbulence kinetic energy at point P

y_P = distance from point P to the wall

μ= dynamic viscosity of the fluid

The logarithmic law for mean velocity is valid for y^+ > about 30 to 60

The law-of-the-wall for temperature is given

$$T^+ \equiv \frac{(T_w - T_P)\rho c_P C_\mu^{0.25} k_P^{0.5}}{q''} = Pry^+ + 0.5\rho.5\ \frac{C_\mu^{0.25} k_P^{0.5}}{q''} U_P^2 \qquad \left(y^+ < y_T^+\right) \qquad \text{(Eq.3.19)}$$

$$= Pr_t\left[\frac{1}{\kappa}\ln\left(Ey^+\right) + P\right] + 0.5\rho\frac{C_\mu^{0.25} k_P^{0.5}}{q''}\left[Pr_t\, U_P^2 + (Pr - Pr_t)U_c^2\right] \qquad \left(y^+ > y_T^+\right) \qquad \text{(Eq.3.20)}$$

where P is computed using the formula

$$P = 9.24\left[\left(\frac{Pr}{Pr_t}\right)^{3/4} - 1\right]\cdot\left[1 + 0.28e^{-0.007 Pr/Pr_t}\right] \qquad \text{(Eq.3.21)}$$

k_f = thermal conductivity of the fluid

ρ = density of fluid

c_P = specific heat of fluid

q" = wall heat flux

T_P = temperature at the cell adjacent to the wall

T_w = temperature at the wall

Pr = molecular Prandtl number ($\mu c_P / k_f$)

Pr_t = turbulent Prandtl number (= 0.85 at the wall)

A = 26 (van Driest constant)

κ = 0.4187 (von Karman constant)

E = 9.793 (wall function constant)

U_c = mean velocity magnitude at $y^+ = y^+_T$

For the k - ε turbulence model, wall adjacent cells are considered to solve the k-equation. The boundary condition for k imposed at the wall is $\partial k/\partial n = 0$, where "n" is the local coordinate normal to the wall. The production of kinetic energy, G_k, and its dissipation rate, ε, at the wall-adjacent cells, which are the source terms in k-equation, are computed on the basis of

equilibrium hypothesis with the assumption that production of k and its dissipation rate is assumed to be equal in the wall-adjacent control volume. The production of k and ε is computed as

$$G_k \approx \tau_w \frac{\partial U}{\partial y} = \tau_w \frac{\tau_w}{\kappa \rho C_\mu^{0.25} k_P^{0.5} y_P} \quad \text{(Eq.3.22)}$$

$$\varepsilon_P = \frac{C_\mu^{0.75} k_P^{1.5}}{\kappa y_P} \quad \text{(Eq.3.23)}$$

3.5 Combustion Model

In this study, two different models, gas combustion model and particle combustion model, are used to simulate the combustion process.. The key difference between these two models is related to how the carbon species is modeled. The gas combustion model treats carbon as gas, while particle combustion model treats carbon as solid particles. The two models focus on different aspects of the combustion processes and have their own advantages. The gas combustion model is simpler in mechanism, making it robust and less costly in computation; however, it is less accurate in describing the real physics. The gas combustion model focuses on the overall process and results. On the other hand, the particle combustion model provides a more accurate modeling of heterogeneous reaction by modeling the complex surface reaction, heat transfer, and species transport. Due to its complex dealing of random particle tracking and the heterogeneous combustion process, intensive computational power is expected.

Gas Combustion Model

In this approach, carbon is modeled as a gas species and the combustion of volatiles and carbon is modeled by a single-step reaction. The mixing and transport of chemical species is modeled by solving the conservation equations describing convection, diffusion, and reaction sources for each component species. The species transport equations are solved by predicting the

local mass fraction of each species, Yi, through the solution of a convection-diffusion equation for the i-th species. The species transport equation in general form is given as:

$$\frac{\partial}{\partial t}(\rho Y_i) + \nabla \bullet (\rho \vec{v} Y_i) = -\nabla \bullet \vec{J}_i + R_i + S_i \qquad \text{(Eq.3.24)}$$

where R_i is the net rate of production of species i by chemical reaction. S_i is the rate of creation (a source term) from the dispersed phase. $\vec{J}_i$ is the diffusion flux of species i, which arises due to concentration gradients. Mass diffusion for laminar flows is given as

$$\vec{J}_i = -\rho D_{i,m} \nabla Y_i \qquad \text{(Eq.3.25)}$$

For turbulent flows, mass diffusion flux is given as

$$\vec{J}_i = -\left(\rho D_{i,m} + \frac{\mu_t}{Sc_t} \right) \nabla Y_i \qquad \text{(Eq.3.26)}$$

where Sc_t is the turbulent Schmidt number given as $\mu_t / \rho D_t$, where μ_t is the turbulent viscosity and D_t is the turbulent diffusivity.

In this study, the reaction rate that appears as a source term in (Eq.3.23) is given by the turbulence-chemistry interaction model called the eddy-dissipation model. The overall rate of reaction for the fastest burning fuels is controlled by turbulent mixing. The net rate of production of species i due to reaction r, $R_{i,r}$, is given by the smaller of the two given expressions below:

$$R_{i.r} = \nu'_{i,r} M_{w,i} A \rho \frac{\varepsilon}{\kappa} \min_R \left(\frac{Y_R}{\nu'_{R,r} M_{w,R}} \right) \qquad \text{(Eq.3.27)}$$

$$R_{i.r} = \nu'_{i,r} M_{w,i} A B \rho \frac{\varepsilon}{\kappa} \frac{\sum_P Y_P}{\sum_j^N \nu''_{j,r} M_{w,j}} \qquad \text{(Eq.3.28)}$$

where Y_P is the mass fraction of any product species, P

Y_R is the mass fraction of a particular reactant, R

A is an empirical constant equal to 4.0

B is an empirical constant equal to 0.5

$\nu'_{i,r}$ is the stoichiometric coefficient for reactant i in reaction r

$\nu''_{j,r}$ is the stoichiometric coefficient for product j in reaction r

In the above equations (Eq.3.27) and (Eq.3.28), the chemical reaction rate is governed by the large-eddy mixing time scale, κ/ε, and an ignition source is not required. This is based on the assumption that the chemical reaction is much faster than the turbulence mixing time scale, so the actual chemical reaction is not important.

In this study, carbon (C) and volatile matters ($CH_{3.086}O_{0.131}$) is used as fuel for combustion. The composition of volatile matters is selected to give medium heating values at approximately 4.12×10^4 kJ/kg. The complete stoichiometric combustion equations are given below:

$$CH_{3.086}O_{0.131} + 1.706O_2 \rightarrow CO_2 + 1.543H_2O \quad \text{(Eq.3.29)}$$

$$C + O_2 \rightarrow CO_2 \quad \text{(Eq.3.30)}$$

Particle Combustion Model

In the particle combustion model, the combustion involves two different types of reaction: homogeneous reaction and heterogeneous combustion. The details of the two types of reactions are explained in detail below.

Homogeneous Reaction

Finite-Rate/Eddy-Dissipation model is used to simulate the homogeneous reactions. Reaction rate based on the Laminar Finite-Rate Model and Eddy-Dissipation Model are calculated and compared. The minimum of the two results is used as the homogeneous reaction rate.

Laminar Finite-Rate Model

The laminar finite-rate model computes the chemical source terms using Arrhenius expressions and ignores the effects of turbulent fluctuations. The net source of chemical species i due to reaction R_i (kg/m^3-s) is computed as the sum of the Arrhenius reaction sources over the N_R reactions that the species participate in, and is given as

$$R_i = M_{w,i} \sum_{r=1}^{N_R} \hat{R}_{i,r} \qquad \text{(Eq.3.31)}$$

where $M_{w,i}$ is the molecular weight of species i and $R_{i,r}$ is the Arrhenius molar rate of creation/destruction of species i in reaction r.

The r-th reaction can be written in a general form as

$$\sum_{i=1}^{N_R} \upsilon'_{i,r} M_i \underset{k_{b,r}}{\overset{k_{f,r}}{\Leftrightarrow}} \sum_{i=1}^{N} \upsilon''_{i,r} M_i \qquad \text{(Eq.3.32)}$$

where

N = number of chemical species in the system

$\upsilon'_{i,r}$ = stoichiometric coefficient for reactant i in reaction r

$\upsilon''_{i,r}$ = stoichiometric coefficient for product i in reaction r

M_i = symbol denoting species i

$k_{f,r}$ = forward rate constant for reaction r

$k_{b,r}$ = backward rate constant for reaction r.

The molar reaction of creation/destruction of species i in reaction r, which is $\hat{R}_{i,r}$ ($kgmol/m^3$-s) in equation (3.30), is given as

$$\hat{R}_{i,r} = \Gamma\left(\upsilon''_{i,r} - \upsilon'_{i,r}\right)\left(k_{f,r} \prod_{j=1}^{N_r} \left[C_{j,r}\right]^{\eta'_{j,r}} - k_{b,r} \prod_{j=1}^{N_r} \left[C_{j,r}\right]^{\eta''_{j,r}} \right) \qquad \text{(Eq.3.33)}$$

where

N_r = number of chemical species in reaction r

$C_{j,r}$ = molar concentration of each reactant and product species j in reaction r (kgmol/m^3)

$\eta'_{j,r}$ = forward rate exponent for each reactant and product species j in reaction r

$\eta''_{j,r}$ = backward rate exponent for each reactant and product species j in reaction r.

Γ represents the net effect of third bodies on the reaction rate and is given by

$$\Gamma = \sum_{j}^{N_r} \gamma_{j,r} C_j \qquad \text{(Eq.3.34)}$$

where $\gamma_{j,r}$ is the third body efficiency of the jth species in the rth reaction.

The forward rate constant for reaction r, $k_{f,r}$, is computed using the Arrhenius expression

$$k_{f,r} = A_r T^{\beta} e^{-E_r/RT} \qquad \text{(Eq.3.35)}$$

where

A_r = pre-exponential factor (consistent unit)

β_r = temperature exponent (dimensionless)

E_r = activation energy for the reaction (J/kgmol)

R = universal gas constant (J/kgmol-K).

If the reaction is reversible, the backward rate constant, $k_{b,r}$, is computed from the forward rate constant using relation below

$$k_{b,r} = \frac{k_{f,r}}{K_r} \qquad \text{(Eq.3.36)}$$

where K_r is the equilibrium constant for the r-th computed from

$$K_r = \exp\left(\frac{\Delta S_r^0}{R} - \frac{\Delta H_r^0}{RT}\right)\left(\frac{p_{atm}}{RT}\right)^{\sum_{r=1}^{N_R}\left(\upsilon''_{j,r} - \upsilon'_{j,r}\right)} \qquad \text{(Eq.3.37)}$$

where p_{atm} is the atmospheric pressure (101,325 Pa). The term within the exponential function represents the change in Gibbs free energy, and its components are computed as

$$\frac{\Delta S_r^0}{R} = \sum_{i=1}^{N}\left(\upsilon''_{i,r} - \upsilon'_{i,r}\right)\frac{S_i^0}{R} \qquad \text{(Eq.3.38)}$$

$$\frac{\Delta H_r^0}{RT} = \sum_{i=1}^{N} \left(\upsilon''_{i,r} - \upsilon'_{i,r}\right) \frac{h_i^0}{R} \qquad \text{(Eq.3.39)}$$

where S_i^0 and h_i^0 are the standard-state entropy and standard-state enthalpy (heat of formation), respectively.

Eddy Dissipation Model

Eddy dissipation model is the same as shown in gas combustion model. The governing equations are (Eqs.3.24-3.28).

The reason for taking the minimum reaction rate calculated from the eddy-dissipation model and finite rate model is that, in practice, the Arrhenius rate acts as a kinetic "switch", preventing reaction before the flame holder; once the flame is ignited, the eddy-dissipation rate is generally smaller than the Arrhenius rate, and reactions are mixing-limited.

In this study, the complete homogeneous reactions are:

$$CH_{3.086}O_{0.131} + 1.706O_2 \rightarrow CO_2 + 1.543H_2O \qquad \text{(Eq.3.40)}$$

$$2CO + O_2 \rightarrow 2CO_2 \qquad \text{(Eq.3.41)}$$

where in (Eq.3.41) CO come from the following carbon particle surface reactions:

$C + CO_2 \rightarrow 2CO$

$C + 0.5O_2 \rightarrow CO$

which are modeled as the heterogeneous reactions described below.

Heterogeneous Reaction

The particle reaction, R (kg/m^2-s), is expressed as

$$R = D_0(C_g - C_s) = R_c(C_s)^N \qquad \text{(Eq.3.42)}$$

Where

D_0 = bulk diffusion coefficient (m/s)

C_g = mean reacting gas species concentration in the bulk (kg/m^3)

C_s = mean reacting gas species concentration at the particle surface (kg/m^2)

R_c = chemical reaction rate coefficient (units vary)

N = apparent reaction order (dimensionless).

The concentration at the particle surface, C_s, is not known, so it is eliminated and the expression is recast as follows,

$$R = R_c \left[C_g - \frac{R}{D_0} \right]^N . \qquad \text{(Eq.3.43)}$$

This equation has to be solved by an iterative procedure, with the exception of the cases when N = 1 or N = 0. When N = 1, equation (Eq.3.43) can be written as

$$R = \frac{C_g R_c D_0}{D_0 + R_c} . \qquad \text{(Eq.3.44)}$$

In the cases of N = 0, if there is a finite concentration of reactant at the particle surface, the solid depletion rate is equal to the chemical reaction rate. If there is no reactant at the surface, the solid depletion rate changes abruptly to the diffusion-controlled rate.

The reaction stoichiometry of a particle undergoing an exothermic reaction in a gas phase is given as

particle species j (s) + gas phase species n $\rightarrow$ products.

Its reaction rate is given as

$$\overline{R}_{j,r} = A_p \eta_r Y_j R_{j,r} \qquad \text{(Eq.3.45)}$$

$$R_{j,r} = R_{kin,r} \left(p_n - \frac{R_{j,r}}{D_{0,r}} \right)^{N_r} \qquad \text{(Eq.3.46)}$$

where

$\overline{R}_{j,r}$ = rate of particle surface species depletion (kg/s)

A_p = particle surface area (m^2)

Y_j = mass fraction of surface species *j* in the particle

η_r = effectiveness factor (dimensionless)

$R_{j,r}$ = rate of particle surface species reaction per unit area (kg/m^2-s)

p_n = bulk partial pressure of the gas phase species (Pa)

$D_{0,r}$ = diffusion rate coefficient for reaction r

$R_{kin,r}$ = kinetic rate of reaction r (units vary)

N_r = apparent order of reaction r.

The effectiveness factor, r, is related to the surface area, and can be used in each reaction in the case of multiple reactions.

$D_{0,r}$ is given by

$$D_{0,r} = C_{1,r} \frac{\left[\left(T_p + T_\infty\right)/2\right]^{0.75}}{d_p} . \qquad \text{(Eq.3.47)}$$

Equation (Eq.3.47) is modification of relationship given by [Smith, 1982] by assuming negligible change in gas density.

The kinetic rate of reaction r is defined as

$$R_{kin,r} = A_p T^{\beta} e^{-(E_r/RT)} . \qquad \text{(Eq.3.48)}$$

The rate of particle surface species depletion for reaction order $N_r = 1$ is given by

$$\overline{R}_{j,r} = A_p \eta_r Y_j p_n \frac{R_{kin,r} D_{0,r}}{D_{0,r} + R_{kin,r}} . \qquad \text{(Eq.3.49)}$$

For reaction order $N_r = 0$,

$$\overline{R}_{j,r} = A_p \eta_r Y_j R_{kin,r} . \qquad \text{(Eq.3.50)}$$

In this study, two heterogeneous reactions are modeled and their reaction rates are:

1. $C + 0.5O_2 \rightarrow CO$

   Rate coefficient: R = T(A+BT)

   where A = -0.067T m/(s-K)

   B = 5.26x10^{-5} m/s-K^2.

The reaction rate is based on the work of Field [1968].

2. $C + CO_2 \rightarrow 2CO$

Rate coefficient: $R = AT^n(-E/RT)$

where $n = 1.0$

$A = -4.4$ m/s-K

$E = 1.62x10^{+8}$ J/kmol.

The reaction rate is based on the work of Mayers [1934]

3.6 Radiation Model

The P-1 radiation model is the simplest case of the more general PN radiation model that is based on the expansion of the radiation intensity I. The P-1 model requires only a little CPU demand and can easily be applied to various complicated geometries. It is suitable for applications where the optical thickness aL is large, where "a" is the absorption coefficient, and L is the length scale of the domain.

The heat sources or sinks due to radiation is calculated using the equation

$$-\nabla q_r = aG - 4aG\sigma T^4 \qquad \text{(Eq.3.51)}$$

where

$$q_r = -\frac{1}{3(a+\sigma_s) - C\sigma_s}\nabla G \qquad \text{(Eq.3.52)}$$

and q_r is the radiation heat flux, a is the absorption coefficient, σ_s is the scattering coefficient, G is the incident radiation, C is the linear-anisotropic phase function coefficient, and σ is the Stefan-Boltzmann constant.

The flux of the radiation, $q_{r,w}$, at walls caused by incident radiation G_w is given as

$$q_{r,w} = -\frac{4\pi\,\varepsilon_w \dfrac{\sigma T_w^4}{\pi} - (1-\rho_w)G_w}{2(1+\rho_w)} \qquad \text{(Eq.3.53)}$$

where ε_w is the emissivity and is defined as

$$\varepsilon_w = 1 - \rho_w \qquad \text{(Eq.3.54)}$$

and ρ_w is the wall reflectivity.

3.6 NO_x Emission Model

NOx emission consists of mostly nitric oxide (NO). Less significant are nitrogen oxide, NO_2 and nitrous oxide (N_2O). To predict NO_x emission, transport equations for nitric oxide (NO) concentration are solved. With fuel NO_x sources, an additional transport equation for an intermediate species (HCN or NH_3) are solved. Since NO_x concentrations generated in a combustion system are generally low, NO_x chemistry has negligible influence on the predicted flow fields and species concentrations. Therefore, the calculation of NO_x concentrations can be post-processed after the thermal flow and major species concentrations are computed.

The NO_x transport equations are solved based on a given flow field and combustion solution. NO_x is post processed from a combustion simulation, thus an accurate combustion solution becomes a prerequisite of NO_x production. For example, thermal NO_x production doubles for every 90 K temperature increase when the flame temperature is about 2200 K. Accurate prediction of NO_x parametric trends can cut down on the number of laboratory tests, allow more design variations to be studied, shorten the design cycle, and reduce product development cost.

In laminar flames and at the molecular level within turbulent flames, the formation of NO_x can be attributed to four distinct chemical kinetic processes: thermal NO_x formation, prompt

NO_x formation, fuel NO_x formation, and reburning. Thermal NO_x is formed by the oxidation of atmospheric nitrogen present in the combustion air. Prompt NO_x is produced by high-speed reactions at the flame front, and fuel NO_x is produced by oxidation of nitrogen contained in the fuel. The reburning mechanism reduces the total NO_x formation by accounting for the reaction of NO with hydrocarbons.

The mass transport equation for the NO species is solved taking into account convection, diffusion, production and consumption of NO and related species. The effect of residence time in NO_x mechanisms, a Lagrangian reference frame concept, is included through the convection terms in the governing equations written in the Eulerian reference frame. For thermal and prompt NO_x mechanisms, only the NO species transport equation is needed and is given as

$$\frac{\partial}{\partial t}(\rho Y_{NO}) + \nabla \cdot (\rho \vec{v} Y_{NO}) = \nabla \cdot (\rho D \nabla Y_{NO}) + S_{NO} \qquad \text{(Eq.3.55)}$$

Thermal NOx

The formation of thermal mechanism dominates in high-temperature combustion over a fairly wide range of equivalence ratios. The formation of thermal NO_x is determined by a set of highly temperature-dependent chemical reactions known as the extended Zeldovich mechanism described

$$O + N_2 \underset{k_1 r}{\overset{k_1 f}{\Leftrightarrow}} NO + N \qquad \text{(Eq.3.56)}$$

$$N + O_2 \underset{k_2 r}{\overset{k_2 f}{\Leftrightarrow}} NO + O \qquad \text{(Eq.3.57)}$$

$$N + OH \underset{k_{3r}}{\overset{k_{3f}}{\Leftrightarrow}} NO + H \qquad \text{(Eq.3.58)}$$

The net rate of formation of NO via extended Zeldovich mechanism reactions described above from equations (E.q.3.56) to (E.q.3.58) is given by

$$d[NO] / dt = K_{1f}[O][N_2] + K_{2f}[N][O_2] + K_{3f}[N][OH] - K_{1r}[NO][N] - K_{2r}[NO][O] - K_{3r}[NO][H] \qquad \text{(Eq.3.59)}$$

where all concentrations have units of gmol/m^3.

To calculate the formation rates of NO and N, the concentrations of O, H, OH are required. The rate constants for these reactions have been measured in numerous experimental studies. The expressions for the rate coefficients for above reactions are:

$$K_{1f} = 1.8*10^{11} \exp [-38{,}370/T\,(K)] \quad m^3 / kmol\text{-}s, \qquad \text{(Eq.3.60)}$$

$$K_{1r} = 3.8*10^{10} \exp[-425/T\,(K)] \quad m^3 / kmol\text{-}s, \qquad \text{(Eq.3.61)}$$

$$K_{2f} = 1.8*10^{7} \exp [-4{,}680/T\,(K)] \quad m^3 / kmol\text{-}s, \qquad \text{(Eq.3.62)}$$

$$K_{2r} = 3.8*10^{6} \exp[-20{,}820/T\,(K)] \quad m^3 / kmol\text{-}s, \qquad \text{(Eq.3.63)}$$

$$K_{3f} = 7.1*10^{10} \exp [-450/T\,(K)] \quad m^3 / kmol\text{-}s, \qquad \text{(Eq.3.64)}$$

$$K_{3r} = 1.7*10^{11} \exp[-24{,}560/T\,(K)] \quad m^3 / kmol\text{-}s \qquad \text{(Eq.3.65)}$$

where K_{1f} is forward reaction rate for reaction 1 and K_{1r} is the backward reaction rate for reaction 1 and in a similar manner for reactions 2 and 3.

The rate of formation of NO_x is significant only at high temperatures because fixation of nitrogen requires the breaking of the strong N_2 triple bond. A quasi-steady state can be established for a fuel-lean flame, where the rate of consumption of free nitrogen atoms becomes equal to the rate of its formation. This assumption is valid for most combustion cases except in

extremely fuel-rich combustion conditions. In a quasi-steady state, the NO formation rate is predicted by the following equation:

$$\frac{d[NO]}{dt} = 2k_1[O][N_2]\frac{\left(1 - \frac{k_{-1}k_{-2}[NO^2]}{k_1[N_2]k_2[O_2]}\right)}{\left(1 + \frac{k_{-1}[NO]}{k_2[O_2] + k_3[OH]}\right)} \quad \text{(Eq.3.66)}$$

where the sub-scripts negative is for backward reaction, and positive is for forward reaction and the number (1,2,3) stands for the reaction number in the Zeldovich mechanism (Eqs.3.56, 3.57, and 3.58).

From the above equation, it is clear that the rate of formation of NO will increase with increasing oxygen concentration. The O-atom concentration is calculated by the equations given below

- For the equilibrium assumption
- $[O]=3.97 * 10^5 T^{-1/2} [O_2]^{1/2} \exp(-31090/T)$ (Eq.3.67)
- For a partial equilibrium assumption

$$[O]=36.64\, T^{1/2} [O_2]^{1/2} \exp(-27123/T) \quad \text{(Eq.3.68)}$$

- Using the local O_2-species mass fraction.

The source term due to thermal NO_x formation in equation (3.55) is calculated as

$$S_{thermal,NO} = M_{w,NO}\frac{d[NO]}{dt} \quad \text{(Eq.3.69)}$$

where $M_{w, NO}$ is the molecular weight of NO, and $\frac{d[NO]}{dt}$ is computed from Equation (Eq.3.66).

Prompt NO_x

During combustion of hydrocarbon fuels, the NO_x formation rate can exceed the rate produced from direct oxidation of nitrogen molecules (i.e., thermal NOx). Prompt NO_x can be formed in a significant quantity in some combustion environments, such as in low-temperature, fuel-rich conditions and where residence times are short. Surface burners, staged combustion systems, and gas turbines can create such conditions.

The formation of prompt NO_x is governed by a set of equations known as Fenimore mechanism given below:

$$CH + N_2 \Leftrightarrow HCN + N \quad \text{(Eq.3.70)}$$

$$C + N_2 \Leftrightarrow CN + N \quad \text{(Eq.3.71)}$$

$$N + O_2 \Leftrightarrow NO + O \quad \text{(Eq.3.72)}$$

$$HCN + OH \Leftrightarrow CN + H_2O \quad \text{(Eq.3.73)}$$

$$N + OH \Leftrightarrow NO + H \quad \text{(Eq.3.74)}$$

The scheme of Fenimore mechanism is that hydrocarbon radicals react with molecular nitrogen to form amines or cyano compounds. The amines and cyano compounds are then converted to inverted compounds that ultimately form NO.

In prompt NO_x mechanism, reaction (E.q.3.70) is of primary importance. The majority of the NO_x at the flame base is prompt NO_x formed by the CH reaction; the prompt NO_x formation rate is given as

$$\frac{d[NO]}{dt} = k_0[CH]\cdot[N_2] \qquad \text{(Eq.3.75)}$$

The prediction of prompt NO_x formation within the flame requires coupling of the NO_x kinetics to an actual hydrocarbon combustion mechanism. Hydrocarbon combustion mechanisms involve many steps, and as mentioned previously, are extremely complex and costly to compute. The rate for most hydrocarbon is given as

$$d[NO]/dt = f\, k'_{pr}\, [O_2]^a\, [N_2]\, [FUEL]\, \exp(-E_a'/RT) \qquad \text{(Eq.3.76)}$$

where "a" is the oxygen reaction order, R is the universal gas constant.

$k_{pr} = 1.2 \times 10^7\, (RT/p)^{a+1}$ and

$E_a = 60$ kcal/gmol

The source term due to prompt NO_x mechanism in equation (E.q.3.55) is given as

$$S_{prompt,NO} = M_{w,NO}\, \frac{d[NO]}{dt} \qquad \text{(Eq.3.77)}$$

where $M_{w,NO}$ is the molecular weight of NO, and $\frac{d[NO]}{dt}$ is computed from Equation (E.q.3.76).

In the above equation (E.q.3.76), f is a correction factor and given as

$$f = 4.75 + 0.0819\,n - 23.2\phi + 32\phi^2 - 12.2\phi^3 \qquad \text{(Eq.3.78)}$$

where n is the number of carbon atoms per molecule for the hydrocarbon fuel, and ϕ is the equivalence ratio that is defined as

ϕ = (Actual air-fuel ratio) / (stoichiometric air-fuel ratio)

CHAPTER FOUR

RESULTS AND DISCUSSIONS

In this study, a total of eight cases using two different models are conducted.

- Gas combustion model:

  Case 1. Baseline case two-stage combustion (100% stoichiometric air distributed as 51% and 49%)

  Case 2. 80% stoichiometric air combustion (for both stages.)

  Case 3. 150% stoichiometric air combustion (for both stages.)

  Case 4. Three-stage combustion (100% stoichiometric air distributed as 41%, 39% and 20%)

  Cases 5-7. Bottom doors opening cases (three cases)

  - Case 5: 100% air injection -- all bottom doors open
  - Case 6: 100% air injection, --partial bottom doors open
  - Case 7: no air injection -- all bottom doors open

- Particle combustion model

  Case 8: 100% stoichiometric air combustion, all bottom doors closed.

Case 1: Baseline Case

To verify the validity of the computational results, the baseline case employs 100% stoichiometric air combustion based on the inlet conditions discussed in Chapter Three. The computed temperature will be compared with the actual measurement during operation at three

locations: center of the high bay, center of the low bay, and center of the exit duct. Also, the computed NO_x emissions will be compared with the plant operating data.

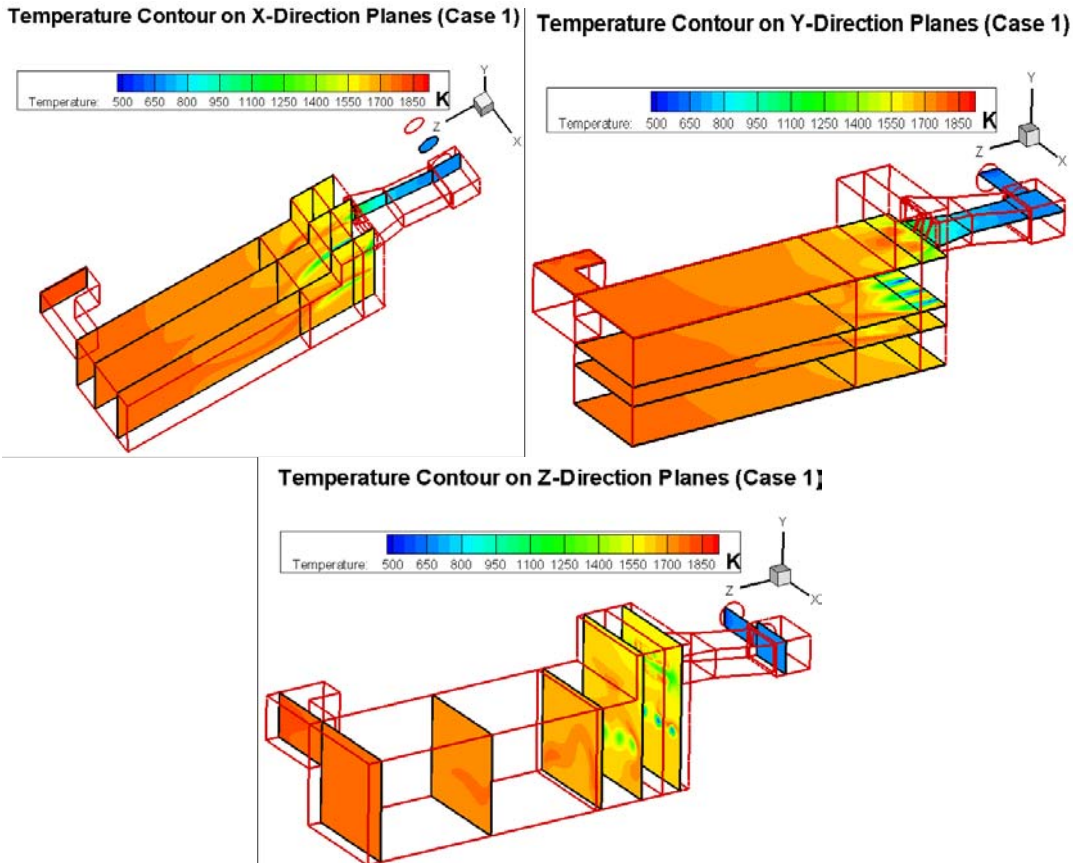

Baseline Case (100% stoichiometric air)

Figure 4.1 Temperature contours inside the pyroscrubber at different planes for the baseline case (100% stoichiometric air)

The 3-D results provide a clear view of flow field and temperature distribution in the pyroscrubber. Temperature contours of different planes are shown in Fig 4.1. Three groups of planes are shown in the direction of X (horizontal), Y (vertical), and Z (main flow direction in the chamber) respectively. Velocity profiles of different planes in X, Y, Z directions are shown

in Figs. 4.3, 4.4, and 4.5 respectively. Figures 4.6, 4.7 and 4.8 present species concentrations and temperature distributions in X, Y, Z directions.

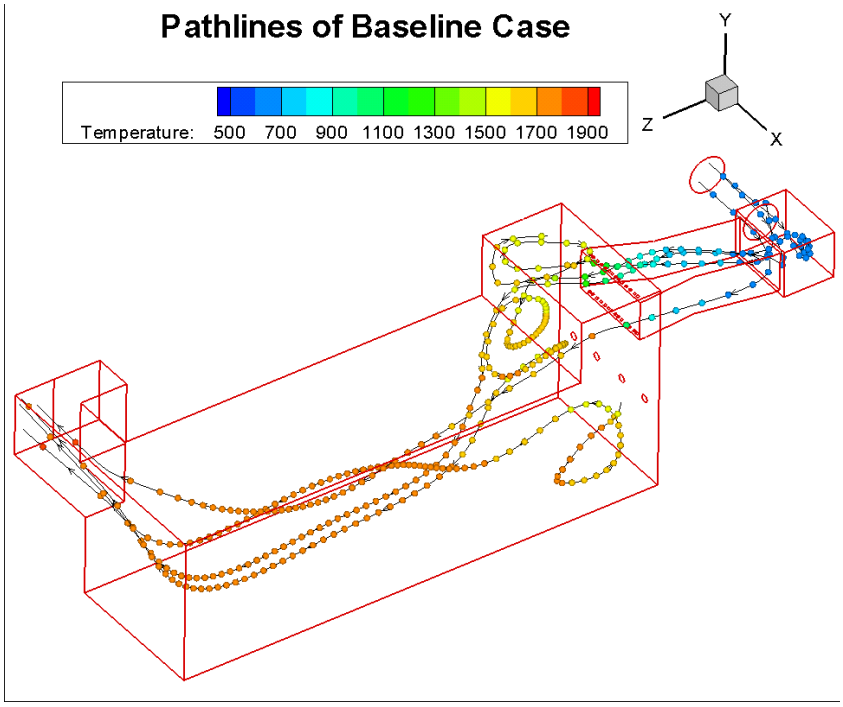

Figure 4.2 Representative pathlines for the baseline case (100% stoichiometric air)

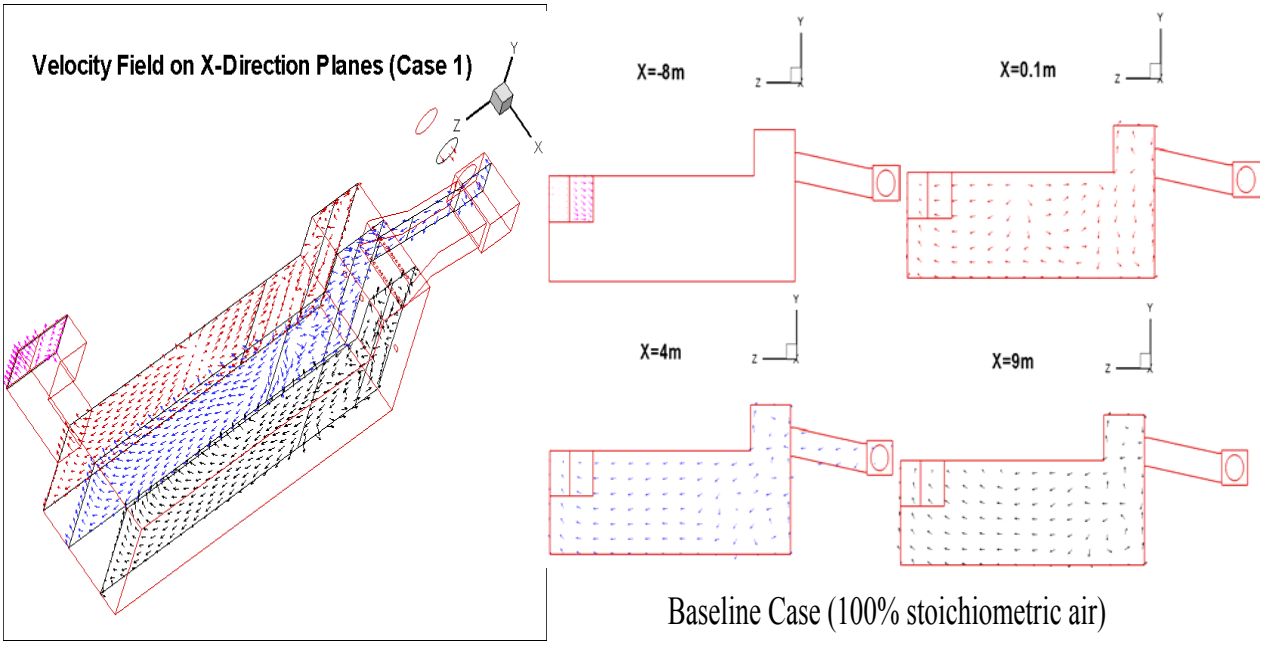

Figure 4.3 Velocity field on X-direction planes for the baseline case (100% stoichiometric air)

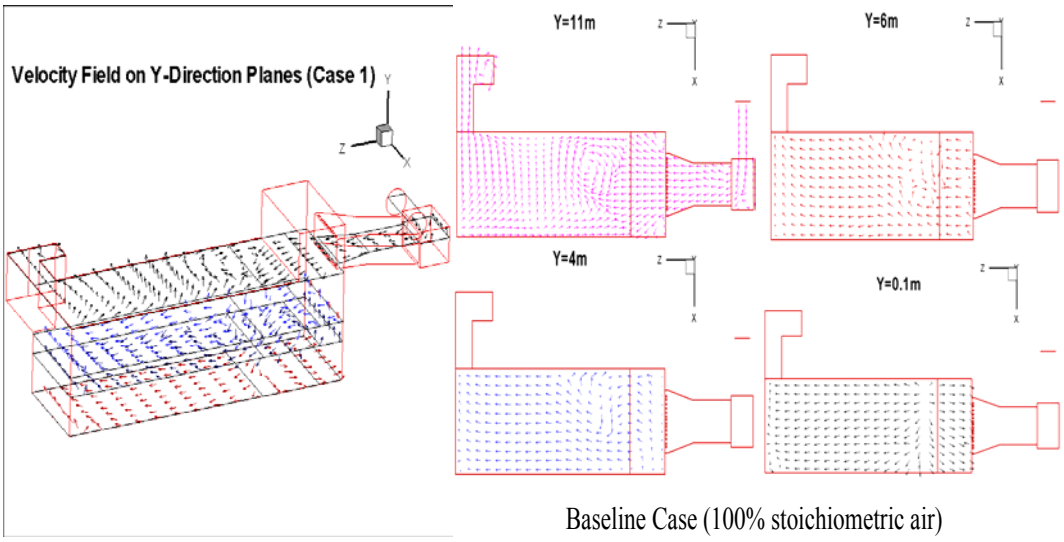

Figure 4.4 Velocity field on Y-direction planes for the baseline case (100% stoichiometric air)

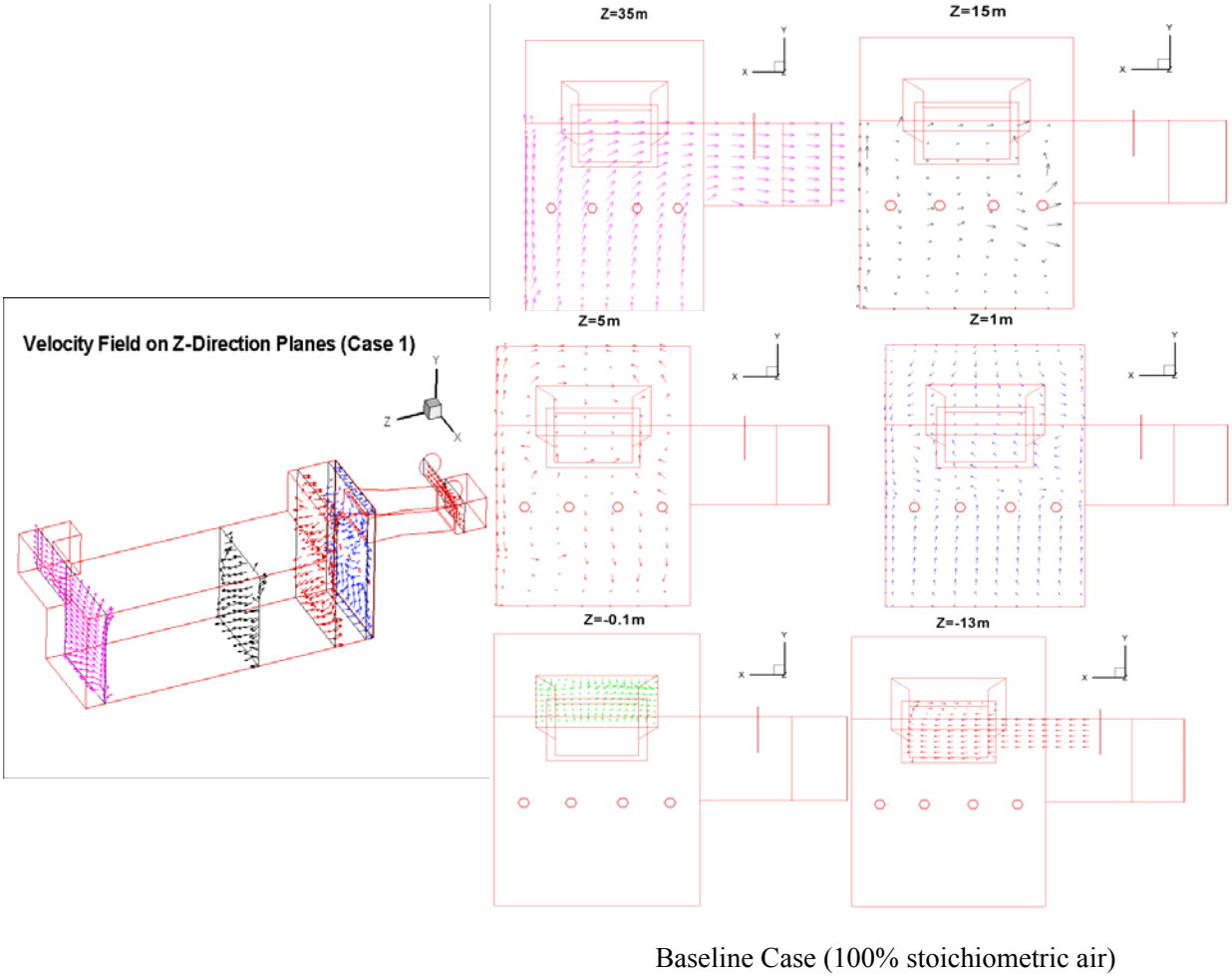

Figure 4.5 Velocity field on Z-direction planes for the baseline case (100% stoichiometric air)

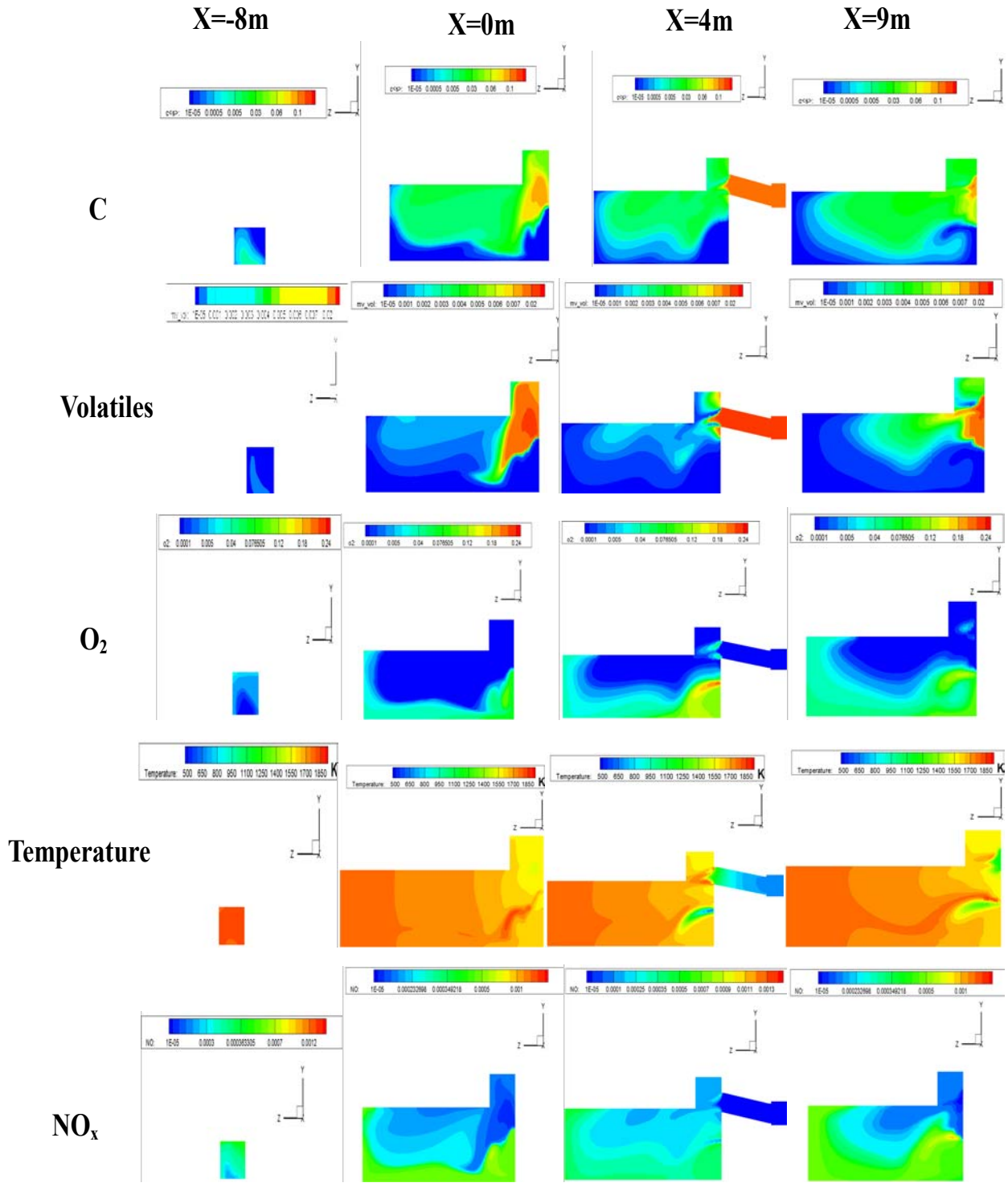

Figure 4.6 Species and temperature contour plots on X-direction planes.

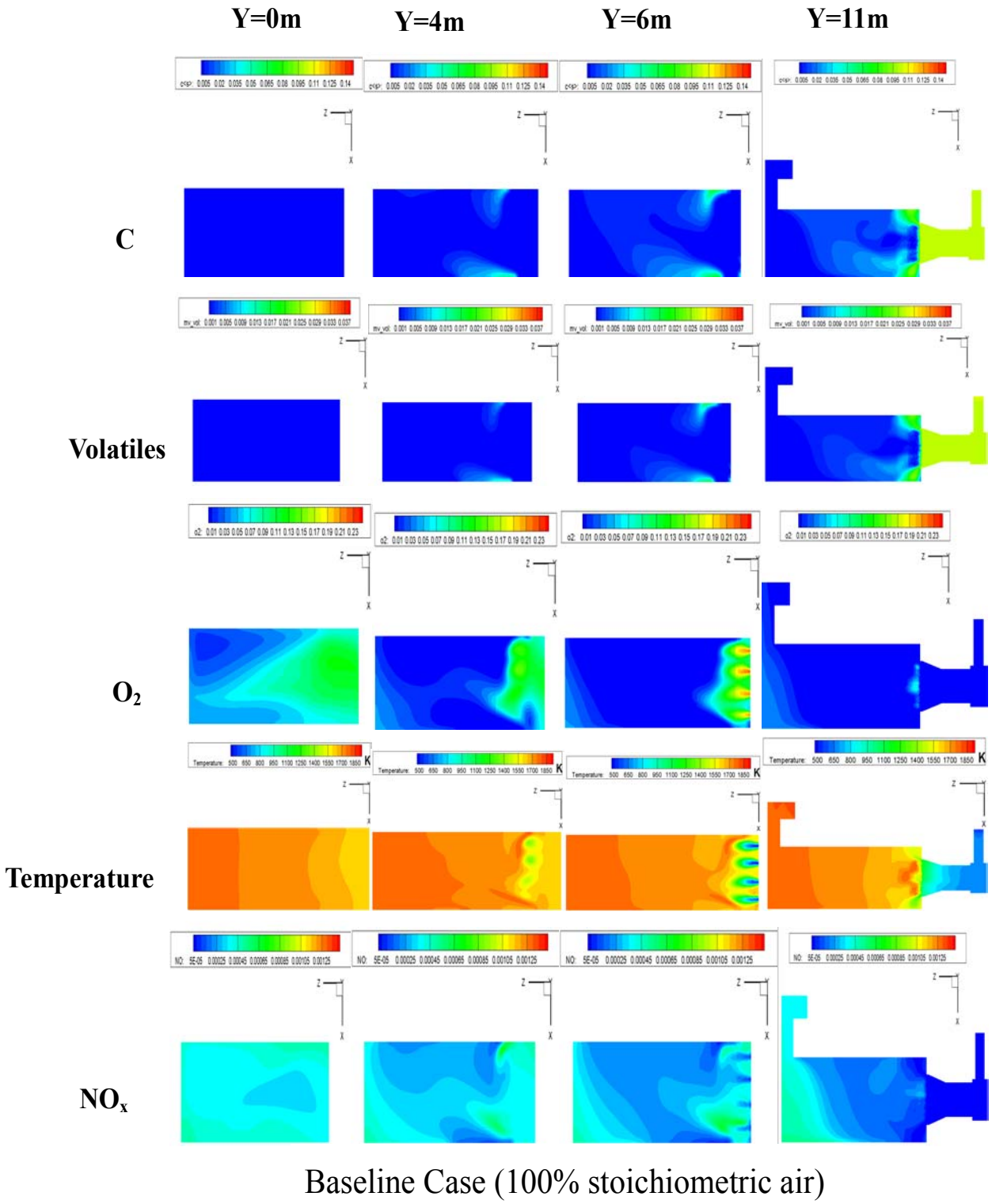

Figure 4.7 Species and temperature contour plots on Y-direction planes.

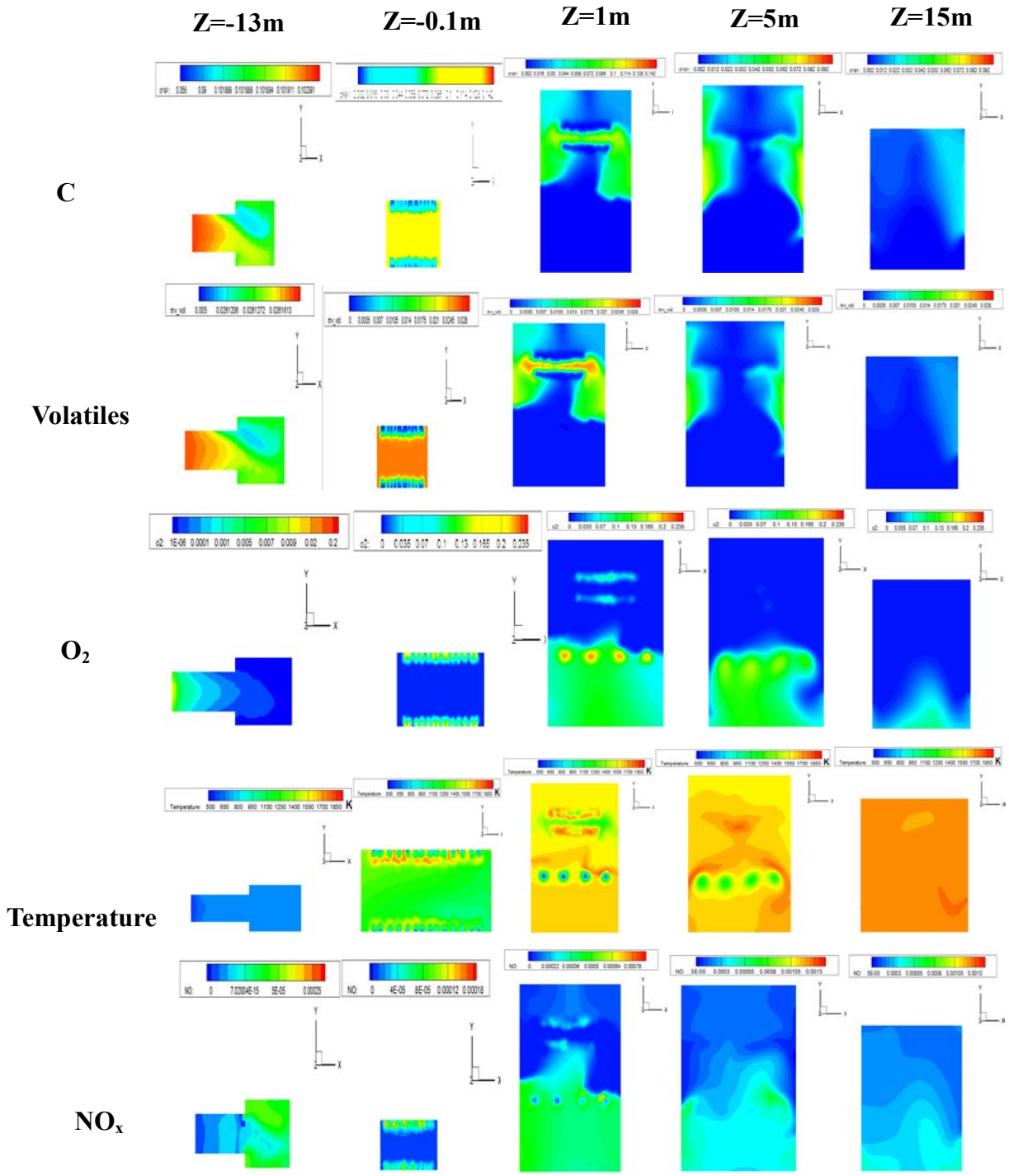

Baseline Case (100% stoichiometric air)

Figure 4.8 Species and temperature contour plots on Z-direction planes

There are three flow streams coming into the main chamber: the first stream comes from the kiln through the inlet duct carrying all the fuels (carbon dusts and volatiles); the second stream is air injected from 28 injection tubes surrounding the high-bay duct for mixing enhancement, and the third air stream comes from the burners at the east wall of the main chamber. The burners supply natural gas fuel during start-up and only provide air during normal operation. The air injection distribution generates two different combustion situations. In the high bay area, the fuel is well mixed with a less-than-stoichiometric amount of air before the combustion starts. The combustion pattern is characterized as pre-mixed and fuel rich. Almost all the volatiles are burned in the high bay area. In the low bay area, air is injected into the chamber and interacts with the leftover fuel (mostly carbon dusts) from the top, generating the non-premixed and oxygen rich diffusion type combustion.

Cold air injection from burners can be easily noticed from the blue color. Hot streaks can be clearly identified through X-direction slices in Fig. 4.1 following the air injection from the burners and the air injection tubes. This can be explained by the following physical process: the fuel (mostly carbon) from the top inlet duct, which is mixed with the air from the air injection tubes, is first partially burned in the high-bay area generating the hot streaks of high-temperature combustion gases; then the remaining fuel, together with the hot combustion gas flow, is directed into the low-bay area to continue to combust with a new supply of the oxygen-rich air flow blown in from the burners. The cold streaks in low-bay area actually show the trace of air flows from the burners. As the combustion intensity decreases along with the air flow moving towards the outlet, mixing effect makes temperature more uniform as shown in temperature contour plots on the Y-direction planes. The function of the high bay wall structure and the distributed second air injection strategy are interesting and will be further examined. From the distributions of

velocity field, species concentration and temperature, observations, and analyses are noted below:

- The high-bay wall blocks the inlet flow from directly shooting into the main chamber and slows down the flow in the high bay. Recirculation zones are generated in the high-bay area, which can be seen in Figs. 4.2, 4.3 and 4.4. Thus the high-bay structure literally slows down the flow velocity, stabilizes the combustion with flow recirculation, and extends the fuel residence time. All of these characteristics help in achieving complete combustion.
- Correspondingly, as shown in Fig 4.6, most of the volatiles are combusted in the high bay area, producing high-temperature gases with the highest temperature around 1850 K (2870 ^{o}F).
- For carbon, its combustion also starts and intensifies in the high-bay area. But different from the volatiles combustion, carbon reaction is slower and extends throughout the main chamber. The current length of the pyroscrubber seems necessary to achieve complete carbon combustion.
- The high-bay wall structure forces the flow from the inlet duct to redirect downward to intersect the second air injection from the burners, creating a strong forced mixing of the partially combusted gas from the top and the fresh air from the burners, thus makes combustion to take place and generates those hot streaks. This effect of forcing combustion to happen at an earlier stage helps to efficiently utilize the main chamber space and avoid using an otherwise bigger main chamber.
- Together with the distributed air injections, the high-bay and low-bay configuration generates a two-stage combustion with 51% stoichiometric air at the first stage in the

high-bay area and 49% air at the second stage in the low-bay area, which yields a lower flame temperature than an otherwise one-stage combustion, and thus less NO_x emission. The details of the two-stage combustion will be discussed in the three-stage combustion case (Case 4)

- In the actual operating condition, volatiles are first to be combusted due to their gas phase rather than the carbon particles in solid phase. The combustion in the high-bay area generates high-temperature gases which heat up the carbon particles. This will speed up the combustion process of the carbon particles and reduce the carbon particle sizes and numbers and allow the smaller carbon particles to remain air borne and prevent more particles from being pulled by gravity to the bottom of the chamber.
- NO_x concentration is generally higher on the bottom of the main chamber than in the upper area, which can be clearly seen from Figs. 4.6 and 4.8. It is noticed that NO_x concentration is consistent with O_2 species distribution. Some scattered high concentration spots of NO_x are also found as hot spots or streaks in Figures. 4.7 and 4.8. This phenomenon can be explained by the two necessary conditions of NOx generation: high temperature and sufficient O_2. High NO_x generation rate only happens at places in accordance with these two conditions.
- Flow goes through the outlet duct at a relatively uniform temperature at about 1500 K.

The combustion performance is evaluated and compared at the exit of the pyroscrubber. Together with the inlet conditions, a summary of the exit conditions are shown in Table 1

including the species mass fractions, mass-weighted average temperature, and exergy (useable energy). From Table 4.1, the following information is noticed:

- Volatiles are fully combusted inside the main chamber.
- Small amounts of both carbon and oxygen are left in the exit gases.
- The exit gases mostly consist of N_2 (71%), CO_2 (24%) and water vapor (5%).

Table 4.1: Simulated results of the baseline case

100% stoichiometric air	main inlet mass flow rate(kg/s)	burner mass flow rate(kg/s)	air injection mass flow rate(kg/s)	outlet mass flow rate(kg/s)	outlet mass fraction
NO_x	0.00E+00	0.00E+00	0.00E+00	1.20E-02	3.24E-04 (321.49 ppm)
Volatiles	0.42	0.00	0.00	0.00	0.00
O_2	0.24	2.66	2.52	0.11	0.00
CO_2	2.16	0.00	0.00	8.73	0.24
H_2O	1.15	0.00	0.00	1.83	0.05
C(s)	1.53	0.00	0.00	0.03	0.00
N_2	9.08	8.82	8.36	26.25	0.71
total	14.58	11.48	10.88	36.95	1.00
Exit Temp	1804K (2788°F)	Exergy (Useful Energy)	57.17MW		

Case 2: 80% Stoichiometric Air Combustion

To find out the effect of less than stoichiometric air injection on the pyroscrubber's combustion performance, 80% stoichiometric air combustion case is simulated with eddy-dissipation model. Temperature and species distribution, flow velocity field, NO_x emission information, and exergy of combusted gases will be evaluated, and comparisons are to be made with the baseline case.

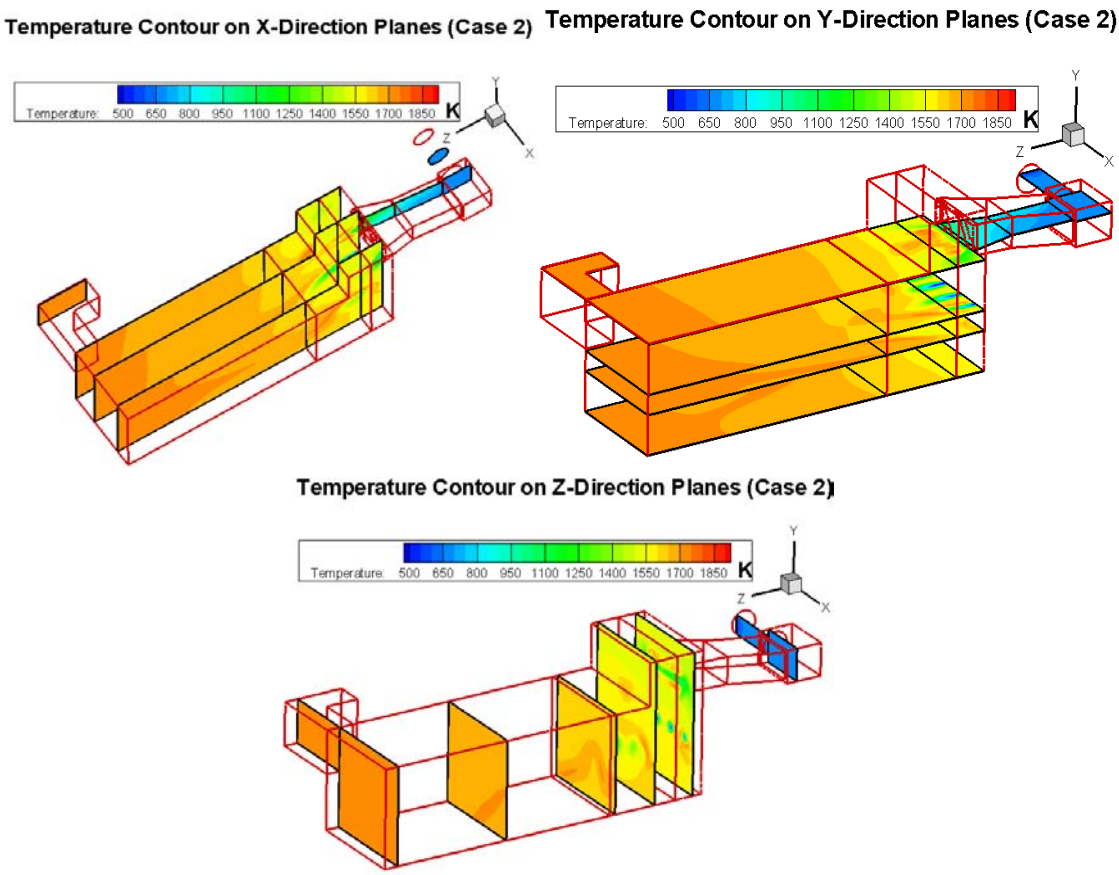

80% stoichiometric air combustion

Figure 4.9 Temperature contour inside the pyroscrubber for different planes for 80% stoichiometric air combustion

Temperature contours of different planes in X, Y and Z directions are shown in Fig 4.9. It can be immediately noticed that the overall temperature is lower than the baseline case. This is expected due to the incompleteness of the fuel combustion and correspondingly less energy being released inside the main chamber. Hot streaks can still be seen but with decreased temperature from the baseline case. The temperature distribution pattern is very similar to the baseline case.

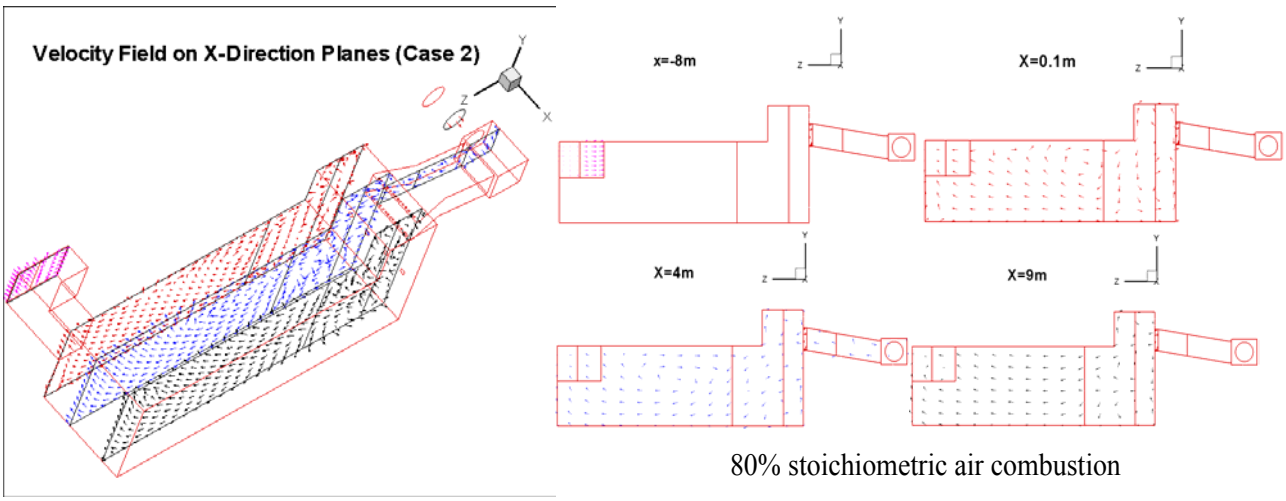

Figure 4.10 Velocity plots on X-direction planes for 80% stoichiometric air combustion

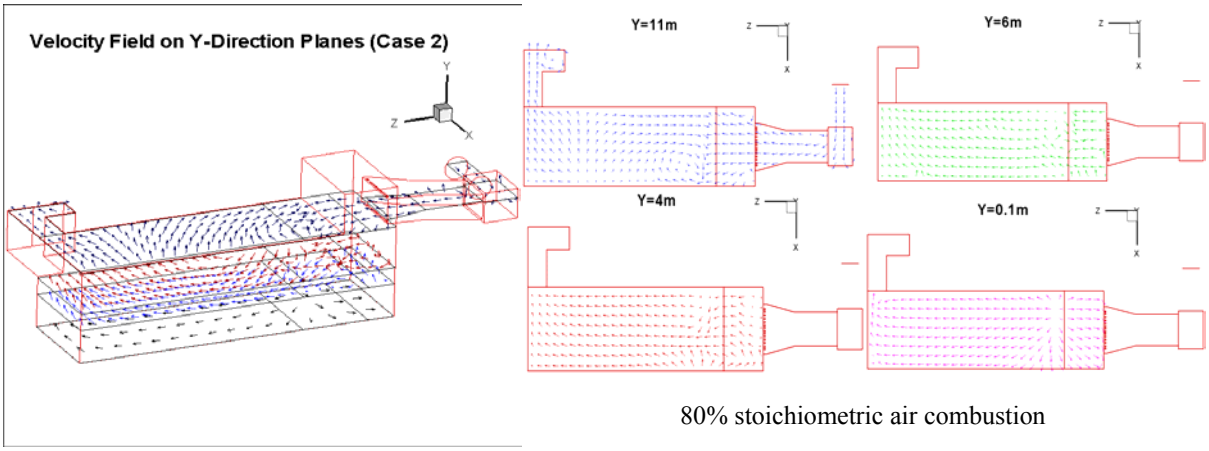

Figure 4.11 Velocity plots on Y-direction planes for 80% stoichiometric air combustion

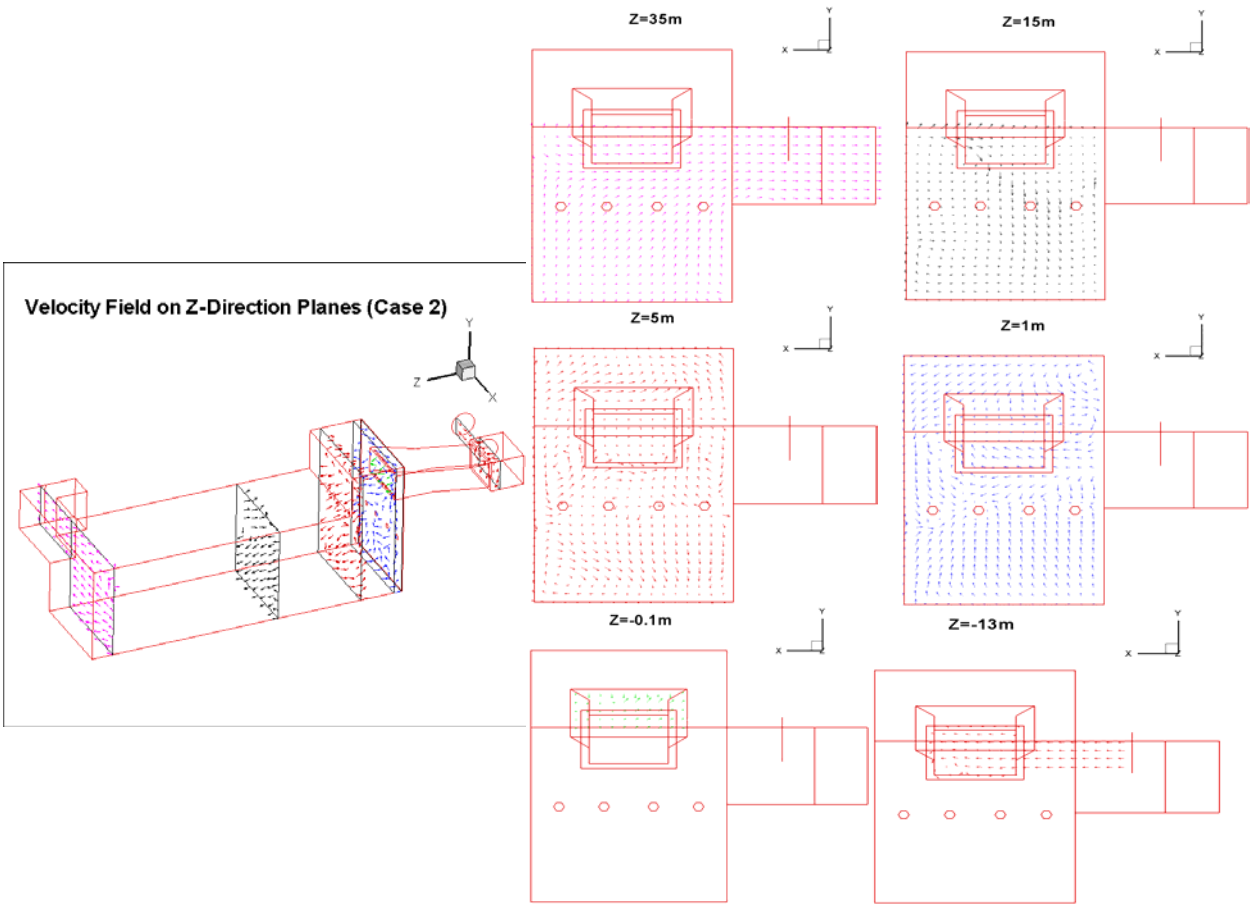

Figure 4.12 Velocity plots on Z-direction planes for 80% stoichiometric air combustion

Different planes of velocity fields are shown in Figs.4.10, 4.11 and 4.12 respectively. Similar to Case 1, swirls and flow recirculation zones are observed in the high-bay and low-bay areas due to the specific high-bay wall structure and the air injection arrangements. Between Z=15m and Z=35m, flow is more uniform compared with the high-bay and low-bay areas.

The inlet conditions and the simulated results of Case 2 with mass weighted species and temperature at the exit are shown in Table 4.2. The results show that:

- Most of the volatiles (88%) are combusted in the main chamber.

- All oxygen is consumed inside the pyroscrubber, which is consistent with the 80% stoichiometric air injection rate (fuel rich).
- 21% of the carbon is not burned.
- The mass-averaged outlet flow temperature is about 100K lower than the baseline case (100% stoichiometric air).
- NO_x emission is greatly reduced to 8.3% of the baseline case. This can be explained as a result of two main reasons: 1) lower combustion temperature, 2) less oxygen. Oxygen is mostly consumed by the fuel (volatiles and carbon) and results in a reduction of NO_x generation. Also, less fuel is combusted resulting in lower combustion temperature, which is another favorable factor to reduce NO_x generation.
- Total exergy is reduced to 83% of the baseline case.

Conclusions of Case 2

- In term of NO_x emission control, the pyroscrubber performance is very good at 80% stoichiometric air injection condition with an order of magnitude reduction of NO_x.
- One major drawback of sub-stoichiometric combustion is the losses of fuel and exergy, which will affect electricity production of the steam power plant.
- 80% air running condition yields lower exit gas temperature, which will result in lower boiler and steam turbine efficiency. Thus less electricity is to be produced.
- CO emission is a concern with the 80% stoichiometric air combustion condition due to reduced combustion temperature and the fuel-rich combustion pattern. No simulation of CO production is performed in gas combustion model, but it will be discussed in the heterogeneous combustion model in Case 8.

- Overall, incomplete combustion at sub-stoichiometric air combustion case is not a favorable running condition for the pyroscrubber. It is necessary to generate a complete combustion condition to utilize all the energy from the fuel.

Table 4.2: Simulated results of 80% stoichiometric air combustion case

80% stoichiometric air	main inlet mass flow rate(kg/s)	burner mass flow rate(kg/s)	air injection mass flow rate(kg/s)	outlet mass flow rate(kg/s)	outlet mass fraction
NO_x	0.00E+00	0.00E+00	0.00E+00	1.00E-03	3.02E-05(29.37 ppm)
Volatiles	0.42	0.00	0.00	0.05	0.00
O_2	0.24	2.13	2.02	0.00	0.00
CO_2	2.16	0.00	0.00	7.53	0.23
H_2O	1.15	0.00	0.00	1.76	0.05
C(s)	1.53	0.00	0.00	0.32	0.01
N_2	9.08	7.06	6.69	22.81	0.71
total	14.58	9.19	8.71	32.47	1.00
Exit Temp	1726K (2647 ^oF)	Exergy (Useful Energy)	47.32MW		

Case 3: 150% Stoichiometric Air Combustion

As an 80% stoichiometric air combustion case is studied as the lower limit of the incomplete combustion running condition of the pyroscrubber, 150% air combustion case is studied as the higher limit of excess air combustion condition. From the discussion of 80% air combustion (Case 2), it is concluded that all fuel must be combusted to fully utilize the fuel's energy and in the meantime the combusted temperature needs to be reduced to decrease NO_x formation. With the 150% stoichiometric air, this goal is expected to be achieved, although it is understood that the energy density could be reduced.

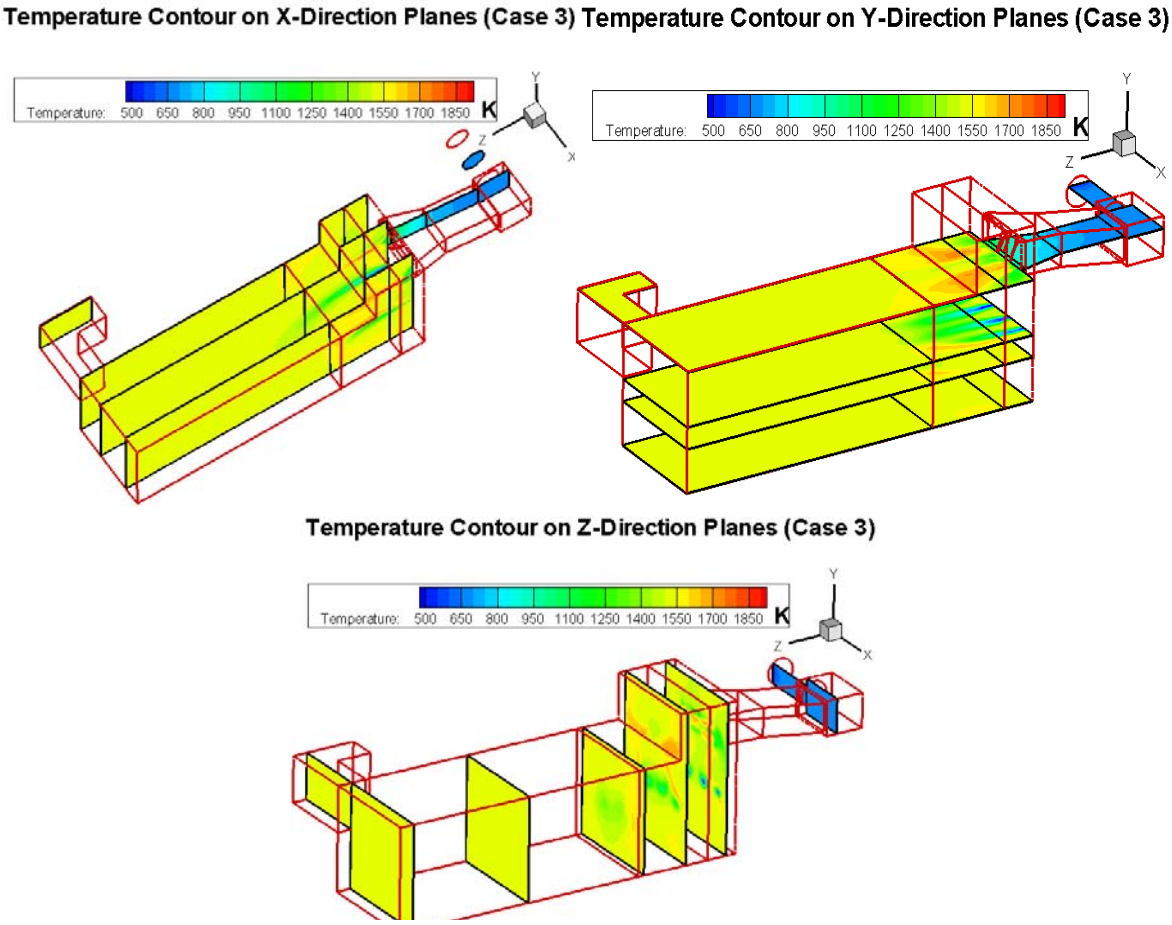

Figure 4.13 Case 3 temperature contour inside the pyroscrubber for different planes for 150% stoichiometric air combustion.

Temperature contour plots for different planes are shown in Fig 4.13, and the velocity plots are shown in Fig 4.14, 4.15 and 4.16. The results indicate:

- The overall combustion temperature is lower than both the baseline case (Case 1) and the 80% stoichiometric combustion case (Case 2).

- Hot streaks can still be identified; but are much weaker, i.e. with smaller volumes and lower temperatures, than in Cases 1 and 2. Temperature distribution in the main chamber is more uniform than both of Cases 1 and 2. This can be explained by the following reasons:

    1) The combustion is less intensive due to diluting effect of the excess air. With more air, the species concentration of fuels is reduced, and thus generates slower reaction rates.

    2) Stronger mixing effect can be found from Figs 4.14, 4.15 and 4.16. Larger amounts of air injected from tubes and burner slot produces higher air speed and stronger mixing effect than in Cases 1 and 2.

- Two visible recirculation zones can be seen from Fig 4.14. One is at the high-bay area, where the flow from the inlet duct impinging to the high-bay walls generates the recirculation zone. The other one is close to the burner slots where burner air injection intersects the gas flow bending down from the top. The strengths of both recirculations are stronger than in Cases 1 and 2.

- From Fig 4.15, at Y=0.1m close to the bottom of the main chamber, flow is found to be separated into two streams in the 2-D plot, indicating the existence of a stagnation region. This is the result of the flow bending down from the top impinging to the bottom floor. Comparing with the velocity profiles of the baseline case and 80% air combustion case, it is noticed that the location of flow separation has moved downstream due to stronger flow injection of the 150% air combustion case.

- At Z=15m, the velocity profile is very different from both Cases 1 and 2. Recirculation can still be clearly identified at this location for the 150% air case, suggesting a much stronger mixing compared with Cases 1 and 2.
- At Z=35m, recirculation zones disappear and the flow becomes more uniform, similar to the baseline case and 80% air case.

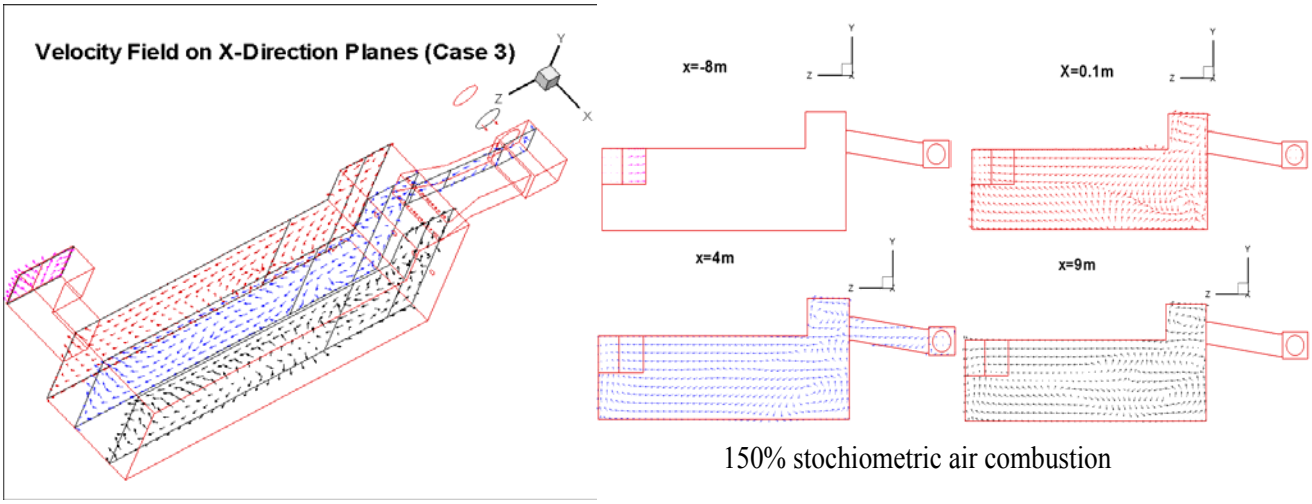

Figure 4.14 Velocity plots on X-direction planes for 150% stoichiometric air combustion

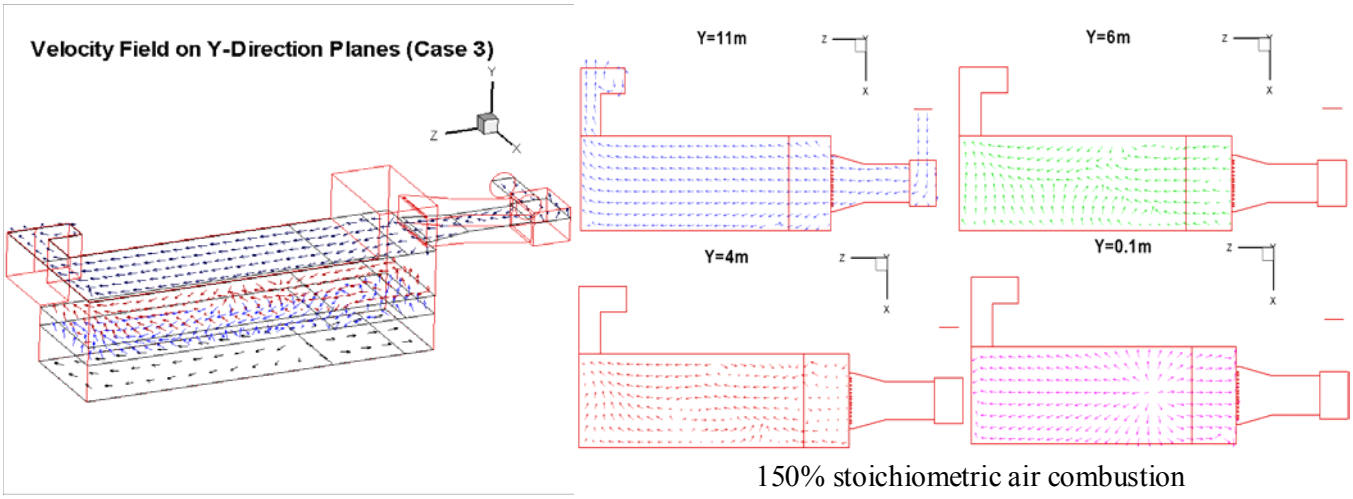

Figure 4.15 Velocity plots on Y-direction planes for 150% stoichiometric air combustion

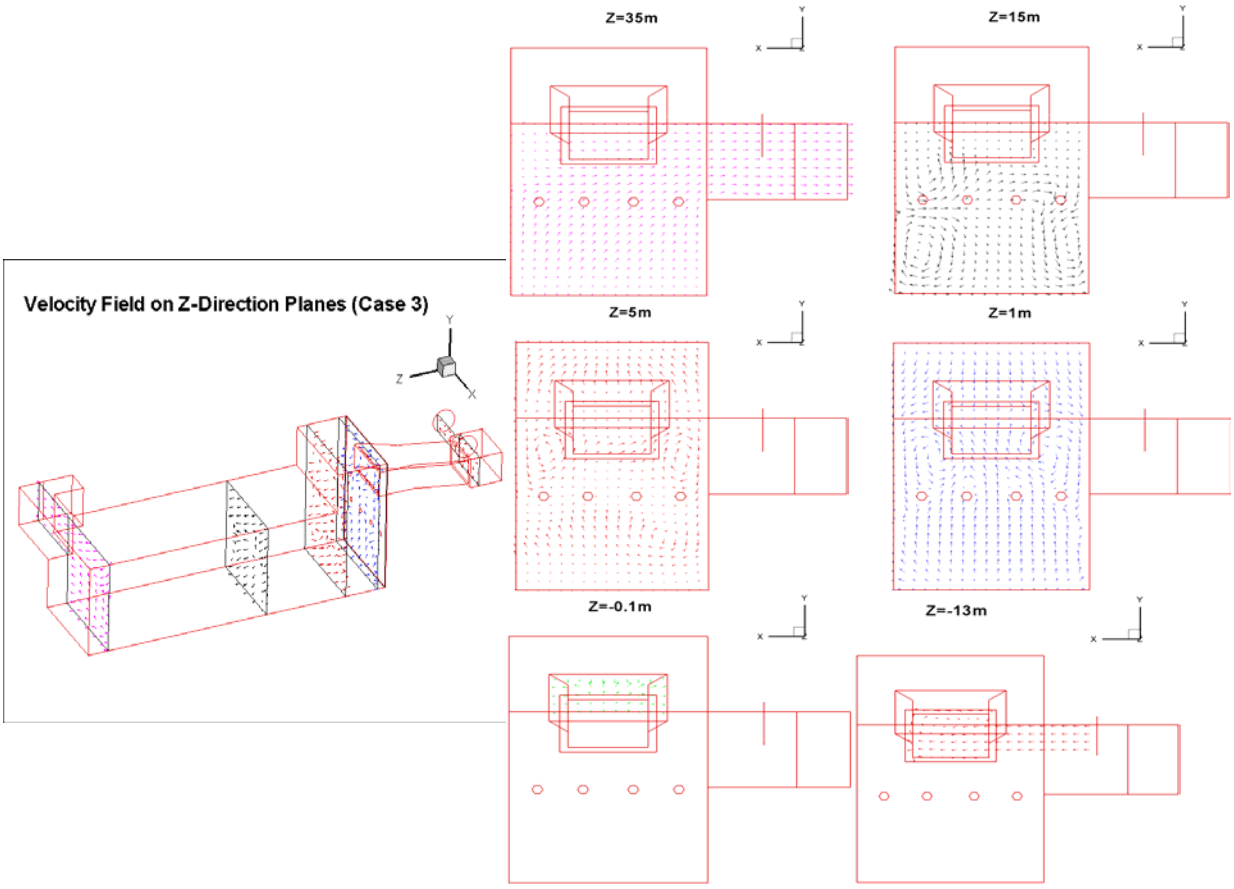

150% stoichiometric air combustion

Figure 4.16 Velocity plots on Z-direction planes for 150% stoichiometric air combustion

The inlet condition and the simulated results at exit are tabulated in Table 4.3. The results show that:

- All the volatiles and carbon are burned inside the pyroscrubber, which is expected for combustion with a large amount of excess air.
- Much lower outflow temperature is found (281K and 203K lower than 100% and 80% air combustion respectively), indicating that cold excess air cools down the combustion gas.

- NO_x emission is significantly reduced to 3.3% of the baseline case and 25% of the 80% stoichiometric combustion case in term of mass fraction. The lower emission value based on mass fraction could be misleading because the mass fraction is diluted by the excessive air mass. So, a more meaningful method is to compare the mass flow rates of the emissions (kg/s), which shows the mass flow rate of NO_x of the 150% case is 3.3% of Case 1 and 40% of Case 2 values, respectively. The result shows that even though there is more oxygen in 150% air combustion case, the reduced combustion temperature seems to effectively cut down the NO_x emission.
- The total exergy is s about the same as the baseline case due to the complete combustion.

Table 4.3: Simulated results of 150% stoichiometric air combustion case (Case 3)

150% stoichiometric air	main inlet mass flow rate(kg/s)	burner mass flow rate(kg/s)	air injection mass flow rate(kg/s)	outlet mass flow rate(kg/s)	outlet mass fraction
NO_x	0.00E+00	0.00E+00	0.00E+00	4.00E-04	7.56E-06(7.45 ppm)
Volatiles	0.42	0.00	0.00	0.00	0.00
O_2	0.24	4.00	3.79	2.64	0.05
CO_2	2.16	0.00	0.00	8.82	0.18
H_2O	1.15	0.00	0.00	1.83	0.04
C(s)	1.53	0.00	0.00	0.00	0.00
N_2	9.08	13.22	12.54	34.84	0.73
total	14.58	17.22	16.33	48.13	1.00
Exit Temp	1523K (2282 ^oF)	Exergy (Useful Energy)	56.17 MW		

Conclusions of Case 3:

- In terms of NO_x emission control, the pyroscrubber performance is best with 150% stoichiometric air. It gives the lowest NO_x emission in either mass fraction or mass flow rate.
- The major draw-back of 150% air running condition is the much lower output gas temperature. When the outflow gas is used in boiler, it will decrease the overall efficiency of the power generation system.
- Overall, Case 3 undergoes a complete combustion that harvests full energy from the fuel. Excess air cools down the combusted gas temperature and significantly cuts down NO_x emission. Balance between these two effects need to be made to obtain the optimum pyroscrubber performance.

Case 4: Three Stage Combustion (41%, 39% and 20%)

Based on the results and discussions from the baseline case, two limiting cases of incomplete combustion (80% stoichiometric air) and excess-air combustion (150% stoichiometric air), a new burning strategy by distributing air injection into three stages is studied. In addition to the existing two-stage combustion of Case 2 in the high-bay and low-bay regions, an additional 20% stoichiometric air is injected through the side doors in the outlet duct walls to burn off all the fuel. The theory of employing the three-stage combustion is to cut down the NO_x emission by distributing the third air injection much further downstream to reduce the flame temperature in the early stage of combustion. The reason for choosing the third stage in the outlet duct is because the main chamber of the pyroscrubber is too spacious to achieve uniform combustion with localized air injection, whereas it is thought that it will be easier to achieve uniform combustion in the outlet duct since the flow converges into much smaller space in the outlet duct. (The latter reasoning is later found not holding as wished.) Meanwhile the exit temperature will not be compromised such as in Cases 2 or 3.

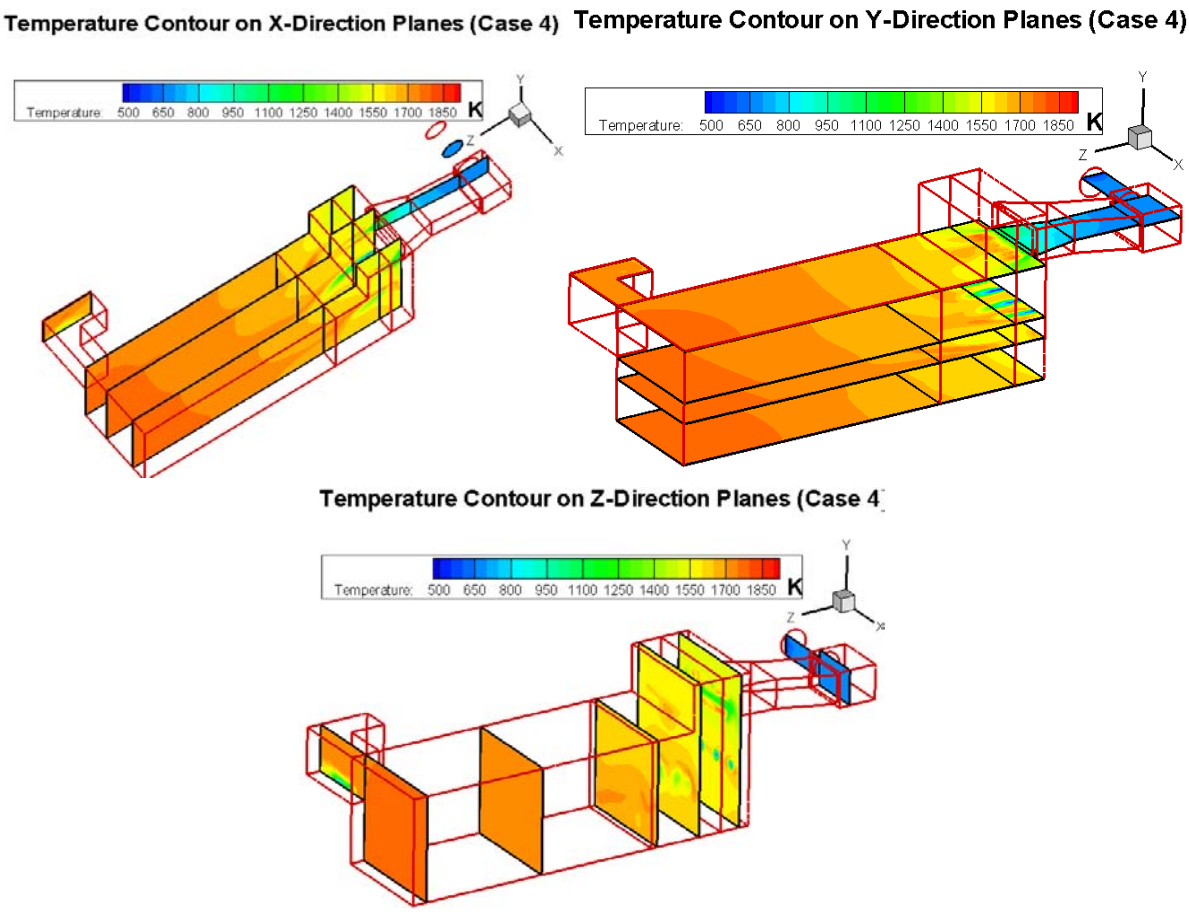

Three stage combustion (41%, 39% and 20%)

Figure 4.17 Case 4 temperature contour inside the pyroscrubber for different planes with three-stage combustion (41%, 39% and 20%)

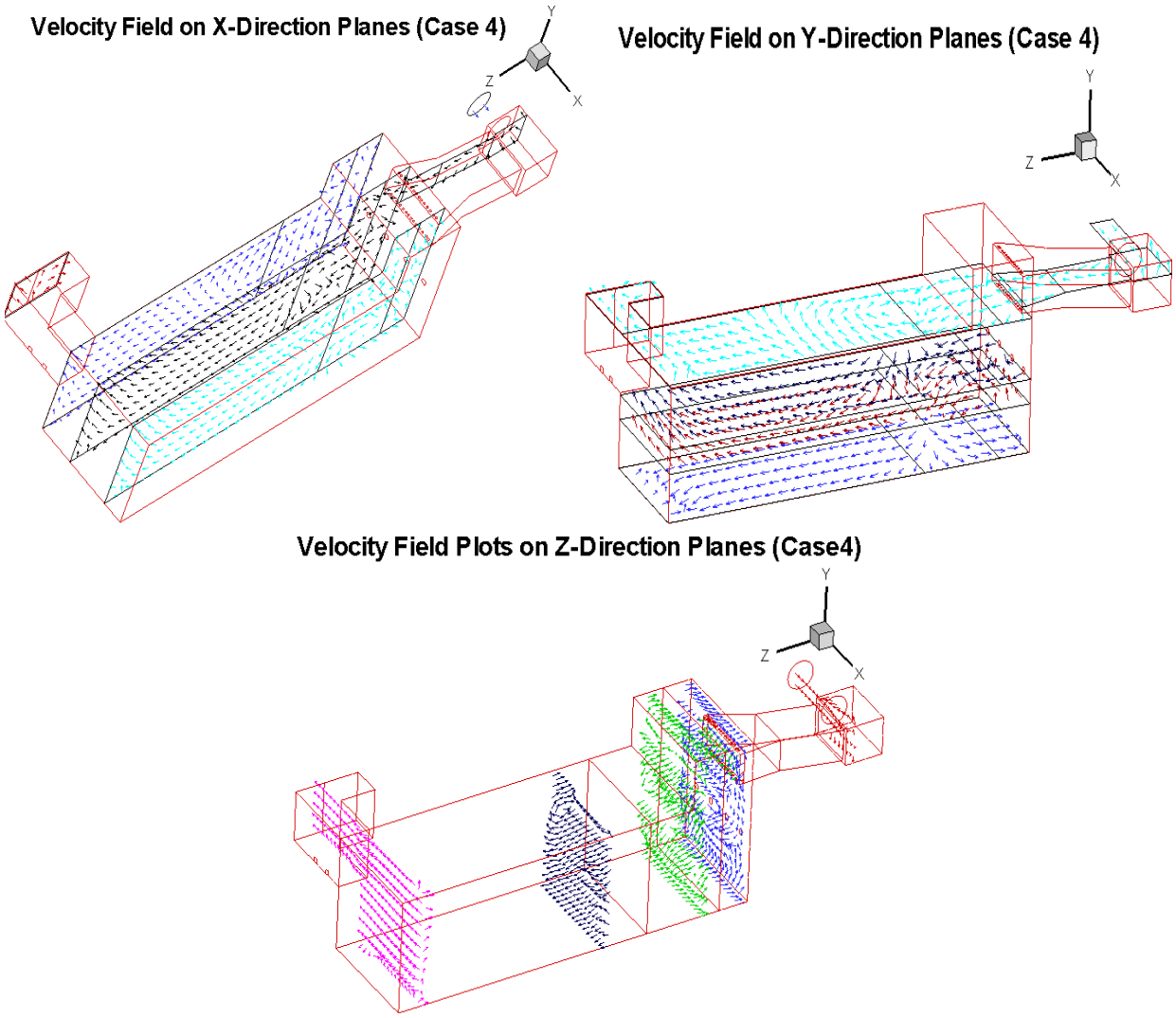

Figure 4.18 Velocity profiles for three-stage combustion in Case 5.

Figures 4.17 and 4.18 show the temperature contour plots and velocity field for the three-stage combustion case (Case 4). The inlet conditions and the results at exit are shown in Table 4.4. The results show:

- As expected, the temperature profiles are very similar to 80% case in regions of inlet duct and the main chamber. The difference occurs in the region close to the third

stage air injection in the outlet duct where the temperature distribution is relatively non-uniform

- The fuels are not completely combusted as there is carbon left in the outlet species as shown in Table 4.3. 5% of the volatiles, and 12% of the carbon are left unburned in the outflow gas.
- Outflow temperature is 100K lower than the baseline case and close to 80% case, but is higher (200k) than the 150% case. This can be explained as that despite the fact more fuel is burned in the three-stage burning case and more energy is released into the gas than Case 2 of 80% air, the combustion is not complete in the third stage, perhaps due to the short residence time inside the outlet duct. Furthermore, introduction of cold air at this late stage cools down the gas. These two factors counteract each other and thus the temperature is about the same as 80% air case (Case 2).
- NO_x emission is cut down to 15.8% of the baseline case, but is 190% higher than the 80% air case (Case 2) and 475% higher than the 150% air case (Case 3).
- The exit exergy is slightly below the baseline case (91%) and 150% air case (93%), but is higher than 80% air case (110%).

Table 4.4 Simulated Case 5 results of three-stage burning case

three-stage combustion (41%, 39% and 20%)	main inlet mass flow rate(kg/s)	burner mass flow rate(kg/s)	air injection mass flow rate(kg/s)	near-exit air injection	outlet mass flow rate(kg/s)	outlet mass fraction
NO_x	0.00E+00	0.00E+00	0.00E+00	0.00E+00	1.90E-03	5.24E-04 (51.36 ppm)
Volatiles	0.42	0.00	0.00	0.00	0.02	0.0005
O_2	0.24	2.13	2.02	1.04	0.72	0.02
CO_2	2.16	0.00	0.00	0.00	8.01	0.22
H_2O	1.15	0.00	0.00	0.00	1.79	0.05
C(s)	1.53	0.00	0.00	0.00	0.19	0.01
N_2	9.08	7.06	6.69	3.44	26.21	0.70
total	14.58	9.19	8.71	4.47	36.94	1.00
Exit Temp	1702K (2604 ^oF)	Exergy (Useful Energy)	52.20 MW			

Conclusions of Case 4:

- For NO_x emission control, the three-stage burning strategy can successfully cut down the emission in comparison with the baseline case.
- Although the NO_x emission of the three-stage burning case is higher than 80% case and 150% case, Case 5 doesn't have the drawbacks of either compromised exergy in the 80% air case or reduced exit temperature in the 150% air case.
- It should be noted that the current 41%, 39% and 20% composition of air injection load is not the optimized air distribution, as can be seen from Table 4.4 that carbon species still exists in the outflow, meaning the fuel is not completely burned under the simulated three-stage air distribution. Further studies will be needed to optimize the multi-stage combustion strategy.
- The existing doors on the side walls of the outlet duct are used for convenience in the third stage air injection. Since the locations of the doors are close to the exit and the space inside the outlet duct is relatively small, two issues are encountered 1) The duct is not long enough to provide sufficient residence time to achieve complete

combustion before the flow exits; 2) Due to the short residence time, the combustion takes place locally without sufficient time to propagate through the entire duct and hence, hot spots form and NO_x emission increases. Further studies are needed to improve the selection of third-stage air injection and the air injection pattern.

Bottom Doors Opening Cases

Bottom doors opening cases are designed to simulate the effect of opening the ventilation doors on the bottom of the pyroscrubber. In this case, natural air is expected to be drafted into the pyroscrubber, thus offering the possibility of saving a portion of air-blowers' power. The locations of the bottom doors are shown in Fig 4.19. Each door sizes at 10 ft x 10 ft.

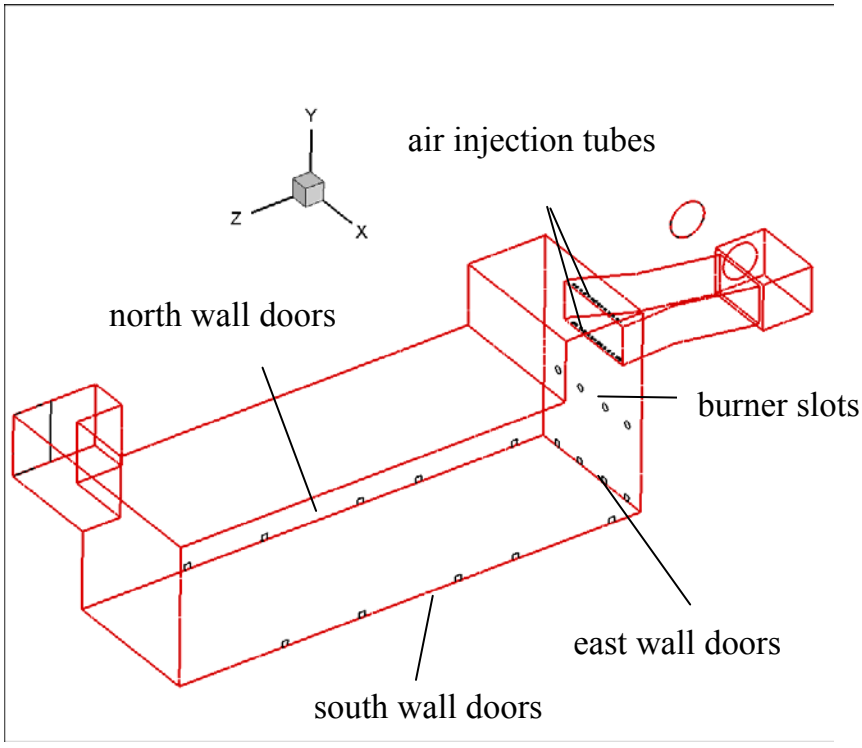

Figure 4.19 Locations for bottom doors, air injections tubes, and burner slots.

Three cases are investigated with open bottom doors:

- Case 5 - All doors open plus 100% air. In this case, all the bottom doors are completely open, and the air is also blown in through injectors at 100% stoichiometric condition.
- Case 6 - Doors partially open plus 100% air. All doors on south and north walls are closed and only the doors on east wall are open. Air injection is at 100% stoichiometric condition.
- Case 7 - All doors open with no air injection. All the air injections from air injection tubes and burner slots are closed, while all the bottom doors are open.

Figure 4.20 shows the wall temperature contours of the three cases involving natural air draft. It is noticed for all three cases that a large amount of ambient air is entrained (sucked) into the chamber by the buoyancy force of the rising hot combusted gas. Combustion is clearly shown being restrained on the upper region of the main chamber. Bottom of the chamber is almost completely occupied with the cold air. Due to the large density difference between the hot gas and the cold air, the flow inside the main chamber is stably stratified without any visible large-scale mixing. The highest temperature of the three cases is about the same as previous cases at 1800K. Cases 5 and 7 with all doors open reduce the high-temperature areas in comparison with the partially open case (Case 6). Simulation results of the three cases are shown in Table 4.5. The induced draft is entrained through the doors with a respectable momentum at an average velocity of 4 m/s (8.95 mph) with mass flow rate at 27.68 kg/s (219,725 lbm/hr), 9.72 kg/s (77,951 lbm/hr), and 32.29 kg/s (256,319 lbm/hr) for Cases 5, 6 and 7 respectively, which is approximately 190%, 67%, and 221% of the total mass flow rate from the pyroscrubber inlet.

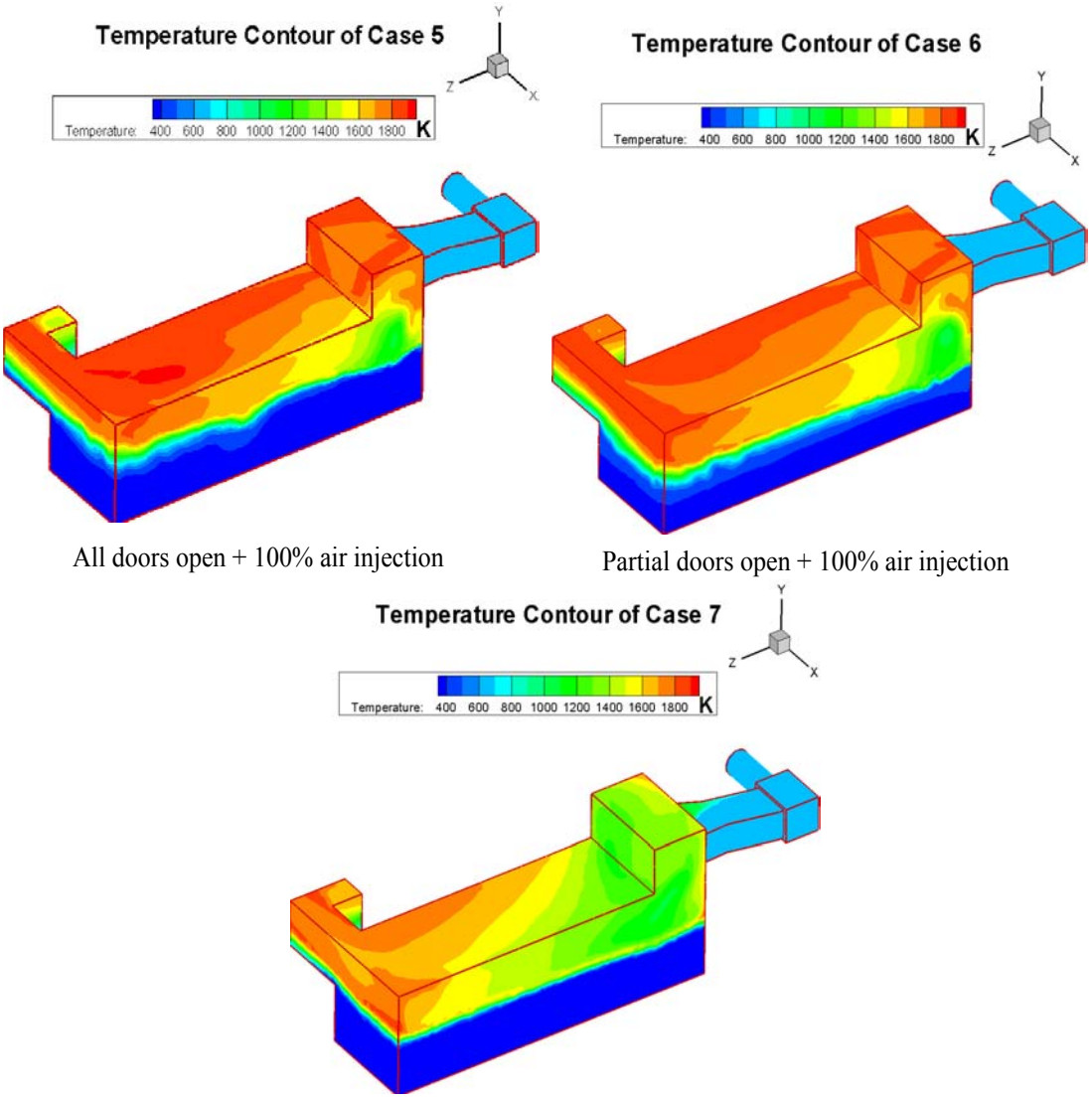

All doors open + 100% air injection

Partial doors open + 100% air injection

All doors open without air injection

Figure 4.20 Wall temperature contours in the pyroscrubber for three bottom doors opening case (Cases 5-7).

Table 4.5: Simulated results of three bottom door opening cases (Cases 5-7)

		mass flow(kg/s)	velocity(m/s)	temperature(K)	exergy (MW)
Case 5	inlet	14.58	4.19	500	-
(All doors open + 100% air injection)	air injection	10.88	14.35	300	-
	burner	11.48	10.15	300	-
	bottom doors	27.68	4.90	300	-
	outlet	64.62	11.58	1190	50.60
Case 6	inlet	14.58	4.19	500	-
(Doors partially open + 100% air)	air injection	10.88	14.35	300	-
	burner	11.48	10.15	300	-
	bottom doors	9.72	6.00	300	-
	outlet	46.66	11.15	1534	55.69
Case 7	inlet	14.58	4.19	-	-
(All doors open, no air)	air injection	0.00	0.00	-	-
	burner	0.00	0.00	-	-
	bottom doors	32.29	5.71	300	-
	outlet	46.86	11.15	1468	52.44

Conclusions of Bottom Doors Opening Cases:

- Strong ambient air is induced into the chamber by opening the bottom doors. The gas flow inside the main chamber is stably stratified with a large amount of the entrained cold air moving at the bottom of the chamber, and the hot combusted gas moving through on the top with minimal mixing.
- Case 6 with all doors open plus 100% air injection is apparently the worst case because the extra air entrained through the bottom doors only cools down the hot combustion gas (about 340 K temperature drop) and downgrades the exergy.

- Closing all air injection and using only the entrained air through opening bottom doors for combustion in Case 7, although is not a controllable way of combustion, it is interesting to see that a comparable amount of air can be entrained as is in 100% air injection. In comparison with the baseline case, the potential saving of blowers' power is 1.71 kW accompanied with a loss of exergy of 4.73 MW. Even the 150% air combustion case yields higher outflow temperature than bottom opening cases. The stratified flow pattern generates a much weaker mixing effect than using the air injection tubes and burner slots; as a result, combustion is not as complete as the 150% case and the temperature is lower.
- Moreover, it is not convenient to control the induced air flow.

Particle Combustion Model

Throughout the study of all the previous cases that used the eddy-dissipation model by assuming the coke particles instantaneously vaporize to gas under intensive heating during volatile combustion, plenty of information has been obtained about the overall aerothermal and combustion performance of the pyroscrubber. To better simulate the solid coke particle combustion, the heterogeneous reaction model between solid and gas is implemented. Particle trajectory and mass change due to diffusion and combustion will be tracked to provide more information about particle reaction behavior. Different particle sizes are used to show the effect of distributed particle diameter on fluid mechanics and combustion processes. Besides, the CO generation mechanism is added to predict CO emission.

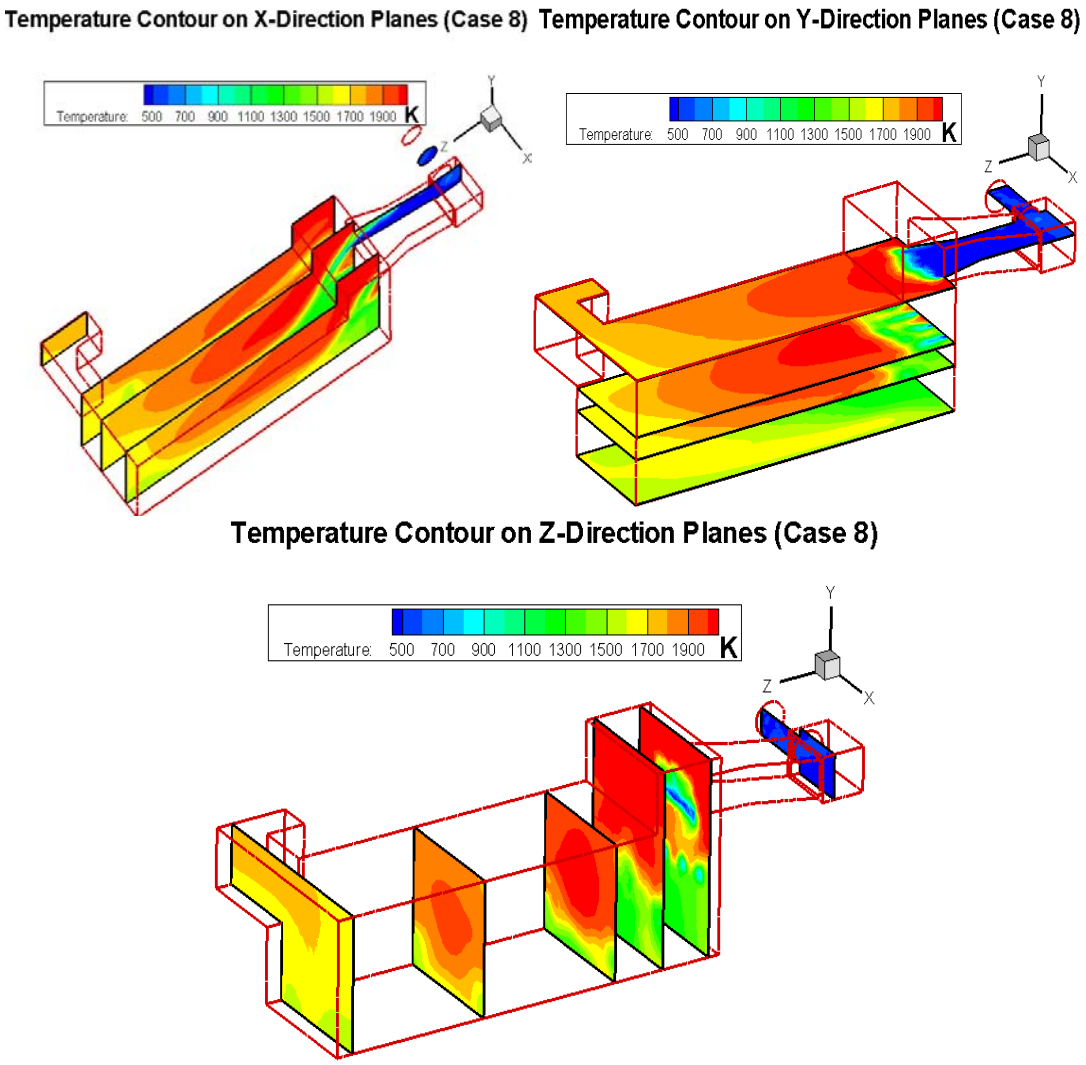

Figure 4.21 Temperature contour inside the pyroscrubber on different planes for coke particle combustion with 100% stoichiometric air.

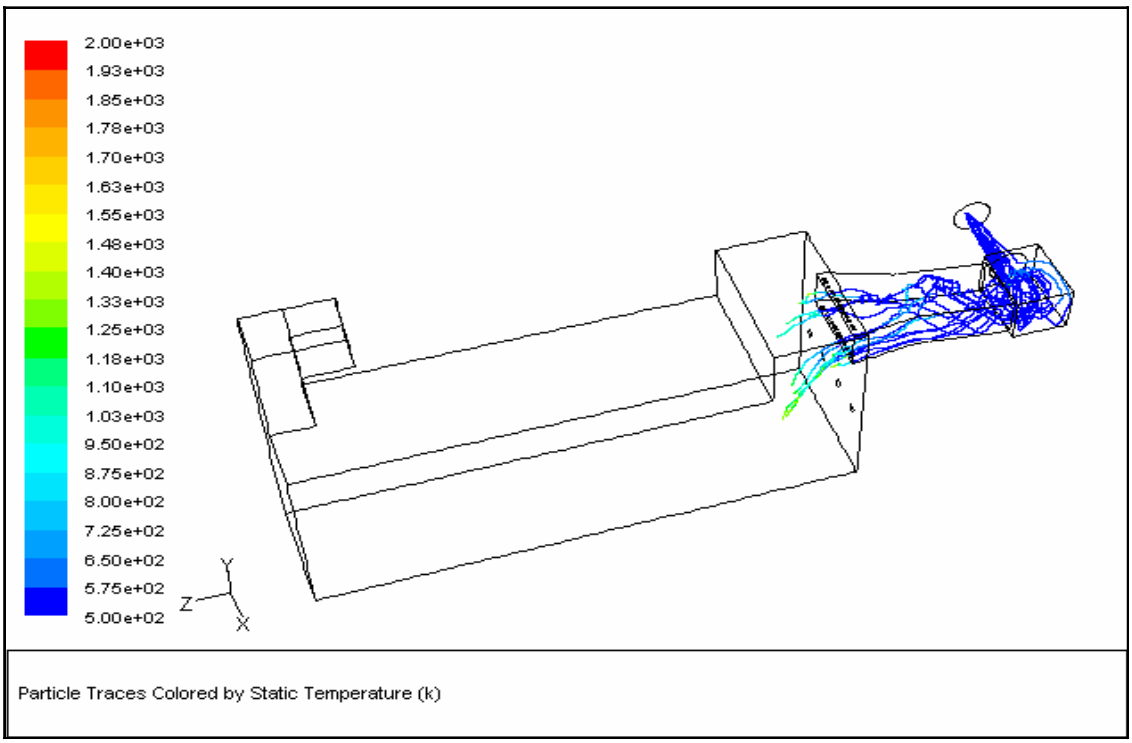

Figure 4.22 Particle pathlines for coke particle combustion (100% stoichiometric air)

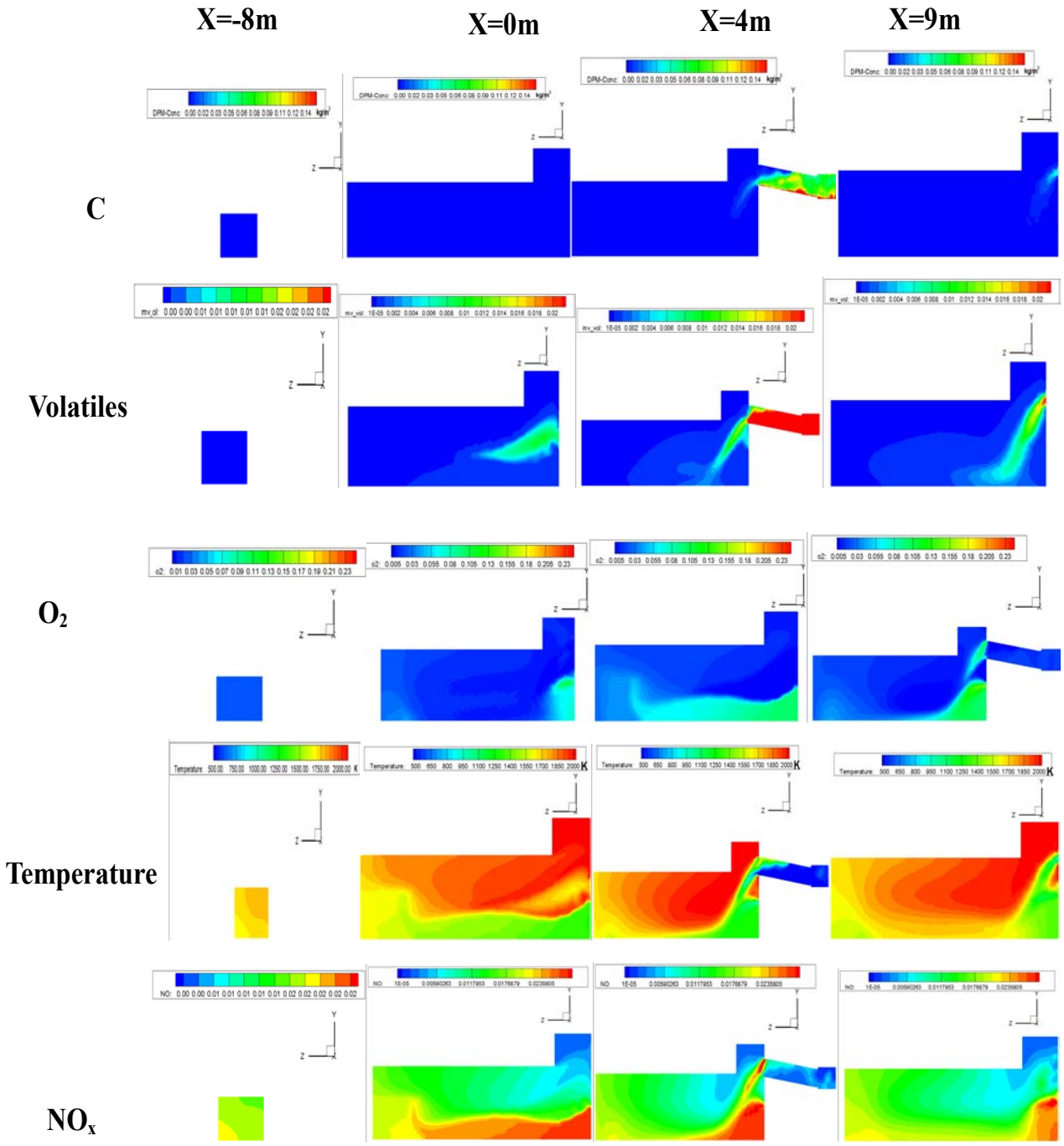

Figure 4.23 Species and temperature contour plots on X-direction planes for coke particle combustion case (100% stoichiometric air).

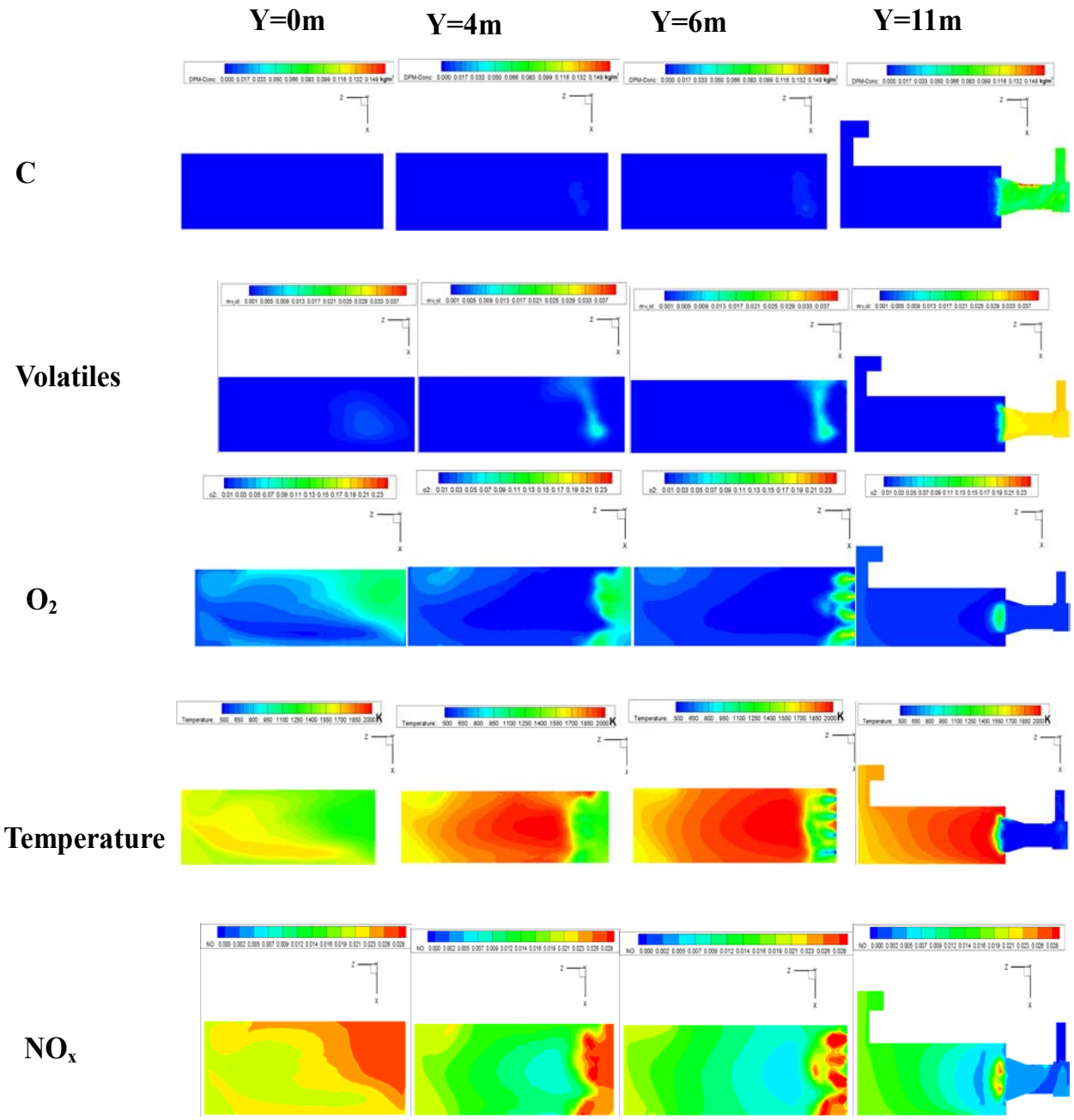

Figure 4.24 Species and temperature contour plots on Y-direction planes for coke particle combustion case (100% stoichiometric air).

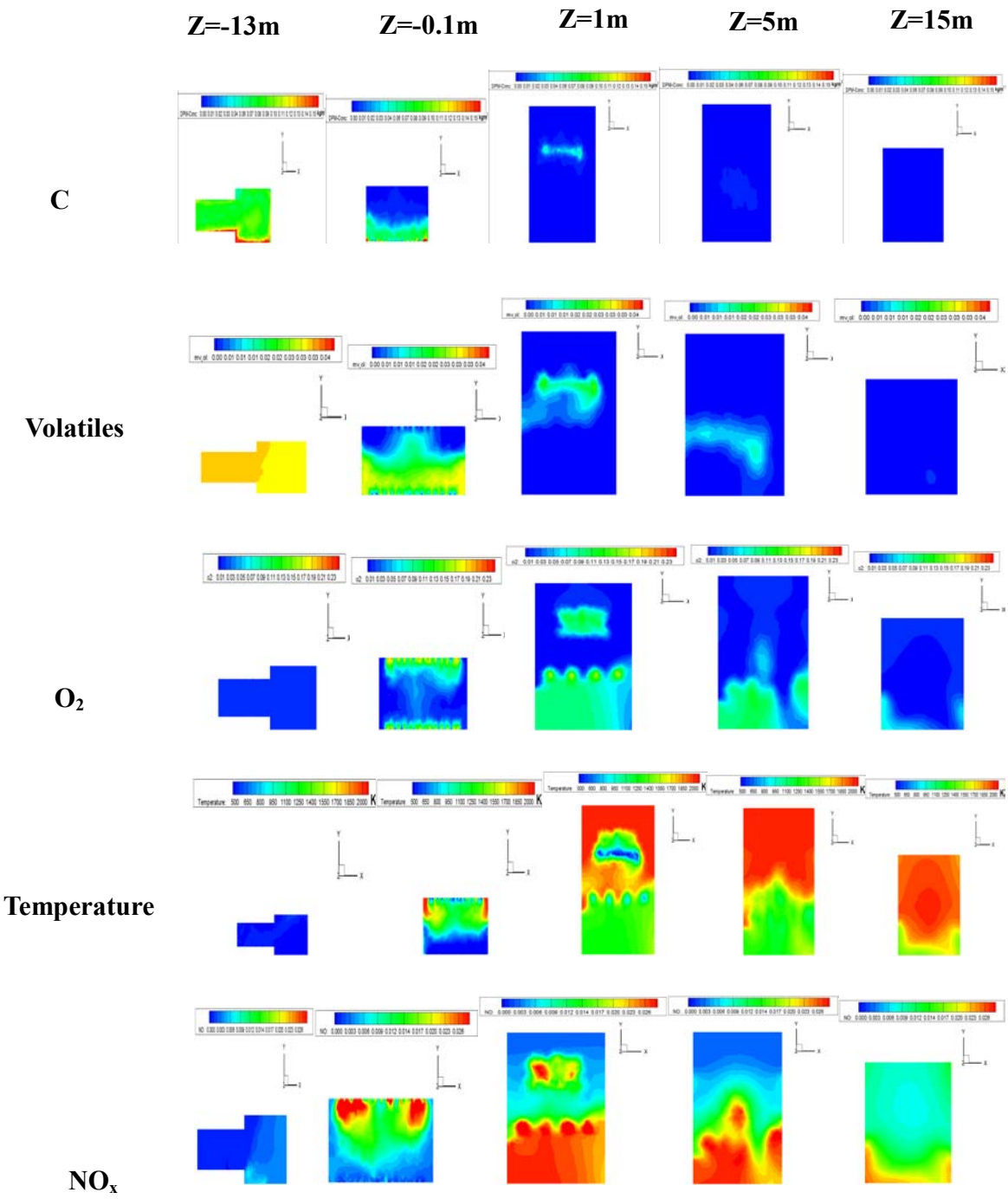

Coke particle combustion (100% stoichiometric air)

.

Figure 4.25 Species and temperature contour plots on Z-direction planes for coke particle combustion case (100% stoichiometric air).

.

Temperature contours on different planes are shown in Fig 4.21. Figure 4.22 shows some typical particle pathlines. Integral results are shown in Table 4.6. Compared with the baseline case, which uses eddy dissipation model and 100% stoichiometric air, the following different features of particle combustion model are noted:

- Particle combustion model generates much higher local flame temperature (2200K) than eddy dissipation model (1800K). This is probably partially caused by less gas volume flow surrounding the solid particles until they completely consumed and becomes gaseous products.
- Particle pathlines in Fig 4.22 shows that all coke particles are burned before or in the high-bay area, and coke particles are burned out very quickly once they enter the high-bay area.
- Intensive combustion and highest temperature occur on top part of the main chamber and close to the high-bay area. On bottom part of the chamber the gas temperature is 300 K lower than in the hot area. This is different from the baseline case of which the highest temperature occurs in the later part of the main chamber and almost uniformly distributed across the vertical cross section of the main chamber.
- For both eddy dissipation model and the particle combustion model, the gas temperature is uniform in the area close to the outlet duct. But the outflow temperature of the particle combustion model is 100k lower than the baseline case as shown in Table 4.6. Total energy of the particle combustion case is 92% of the baseline case.

- The NO_x production is unexpectedly high. It seems the NOx is produced more in the areas with more available oxygen and not necessarily in the locations with the highest temperatures. For example, NO_x is high on the bottom of the pyroscrubber, especially close to the corner of the East Wall where both abundant oxygen and comparatively high temperature exist. NO_x is also noticeably high at the region close to the air injection tubes on the high-bay area where fast combustion makes a trace of high NO_x production almost coincide with the inject air pathway. It is not clear why the NO_x is predicted unreasonable high. It is speculated that the adopted NO_x models are developed from gaseous combustion. Further examination of the NO_x specifically developed for solid combustion needs to be conducted in future study.
- Particle size affects its trajectory inside the pyroscrubber, affecting the combustion process. Particles larger than 200 μm in diameter can be easily trapped at the corners of the flue passage, especially in the front-facing walls between different chambers. Only approximately 10% of the particles larger than 200 μm can be transported into the main chamber. Most of the particles less than 20 μm can be successfully transported through the flue passage into the main chamber.

Table 4.6: Simulated results of particle combustion (100% stoichiometric air)

100% air(particle combustion)	main inlet mass flow rate(kg/s)	burner mass flow rate(kg/s)	air injection mass flow rate(kg/s)	outlet mass flow rate(kg/s)	outlet mass fraction
NO_x	0.00E+00	0.00E+00	0.00E+00	6.48E-01	1.76E-02(17436 ppm)
CO	0.00E+00	0.00E+00	0.00E+00	4.91E-08	1.33E-09(0.0015 ppm)
Volatiles	0.42	0.00	0.00	0.00	0.00E+00
O_2	0.24	2.66	2.53	0.92	2.49E-02
CO_2	2.16	0.00	0.00	8.63	2.34E-01
H_2O	1.15	0.00	0.00	1.84	4.98E-02
C(s)	1.53	0.00	0.00	0.00	0.00E+00
N_2	9.78	8.82	8.35	25.56	6.92E-01
total	14.58	11.48	10.88	36.94	1.02E+00
Exit Temp	1717K	Exergy (Useful Energy)	52.20MW		

CHAPTER FIVE

CONCLUSIONS

In this study, computational simulation of combustion inside a pyroscrubber downstream from a petroleum coke calcinator has been conducted using the commercial code FLUENT. The fuel consists of volatiles and coke dust coming from the petcoke calcinator. A total of eight cases have been simulated and different fuel/air ratios, different deployments of multistage air injection, and with/without natural air aspiration have been employed. The carbon combustion has been modeled using both instantaneous gasification model and finite rate heterogeneous model. The exhaust gas will be used to generate steam and produce electricity via a steam turbine power plant. The combustion performance is evaluated by three parameters: the exit gas temperature, the exit exergy, and the emission. The results provide comprehensive information concerning the thermal-flow behavior and combustion inside an industrial pyroscrubber. The major conclusions are:

Case 1: Baseline Case (100% stoichiometric air)

The simulated temperature is reasonably consistent with the plant running data at several locations: simulated 2450 ^{o}F (1600K) in the high bay and low bay versus plant running data below approximately 2500 ^{o}F, and simulated 2300 ^{o}F (1500K) versus plant running data around 1400K in the duct work connected to the boiler. The simulated NO_x emission of 95lbs/hr (43kg/hr) in the baseline case (100% stoichiometric air) is within the range of actual measurement of 50-110 lbs/hr. The high-bay wall structure forces the flow from the inlet duct to move downward and redirects it to intersect the second air injection from the burners, which creates a strong forced mixing of the partially combusted gas from the top and the fresh air

from the burners, making combustion take place and generating those hot streaks. This effect of forcing combustion to happen at an earlier stage helps to efficiently utilize the main chamber space and avoid using an otherwise bigger main chamber.

Case 2: 80% Stoichiometric Air Combustion

NO_x emission is effectively reduced. However, some major concerns are lower exit gas temperature and the losses of unburned fuel and exergy, which will reduce electricity production of the steam power plant. CO emission also needs to be watched.

Overall, incomplete combustion at sub-stoichiometric air combustion case is not a favorable running condition for the pyroscrubber. It is necessary to generate a complete combustion condition to utilize all the energy from the fuel.

Case 3: 150% Stoichiometric Air Combustion

In terms of NO_x emission control, the pyroscrubber performance is best with 150% stoichiometric air. It gives the lowest NO_x emission in either mass fraction or mass flow rate. Consequently, lower output gas temperature resulting in low overall efficiency of the power generation system is a major draw-back.

Complete combustion harvests full energy from the fuel. Excess air cools down the combusted gas temperature and significantly cut down NO_x emission. Balance between these two effects need to be made to obtain the optimum pyroscrubber performance.

Case 4: Three Stage Combustion (41%, 39% and 20%)

Three-stage burning strategy can successfully cut down the emission in comparison with the baseline case. Although the NO_x emission is higher than 80% and 150% cases, this case doesn't have the drawbacks of either compromised exergy in the 80% air case or reduced exit temperature in the 150% air case. The third stage air injection does not work well as planned due to short residence time for mixing, resulting in nonuniform temperature distribution and formation of hot spots with an increase of NO_x emission. Modifications of the multi-stage combustion in many aspects, e.g. air injection composition, location, construction of different combustion stages, can be made by further studies to optimize the multi-stage combustion strategy.

Comparisons of Cases 1-4 (100%, 80%, 150% and Three-Stage Cases)

Comparison of four cases is listed in Table 5.1.:

Table 5.1: Summary of simulated results

cases	total energy output(MW)	estimated power generation (MW)#	mass flow rate (kg/s)	temperature (K)	NOx emission (kg/s)	NOx emission (ppm)
100%	57.17	17.01	36.94	1804	0.0120	321.49
80%	47.32	14.08	32.47	1726	0.0010	29.37
150%	56.17	16.71	48.13	1523	0.0004	7.45
3-stage	52.20	15.53	36.94	1702	0.0019	51.36

#The estimated power generation is based on 85% of boiler efficiency and 35% of steam turbine efficiency. For 150% case, the estimated power generation shown is over-estimated because its exit temperature is 300K lower than other cases and the boiler efficiency will be lower than 85%.

- The results show: The three-stage burning strategy can effectively reduce NO_x emission without compromising total energy output.
- Excess air can help to reduce NO_x emission and increase total energy output, but yields lower output gas temperature which will reduce boiler efficiency. A well balanced amount of excess air is favorable.
- Incomplete combustion with sub-stoichiometric air cuts NO_x emission, but leads to less total energy output, lowers gas temperature and increased CO emission.

Cases 5, 6 and 7: Bottom Doors Opened

Strong ambient air is induced into the pyrocrubber. The gas flow is stably stratified with a large amount of the entrained cold air moving at the bottom of the chamber and the hot combusted gas moving through the top. Running with all doors open plus 100% air injection is the worst case due to the cooling effect of the excess air (about 340 K temperature drop) and the downgraded exergy. One concern of the bottom doors opening cases is that the induced air flow is not convenient to be controlled.

Particle Combustion Model

Particle combustion model generates much higher local flame temperature (2200K) than eddy dissipation model used in instantaneous gasification model (1800K). All coke particles are burned before or in the high-bay area, and coke particles are burned out very quickly once they enter the high-bay area. Intensive combustion and the highest temperatures occur on the top part of the main chamber and close to the high-bay area. On the bottom part of the chamber, the gas temperature is 300 K lower than in the hot area. Particle size affects its trajectory inside

the pyroscrubber, thus affecting the combustion process. Particles larger than 200 μm in diameter can be easily trapped at the corners of the flue passage, especially in the front-facing walls between different chambers, and approximately 10% can be transported into the main chamber. Most of the particles less than 20 μm can be successfully transported through the flue passage either be combusted or escape through the exit. Total energy output of the particle combustion case is 92% of the baseline case.

Recommendation for Future Studies

1. Develop and incorporate a coke fines entrainment model to predict the effect of the flow field on coke fines entrainment rates.
2. Include the pyroscrubber walls into the simulation to study the temperature and heat flux distribution over different walls.
3. Study effects of different turbulence and gas combustions model on the results.
4. Incorporate different particle combustion models and investigate the effects.
5. Investigate different pyroscrubber geometries and structures.

REFERENCES

[1] Allred, V. D., "Rotary Hearth Calcining of Petroleum Coke," Light Metals, 1971, pp. 313-329.

[2] Anderson, J. D. Jr, "Computational Fluid Dynamics, the basics with application," McGraw-Hill Inc., 1995.

[3] Bagdoyan, E. A., and Gootzait, E., "Refiners Calcine Coke," Hydrocarbon Processing, September 1985, pp.85-90.

[4] Byrne, Henry James, United States Patent 4,012,202, 1977.

[5] Burmeister, L. C., "Convective Heat Transfer," John Wiley & Sons Inc., 1983.

[6] CII Carbon L.L.C., "Canadian Rotary Coke Calciner Modeling," 2004.

[7] Field, M.A., "Rate of Combustion of Size-Graded Fractions of Char From a Low-Rank Between 1200 K and 2000 K," Combustion and Flame 13, 237, 1968.

[8] Fluent 6.3 User's Guide, September 2006, Fluent Inc.

[9] Incropera, F. P., and DeWitt, D. P., "Introduction to Heat Transfer," 4th Edition, John Wiley & Sons Inc., 1996.

[10] Kaftori, D., Hetsroni, G. and Banerjee, S., "Particle behavior in the turbulent boundary layer," Phys. Fluids, Vol. 7, No. 5, May 1995

[11] Liu, G., Tate, A.G., Bryant, G.W., Wall, T.F., "Mathematical modeling of coal char reactivity with CO_2 at high pressures and temperatures," Fuel 79, 1145-1154, 2000.

[12] Marvin, M. S., "NO_X Emission Control for Gas Turbines: A 1992 Update on Regulations and Technology," ASME COGEN-TURBO ASME, 1992.

[13] Mayers, M.A., "The Rate Reduction of Carbon Dioxide by Graphite," Journal of American Chemical Society 56, 70, 1934.

[14] Munson, Young, and Okiishi, "Fundamentals of Fluid Mechanics," 3rd Edition, John Wiley & Sons Inc., 1998.

[15] Patankar, S.V., "Numerical Heat Transfer and Fluid Flow," McGraw-Hill Inc., Hemisphere, 1980.

[16] Eggels, R.L.G.M., "Modeling of NO_X Formation of a Premixed DLE Gas Turbine Combustor," Proceedings of ASME TURBO EXPO, June 2001.

[17] Siegel, R., and Howell, J. R., "Thermal Radiation Heat Transfer," Hemisphere Publishing

Corporation, Washington D.C., 1992.

[18] Stovin, V.R., Saul, A.J. “Computational fluid dynamics (CFD) particle tracking approach to efficiency prediction,” Proceedings of the 1997 2nd IAWQ International Conference on the Sewer as a Physical, Chemical and Biological Reactor, May 25-28 1997.

[19] Tennekes, H., and Lumley, J. L., “A First Course in Turbulence,” The Massachusetts Institute of Technology, 1972.

[20] Thomas, L. C., “Heat Transfer,” 2nd edition, Capstone Publishing Corporation., 2000.

[21] Turns, Stephen R., “An Introduction to Combustion,” 2nd Edition, McGraw-Hill Inc., 2000.

[22] Van Wylen, G. J., Sonntag, R. E., “Fundamentals of Classical Thermodynamics,” 3rd Edition, John Wiley & Sons Inc., 1986.

[23] Vivek, S., Cheng, D. Y., “Reduction of NO_x and CO to Below 2PPM in Diffusion Flame,” Proceedings of ASME Turbo Expo 2003 Power for Land , Sea and Air, June 16, 2003.

[24] White, F. “Viscous Flow,” 2nd edition, McGraw-Hill Inc., 1991.

[25] Zhang, Z. and Wang, T.," Thermal-Flow and Combustion Simulation in a Rotational Calcining Kiln," ECCC Report 2007-02, Energy Conversion and Conservation Center, University of New Orleans, submitted to CII Carbon, LLC. 2007.

APPENDIX A

APPLICATION OF FLUENT CODE

The model set-up process in Fluent is shown below.

Step 1: Grids

1. Read the grid file

   FILE → READ → CASE

   After importing the grid file, FLUENT will report the number of cells that has been read, along with number of boundary faces with their zone identifiers.

2. Check the grid

   GRID → CHECK

   The grid check lists the minimum and maximum X, Y and Z values from the grid, and reports on a number of other grid features that are checked. Any errors in the grid would be reported at this time.

3. Scale the grid

   Since this grid was created in units of feet, the SCALE GRID panel will be used to scale the grid into meters.

   GRID → SCALE

   a. Under UNIT CONVERSION, select FT from the drop-down list to confirm that the GRID WAS CREATED IN FEET.

   b. Click on SCALE.

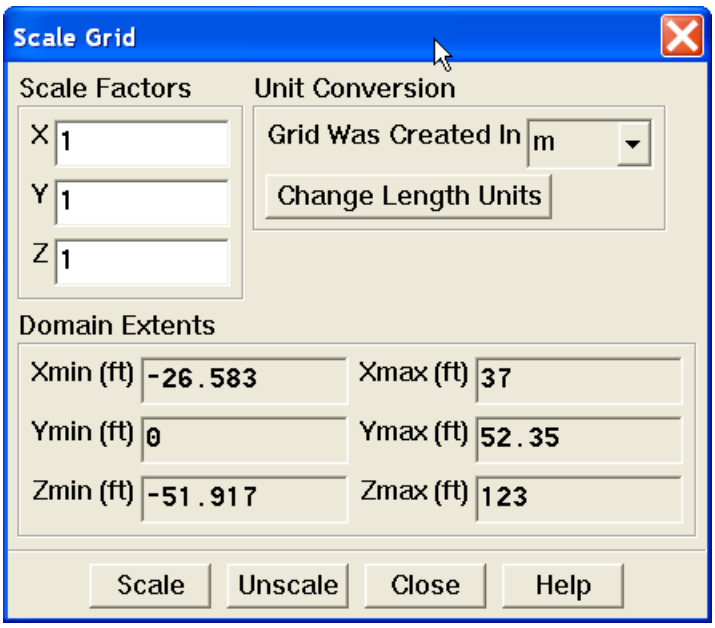

4. Display the grid

   DISPLAY → GRID

Step 2: Models

1. Define the domain space as 3-D, and choose segregated solver.

   DEFINE → MODELS → SOLVER

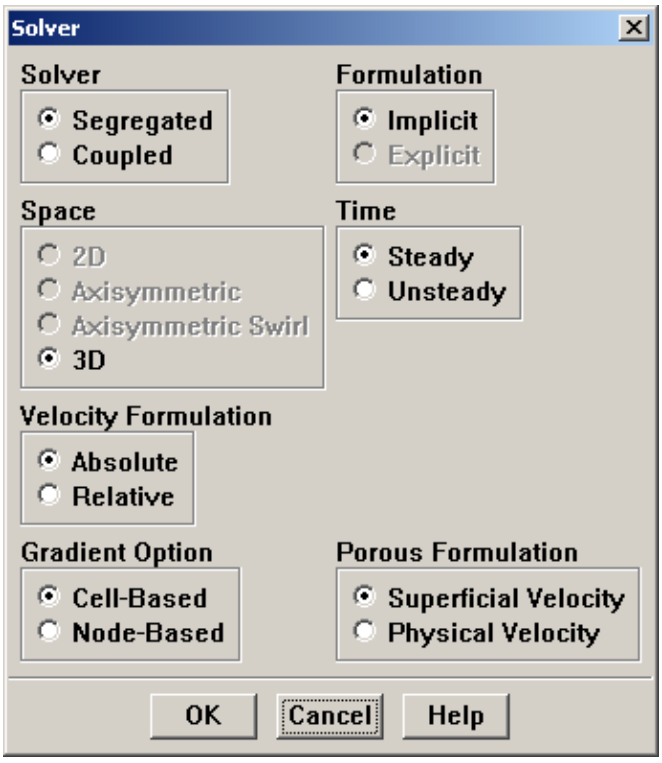

2. Enable heat transfer by activating the energy equation

   DEFINE → MODELS → ENERGY

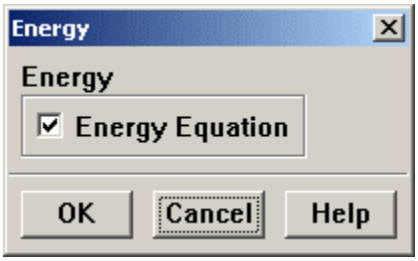

3. Enable the k – ε turbulence model

   DEFINE → MODELS → VISCOUS

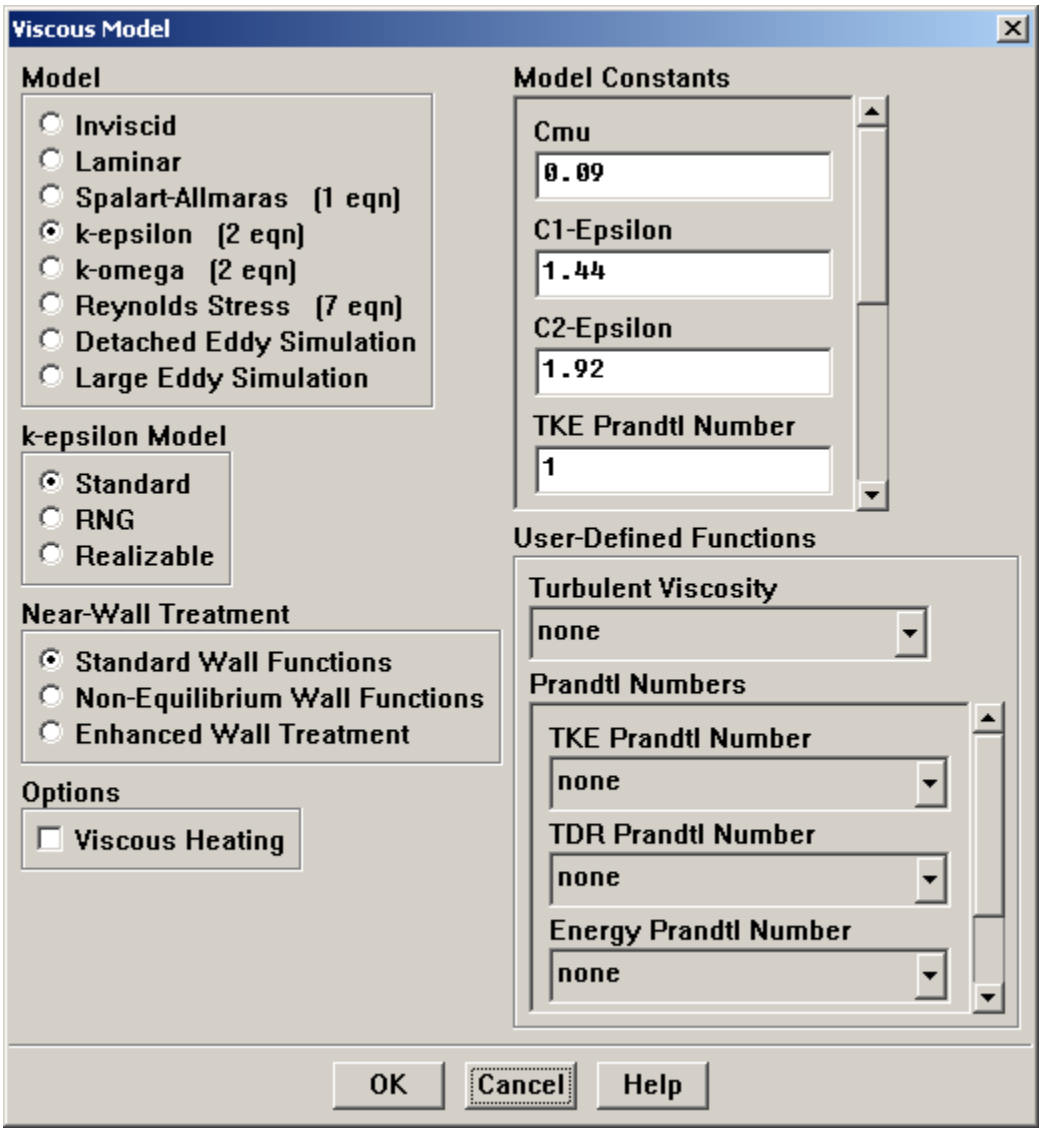

4. Enable P1 radiation model

DEFINE → MODELS → RADIATION

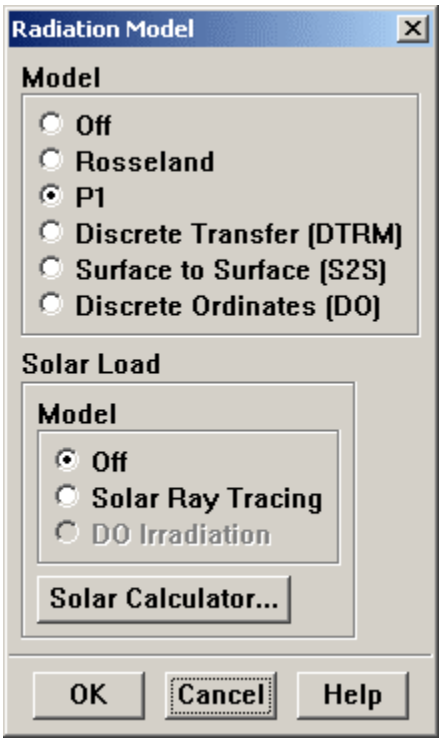

5. Enable chemical species transport and reaction

   DEFINE → MODELS → SPECIES

   - Select SPECIES TRANSPORT under MODEL.
   - Select VOLUMETRIC under REACTIONS.
   - Choose COAL-MV-VOLATILES-AIR in the MIXTURE MATERIAL drop-down list.
   - Select the EDDY-DISSIPATION option under TURBULENCE-CHEMISTRY INTERACTION.
   - Click OK.

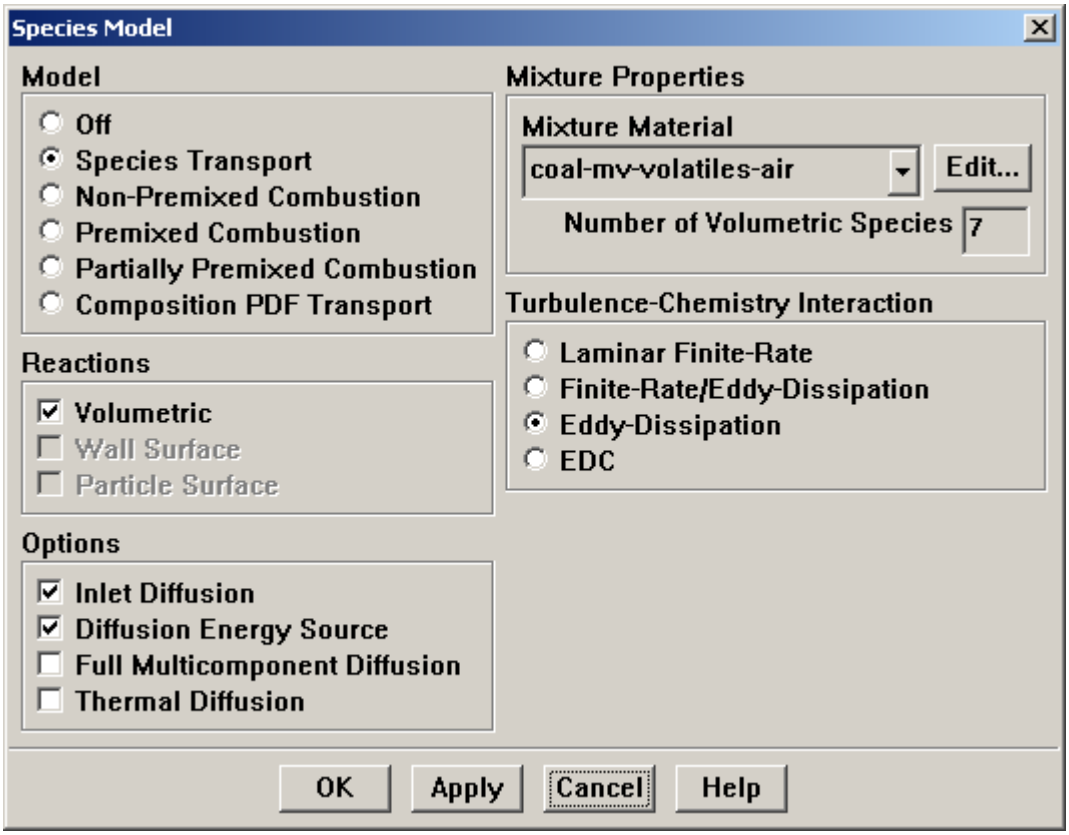
Species Model
Model
Off
Species Transport
Non-Premixed Combustion
Premixed Combustion
Partially Premixed Combustion
Composition PDF Transport
Reactions
Volumetric
Wall Surface
Particle Surface
Options
Inlet Diffusion
Diffusion Energy Source
Full Multicomponent Diffusion
Thermal Diffusion
Mixture Properties
Mixture Material
coal-mv-volatiles-air
Edit...
Number of Volumetric Species
7
Turbulence-Chemistry Interaction
Laminar Finite-Rate
Finite-Rate/Eddy-Dissipation
Eddy-Dissipation
EDC
OK
Apply
Cancel
Help

Step 3: Materials and Reactions

DEFINE → MATERIALS

1. The MATERIALS panel shows the mixture material, COAL-MV-VOLATILES-AIR, which was enabled in the SPECIES MODEL panel.

   Set ABSORPTION COEFFICIENT to 0.2 m^{-1}.

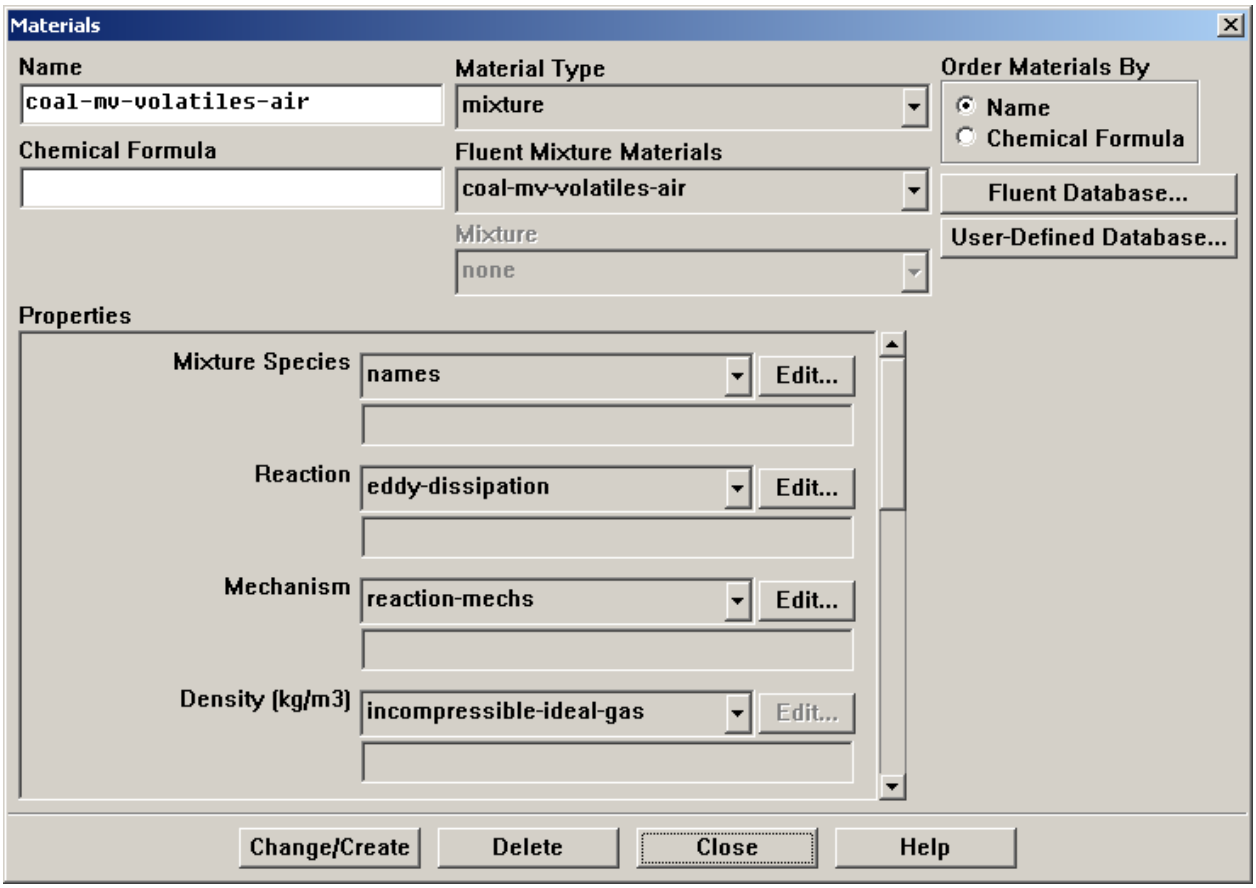

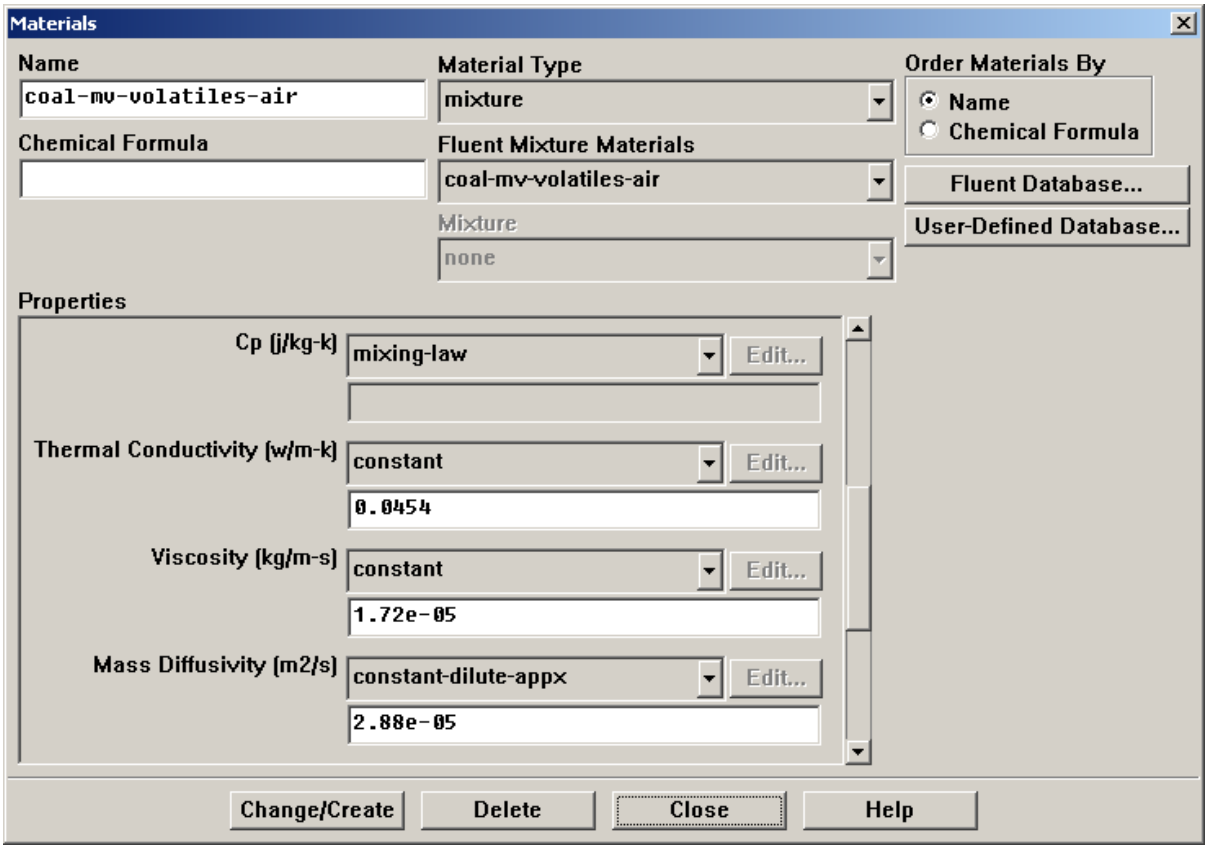
Materials
Name
coal-mv-volatiles-air
Material Type
mixture
Order Materials By
Name
Chemical Formula
Chemical Formula
Fluent Mixture Materials
coal-mv-volatiles-air
Fluent Database...
User-Defined Database...
Mixture
none
Properties
Cp (j/kg-k)
mixing-law
Edit...
Thermal Conductivity (w/m-k)
constant
Edit...
0.0454
Viscosity (kg/m-s)
constant
Edit...
1.72e-05
Mass Diffusivity (m2/s)
constant-dilute-appx
Edit...
2.88e-05
Change/Create
Delete
Close
Help

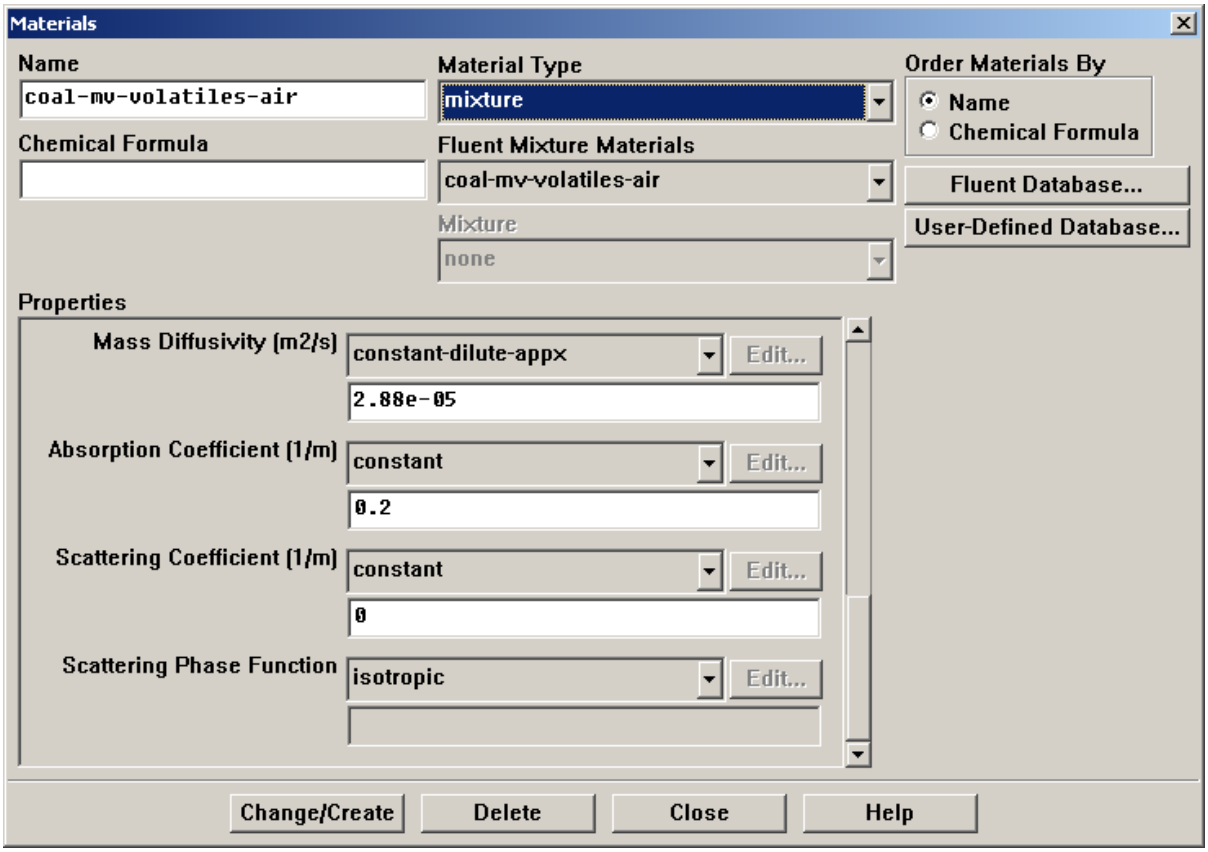
Materials
Name
coal-mv-volatiles-air
Material Type
mixture
Order Materials By
Name
Chemical Formula
Chemical Formula
Fluent Mixture Materials
coal-mv-volatiles-air
Fluent Database...
User-Defined Database...
Mixture
none
Properties
Mass Diffusivity (m2/s)
constant-dilute-appx
Edit...
2.88e-05
Absorption Coefficient (1/m)
constant
Edit...
0.2
Scattering Coefficient (1/m)
constant
Edit...
0
Scattering Phase Function
isotropic
Edit...
Change/Create
Delete
Close
Help

2. Add other fluid species into the computational domain.

From FLUENT DATABASE, in the MATERIAL TYPE drop-down list, choose FLUID.

Select METHANE, CARBON, and click COPY.

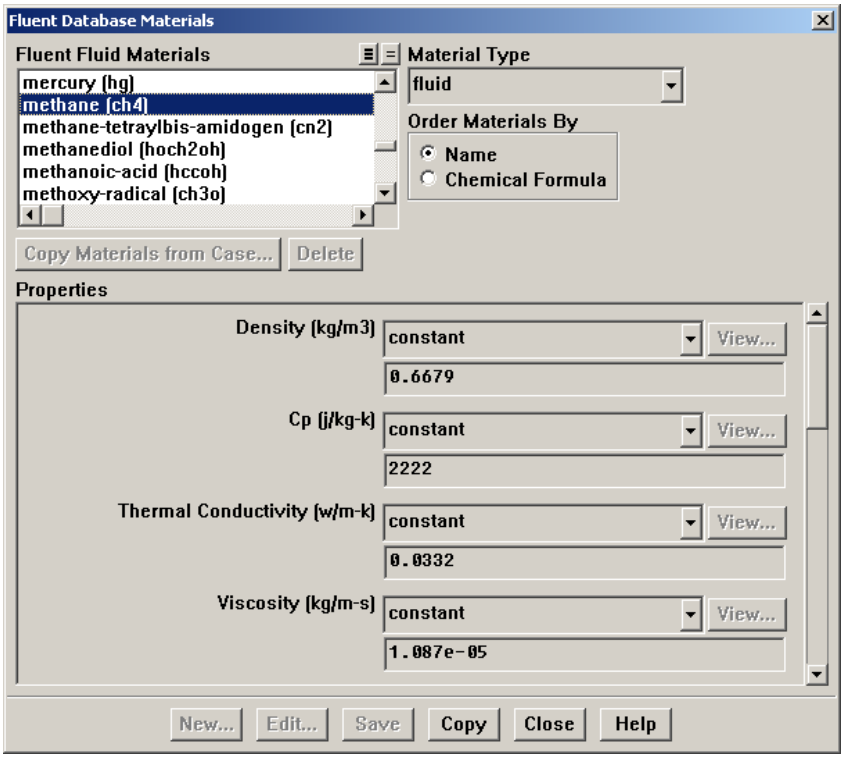

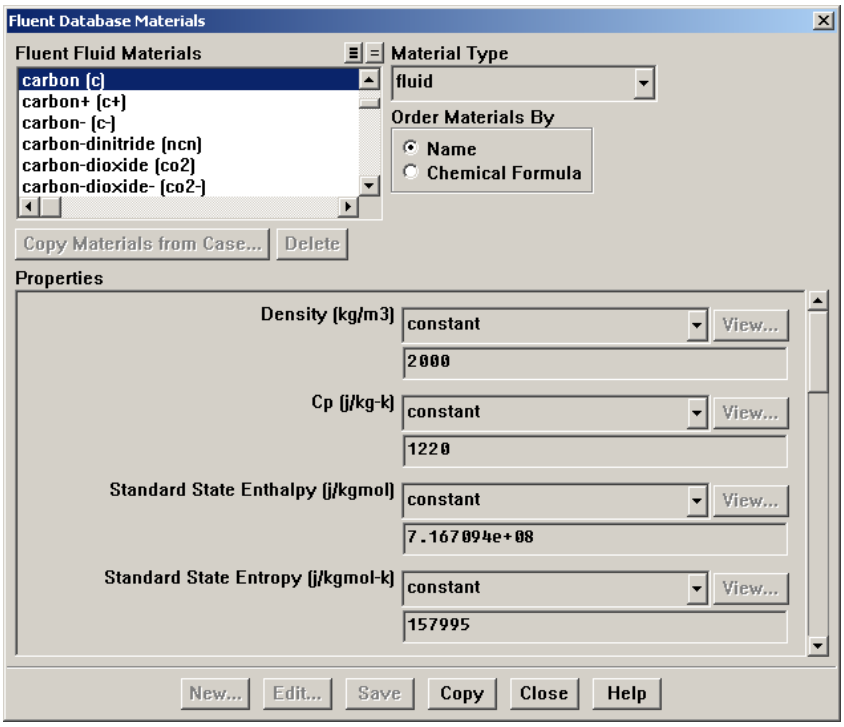

3. In the MATERIALS panel, choose FLUID from the MATERIAL TYPE drop-down list.

   a. Select CARBON (SOLID).

   b. Select COAL-MV-VOLATILES

   c. Select WATER-VAPOR

   d. Select CARBON DIOXIDE

   e. Select OXYGEN

   f. Select NITROGEN

   g. Select COAL-MV-VOLATILES

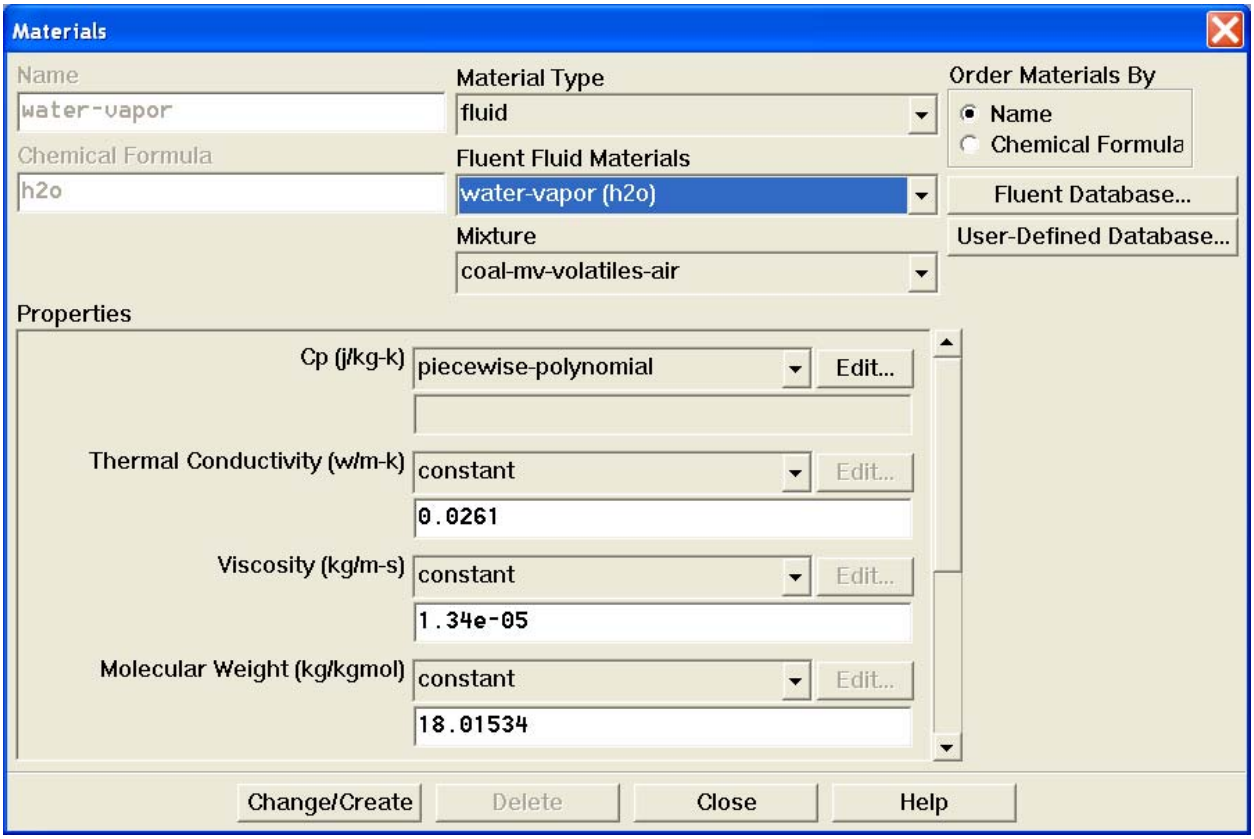

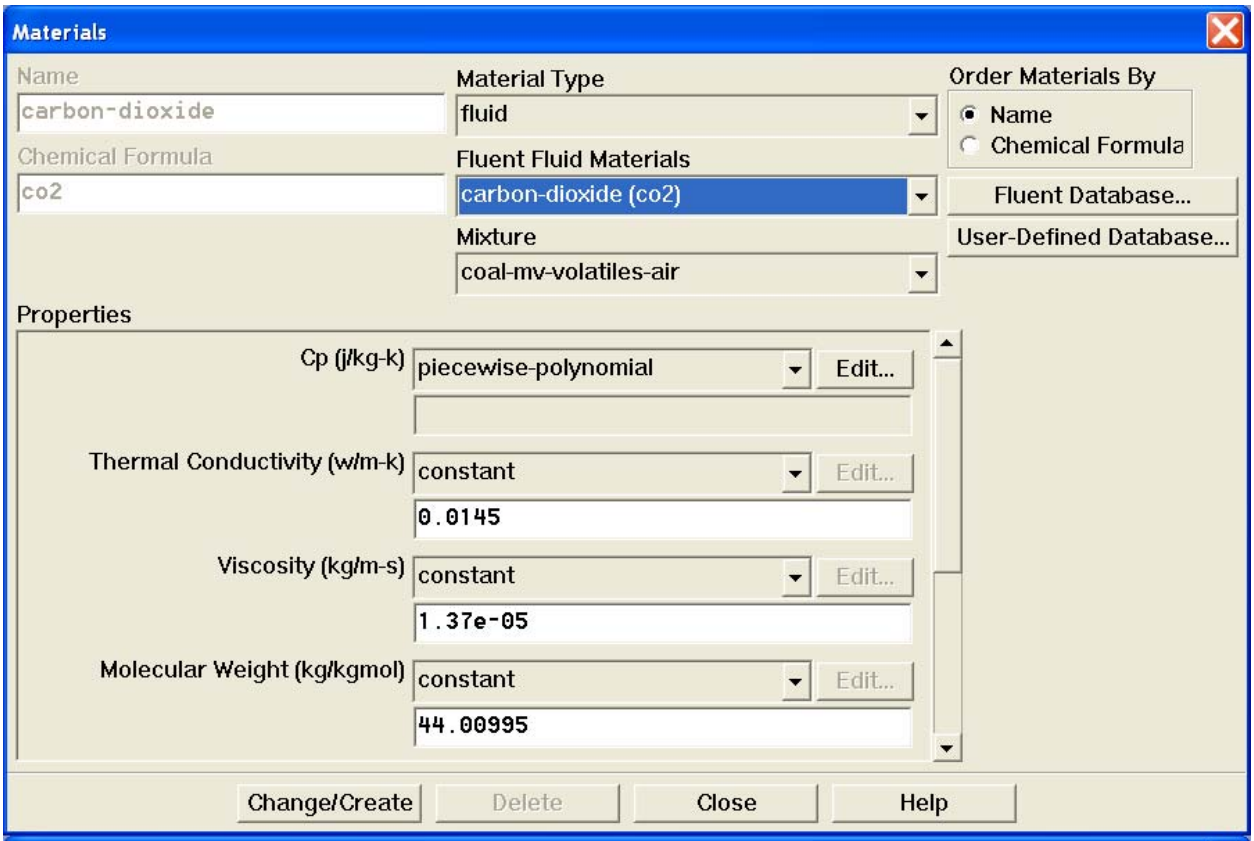
Materials
Name
carbon-dioxide
Material Type
fluid
Order Materials By
Name
Chemical Formula
Chemical Formula
co2
Fluent Fluid Materials
carbon-dioxide (co2)
Fluent Database...
Mixture
coal-mv-volatiles-air
User-Defined Database...
Properties
Cp (j/kg-k)
piecewise-polynomial
Edit...
Thermal Conductivity (w/m-k)
constant
Edit...
0.0145
Viscosity (kg/m-s)
constant
Edit...
1.37e-05
Molecular Weight (kg/kgmol)
constant
Edit...
44.00995
Change/Create
Delete
Close
Help

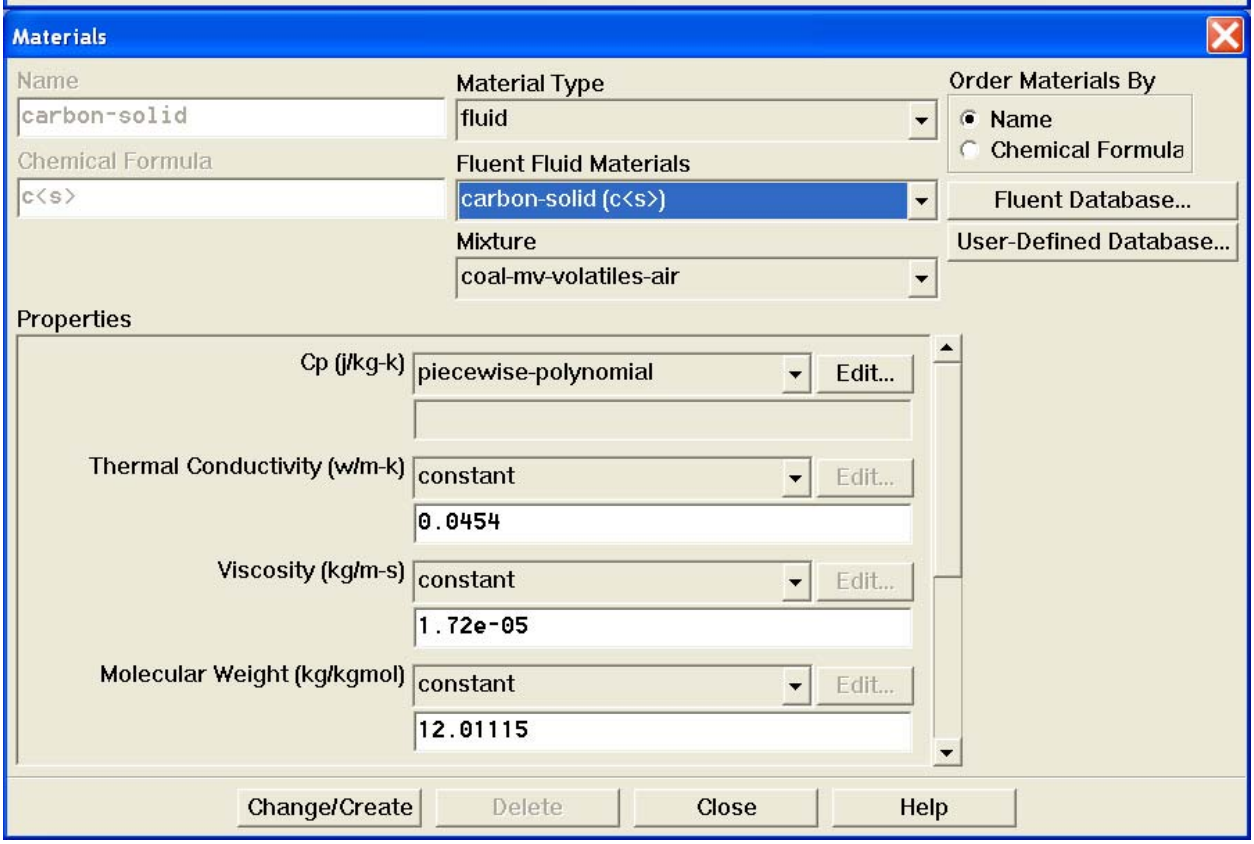
Materials
Name
carbon-solid
Material Type
fluid
Order Materials By
Name
Chemical Formula
Chemical Formula
c<s>
Fluent Fluid Materials
carbon-solid (c<s>)
Fluent Database...
Mixture
coal-mv-volatiles-air
User-Defined Database...
Properties
Cp (j/kg-k)
piecewise-polynomial
Edit...
Thermal Conductivity (w/m-k)
constant
Edit...
0.0454
Viscosity (kg/m-s)
constant
Edit...
1.72e-05
Molecular Weight (kg/kgmol)
constant
Edit...
12.01115
Change/Create
Delete
Close
Help

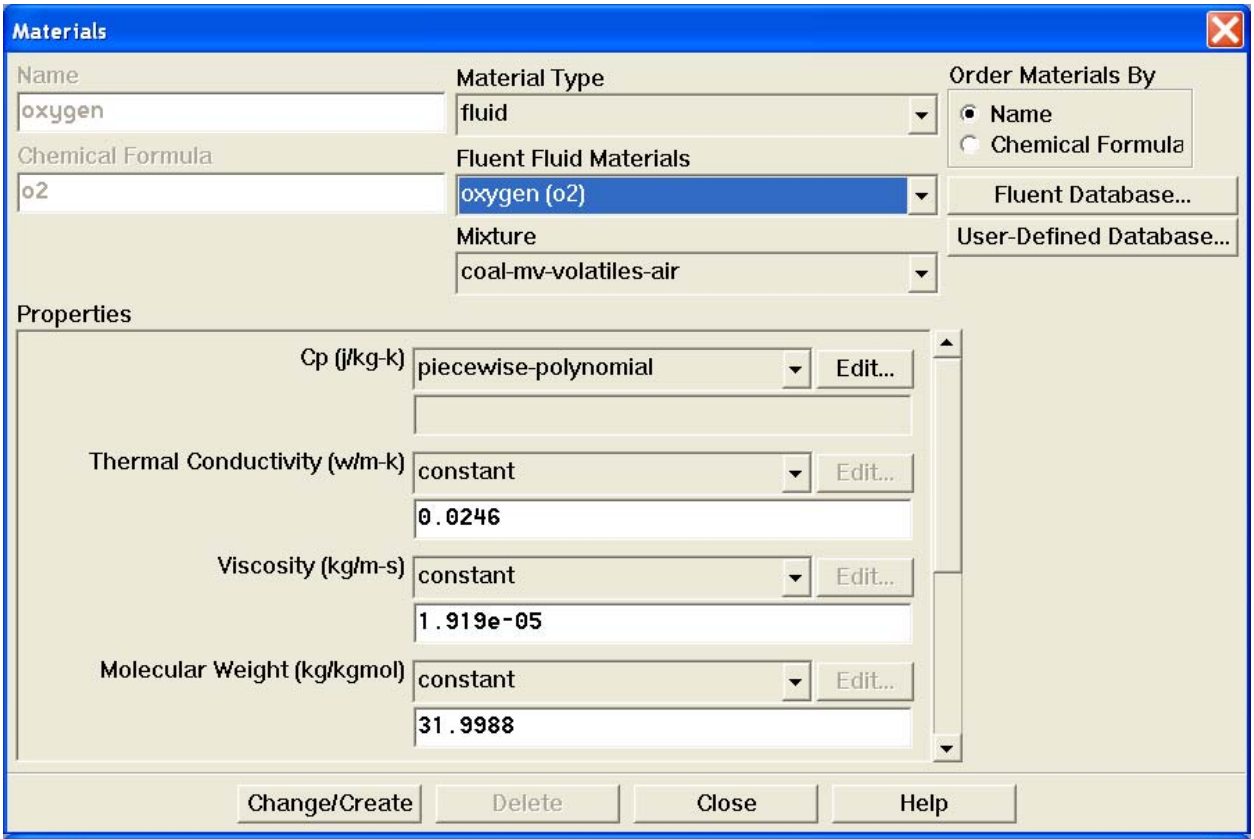
Materials
Name
oxygen
Material Type
fluid
Order Materials By
Name
Chemical Formula
Chemical Formula
o2
Fluent Fluid Materials
oxygen (o2)
Fluent Database...
Mixture
coal-mv-volatiles-air
User-Defined Database...
Properties
Cp (j/kg-k)
piecewise-polynomial
Edit...
Thermal Conductivity (w/m-k)
constant
Edit...
0.0246
Viscosity (kg/m-s)
constant
Edit...
1.919e-05
Molecular Weight (kg/kgmol)
constant
Edit...
31.9988
Change/Create
Delete
Close
Help

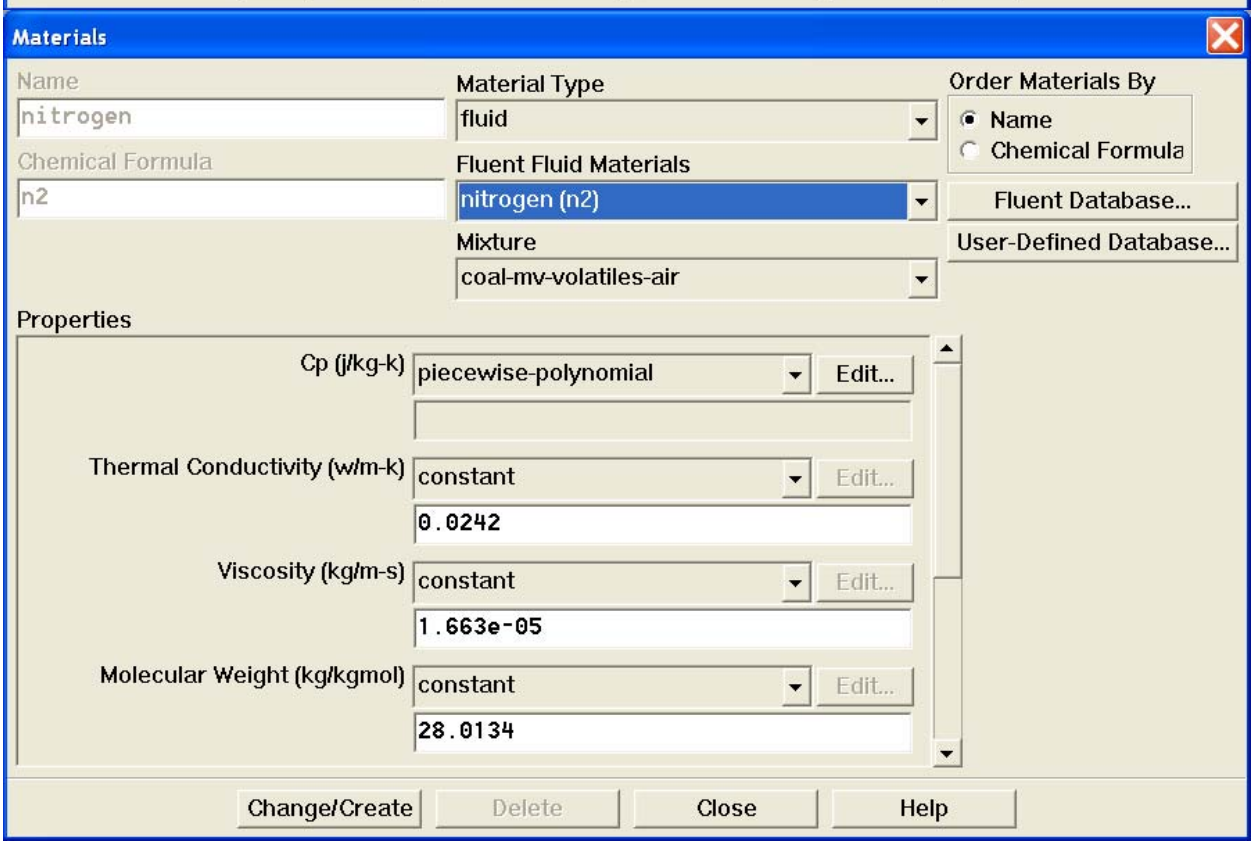
Materials
Name
nitrogen
Material Type
fluid
Order Materials By
Name
Chemical Formula
Chemical Formula
n2
Fluent Fluid Materials
nitrogen (n2)
Fluent Database...
Mixture
coal-mv-volatiles-air
User-Defined Database...
Properties
Cp (j/kg-k)
piecewise-polynomial
Edit...
Thermal Conductivity (w/m-k)
constant
Edit...
0.0242
Viscosity (kg/m-s)
constant
Edit...
1.663e-05
Molecular Weight (kg/kgmol)
constant
Edit...
28.0134
Change/Create
Delete
Close
Help

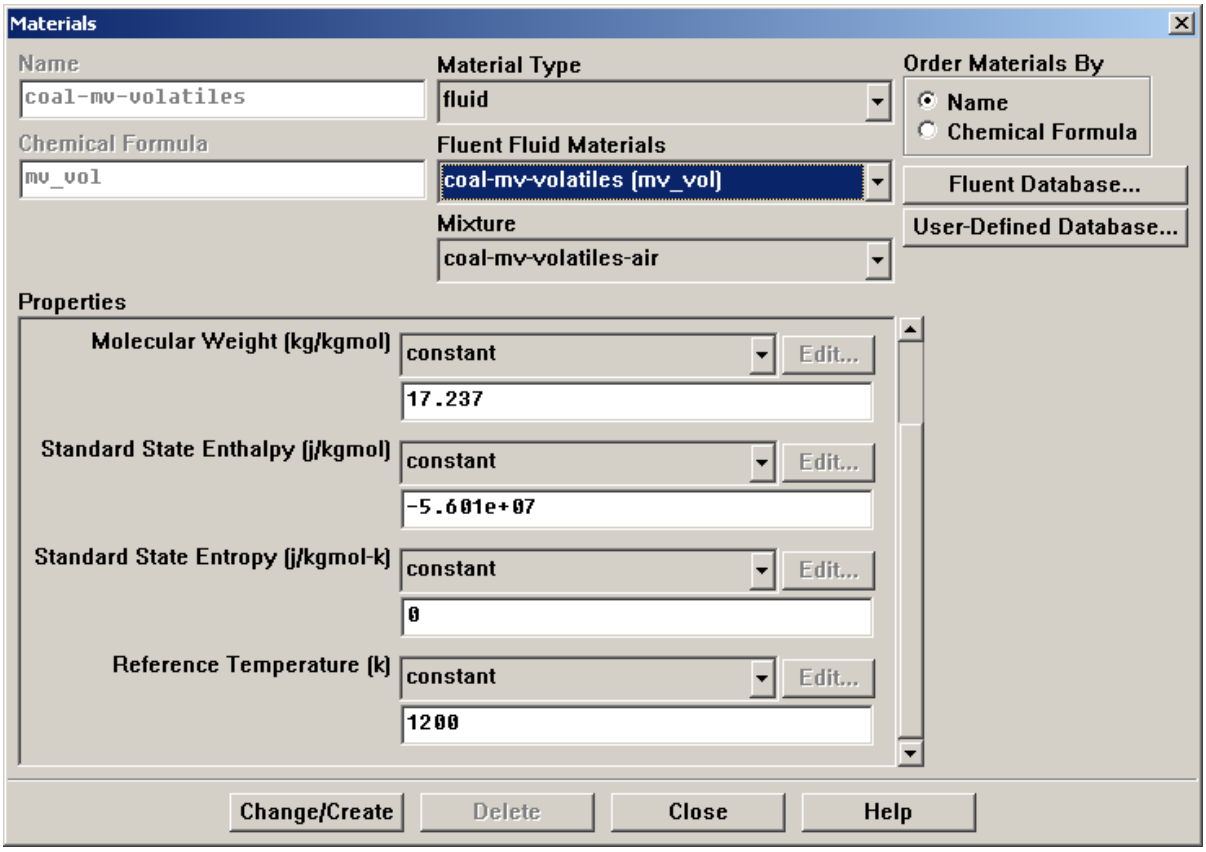
Materials
Name
coal-mv-volatiles
Chemical Formula
mv_vol
Material Type
fluid
Fluent Fluid Materials
coal-mv-volatiles (mv_vol)
Mixture
coal-mv-volatiles-air
Order Materials By
Name
Chemical Formula
Fluent Database...
User-Defined Database...
Properties
Molecular Weight (kg/kgmol)
constant
Edit...
17.237
Standard State Enthalpy (j/kgmol)
constant
Edit...
-5.601e+07
Standard State Entropy (j/kgmol-k)
constant
Edit...
0
Reference Temperature (k)
constant
Edit...
1200
Change/Create
Delete
Close
Help

In the MATERIALS panel, choose MIXTURE from the MATERIAL TYPE drop-down list. Under PROPERTIES, click EDIT for MIXTURE SPECIES. Add all AVAILABLE MATERIALS into SELECTED SPECIES. Note: Make sure N_2 is the last species in the list.

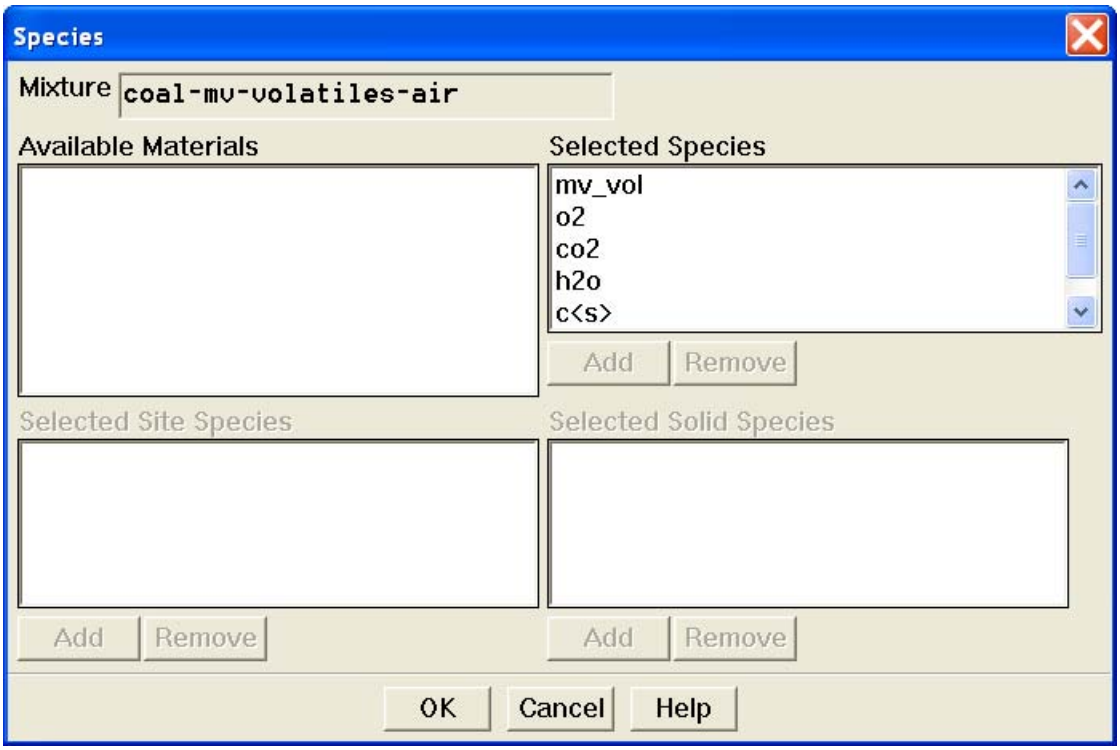

4. In the MATERIALS panel, choose MIXTURE from the MATERIAL TYPE drop-down list. Under PROPERTIES, click EDIT for REACTION.
   a. Increase TOTAL NUMBER OF REACTIONS to 2.
   b. Set up the reactions as shown below.

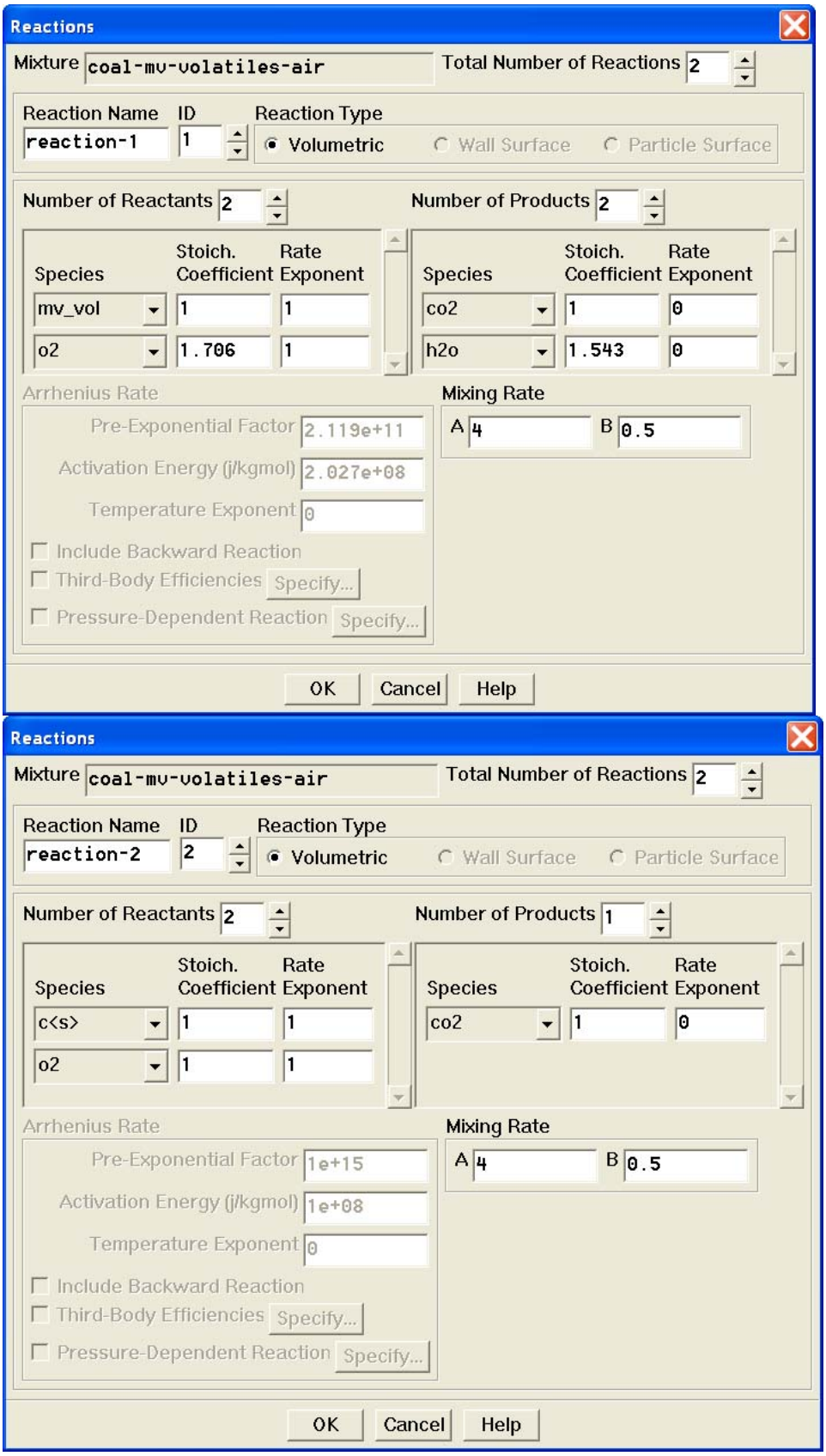
Reactions
Mixture
coal-mv-volatiles-air
Total Number of Reactions
2
Reaction Name
reaction-1
ID
1
Reaction Type
Volumetric
Wall Surface
Particle Surface
Number of Reactants
2
Number of Products
2
Species
Stoich. Coefficient
Rate Exponent
mv_vol
1
1
o2
1.706
1
Species
Stoich. Coefficient
Rate Exponent
co2
1
0
h2o
1.543
0
Arrhenius Rate
Pre-Exponential Factor
2.119e+11
Activation Energy (j/kgmol)
2.027e+08
Temperature Exponent
0
Include Backward Reaction
Third-Body Efficiencies
Specify...
Pressure-Dependent Reaction
Specify...
Mixing Rate
A
4
B
0.5
OK
Cancel
Help
Reactions
Mixture
coal-mv-volatiles-air
Total Number of Reactions
2
Reaction Name
reaction-2
ID
2
Reaction Type
Volumetric
Wall Surface
Particle Surface
Number of Reactants
2
Number of Products
1
Species
Stoich. Coefficient
Rate Exponent
c<s>
1
1
o2
1
1
Species
Stoich. Coefficient
Rate Exponent
co2
1
0
Arrhenius Rate
Pre-Exponential Factor
1e+15
Activation Energy (j/kgmol)
1e+08
Temperature Exponent
0
Include Backward Reaction
Third-Body Efficiencies
Specify...
Pressure-Dependent Reaction
Specify...
Mixing Rate
A
4
B
0.5
OK
Cancel
Help

Step 4: Interface Coupling

DEFINE → GRID INTERFACES

- Name the interfaces first and then select pairs of surfaces that form the interface wanted.
- Repeat until all interfaces are made.

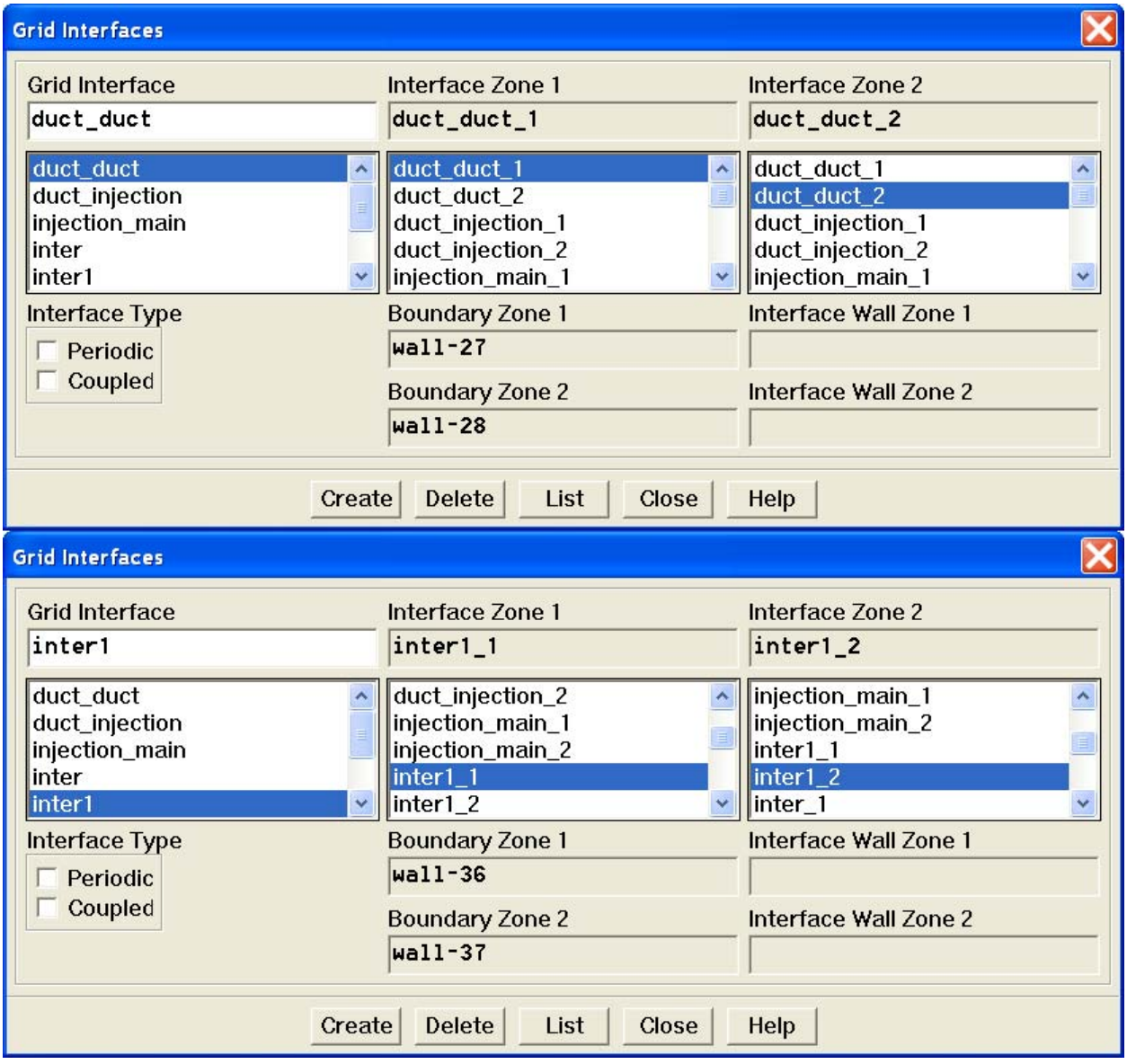

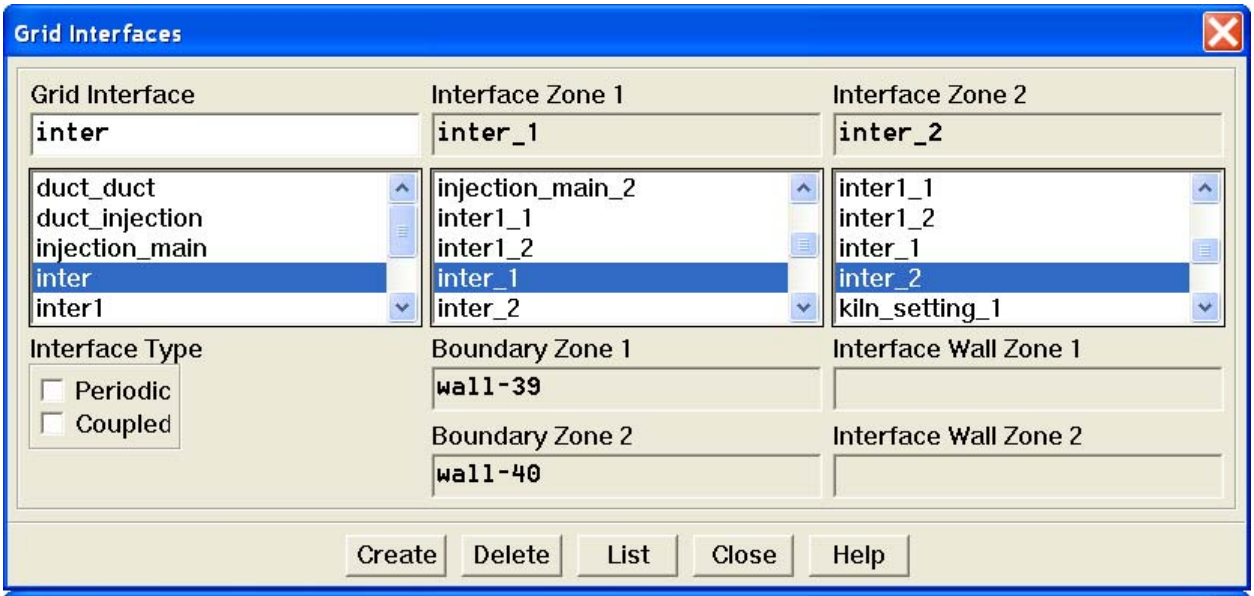
Grid Interfaces
Grid Interface
inter
Interface Zone 1
inter_1
Interface Zone 2
inter_2
duct_duct
duct_injection
injection_main
inter
inter1
injection_main_2
inter1_1
inter1_2
inter_1
inter_2
inter1_1
inter1_2
inter_1
inter_2
kiln_setting_1
Interface Type
Periodic
Coupled
Boundary Zone 1
wall-39
Interface Wall Zone 1
Boundary Zone 2
wall-40
Interface Wall Zone 2
Create
Delete
List
Close
Help

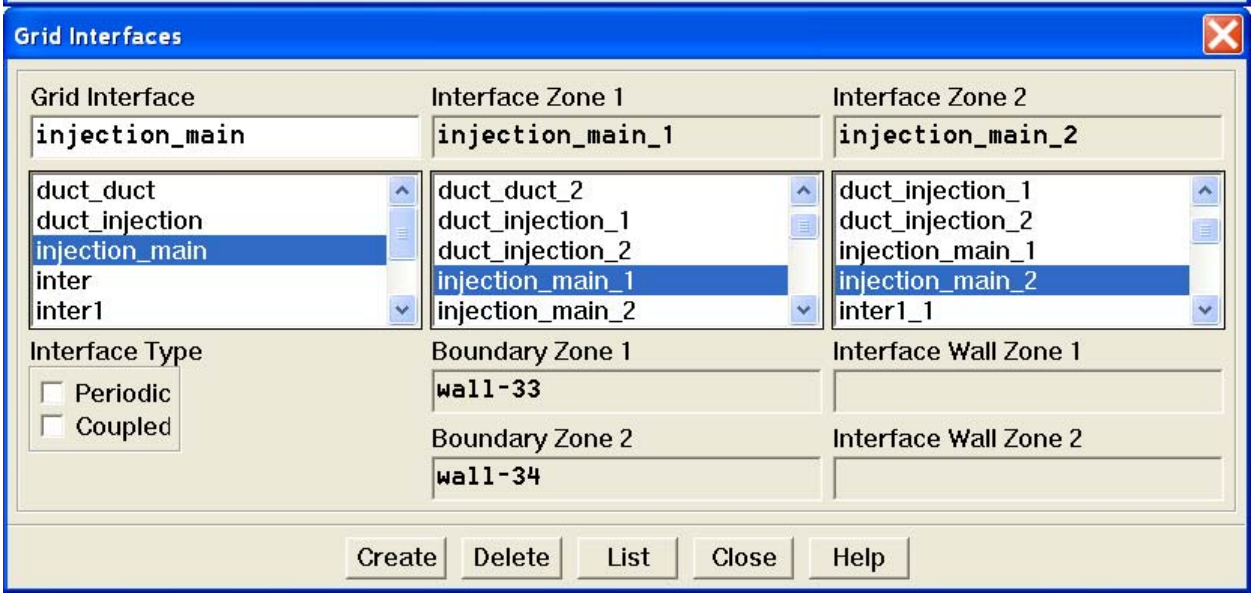
Grid Interfaces
Grid Interface
injection_main
Interface Zone 1
injection_main_1
Interface Zone 2
injection_main_2
duct_duct
duct_injection
injection_main
inter
inter1
duct_duct_2
duct_injection_1
duct_injection_2
injection_main_1
injection_main_2
duct_injection_1
duct_injection_2
injection_main_1
injection_main_2
inter1_1
Interface Type
Periodic
Coupled
Boundary Zone 1
wall-33
Interface Wall Zone 1
Boundary Zone 2
wall-34
Interface Wall Zone 2
Create
Delete
List
Close
Help

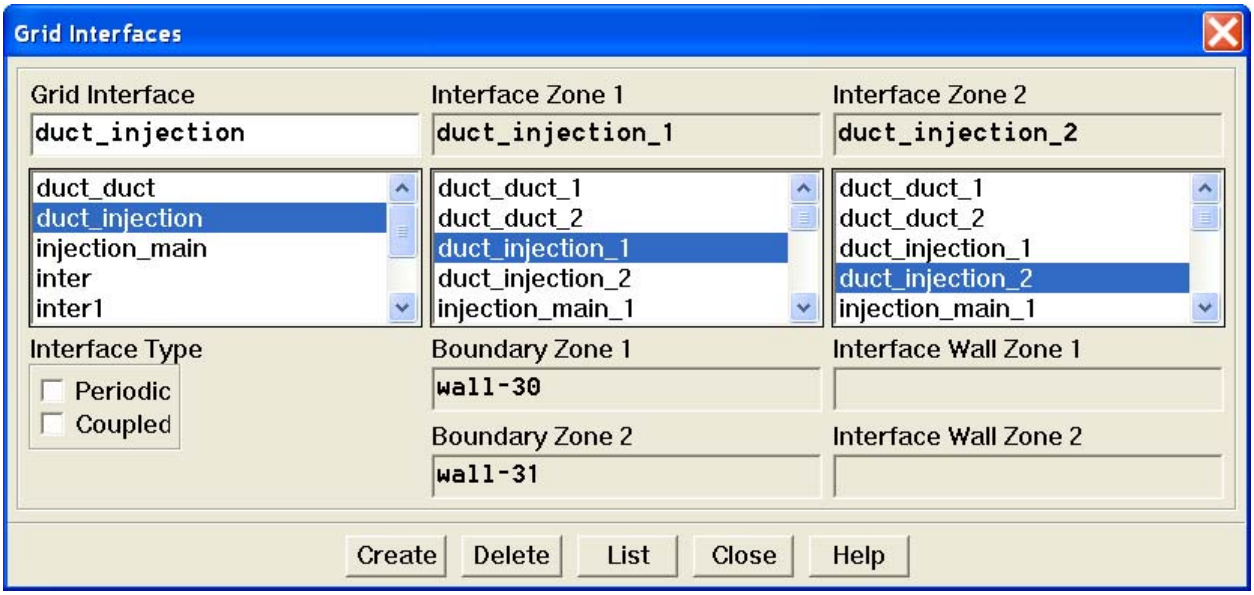

Step 5: Boundary Conditions

DEFINE → BOUNDARY CONDITIONS

1. Set up main inlet as shown below.

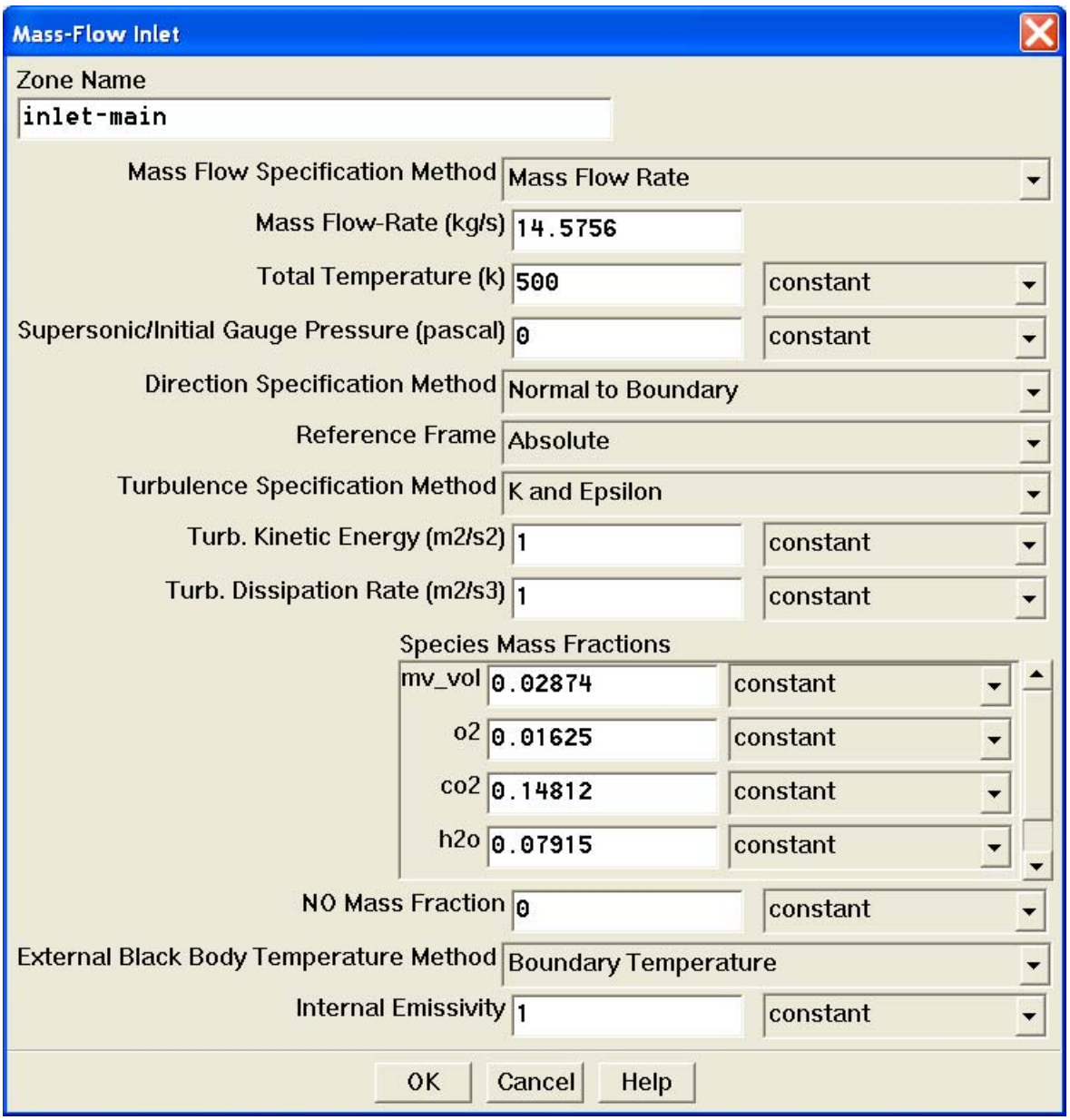

2. Set up injection tubes boundary condition as mass-flow-inlet. Note the air velocity direction is 45^{o} to the normal direction.

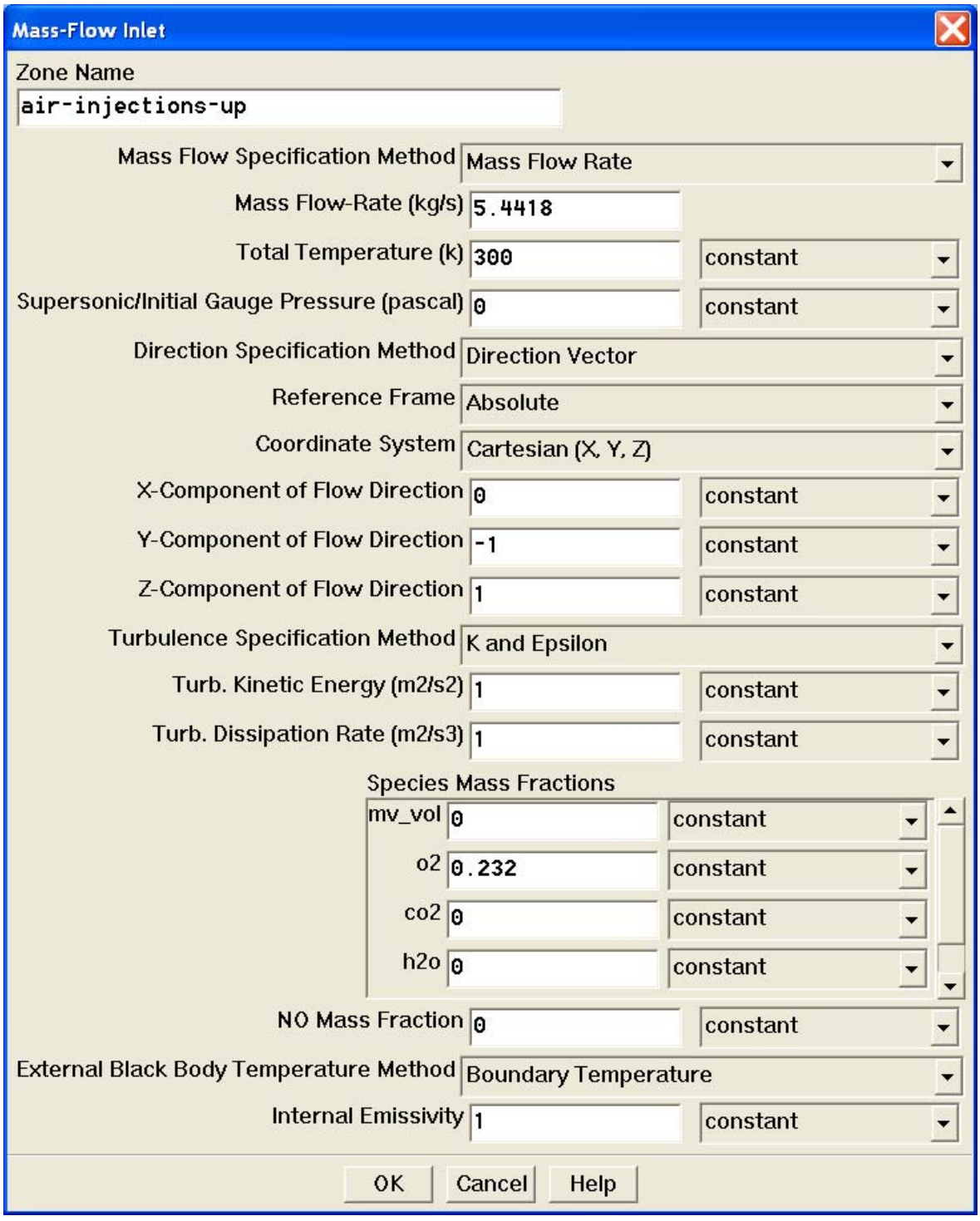
Mass-Flow Inlet
Zone Name
air-injections-up
Mass Flow Specification Method
Mass Flow Rate
Mass Flow-Rate (kg/s)
5.4418
Total Temperature (k)
300
constant
Supersonic/Initial Gauge Pressure (pascal)
0
constant
Direction Specification Method
Direction Vector
Reference Frame
Absolute
Coordinate System
Cartesian (X, Y, Z)
X-Component of Flow Direction
0
constant
Y-Component of Flow Direction
-1
constant
Z-Component of Flow Direction
1
constant
Turbulence Specification Method
K and Epsilon
Turb. Kinetic Energy (m2/s2)
1
constant
Turb. Dissipation Rate (m2/s3)
1
constant
Species Mass Fractions
mv_vol
0
constant
o2
0.232
constant
co2
0
constant
h2o
0
constant
NO Mass Fraction
0
constant
External Black Body Temperature Method
Boundary Temperature
Internal Emissivity
1
constant
OK
Cancel
Help

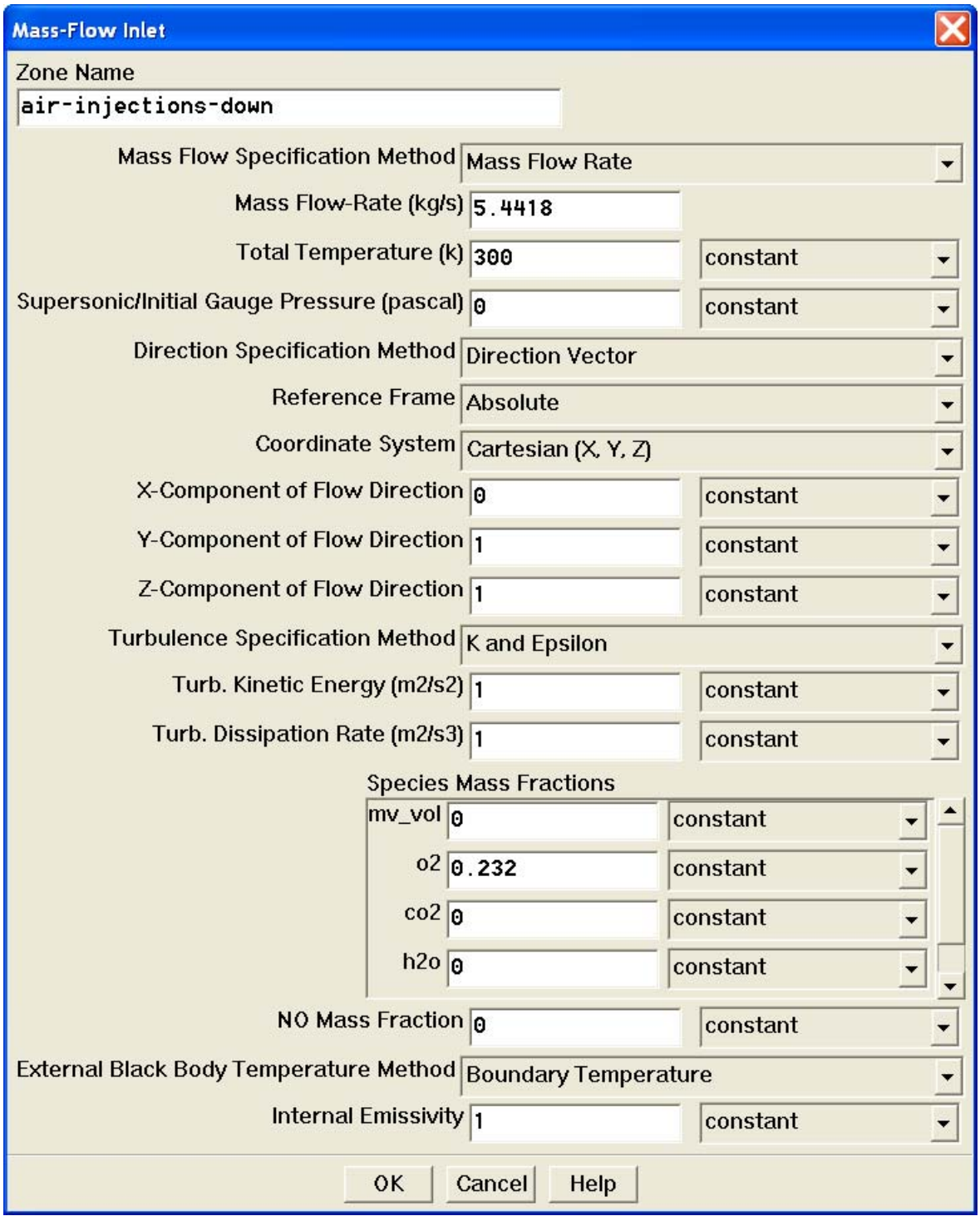

3. Set up the outlet condition as pressure-outlet.

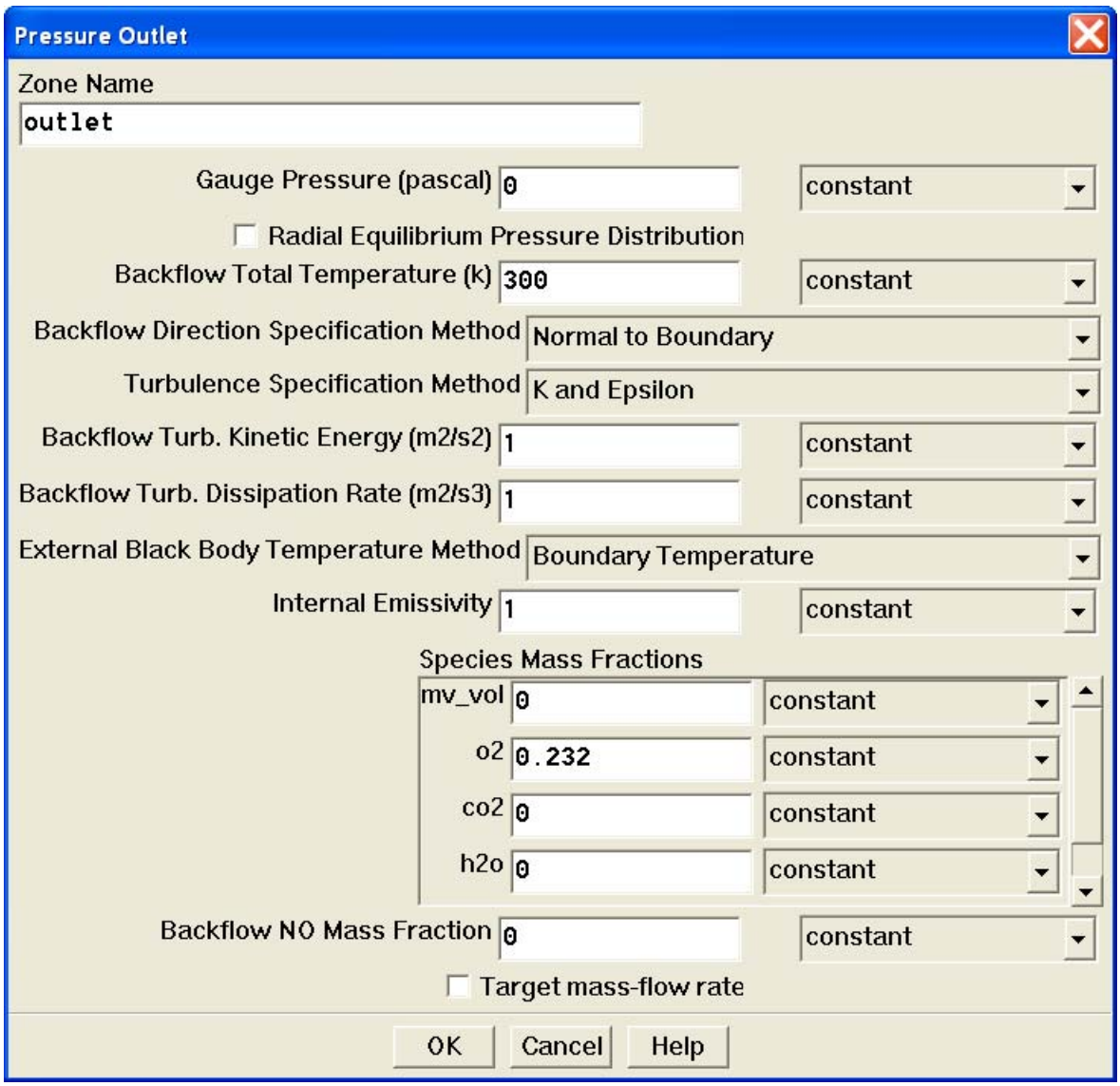

4. Leave the interfaces as they are.

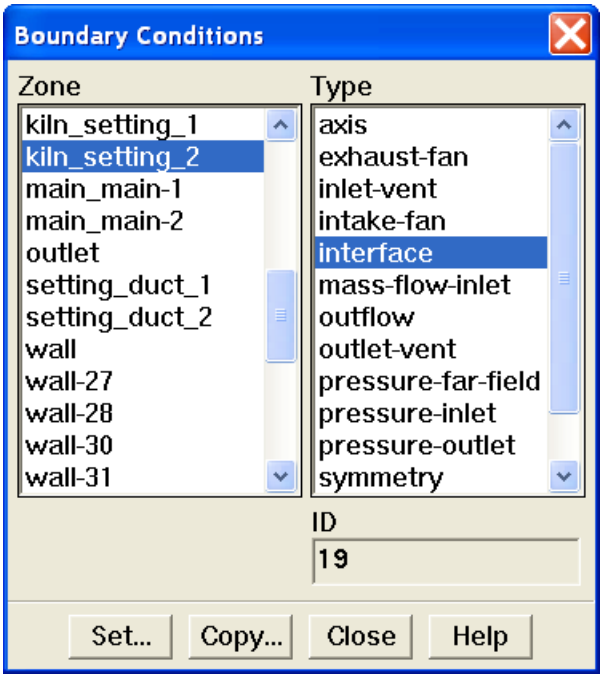

Step 6: Solution Initialization

SOLVE → INITIALIZE → INITIALIZE

1. Initialize the field variables. Choose ALL-ZONES from COMPUTE FROM drop-down list. Use all other default values. Click INIT.
2. Set under-relaxation factors.

SOLVE → CONTROLS → SOLUTION

a. Select all under EQUATIONS.

b. For UNDER-RELAXATION FACTORS, adjust the number according to different cases. If the solution is easily diverged, reduce the number; otherwise use larger numbers to get fast convergence.

c. Under DISCRETIZATION, set all others to SECOND ORDER UPWIND except pressure.

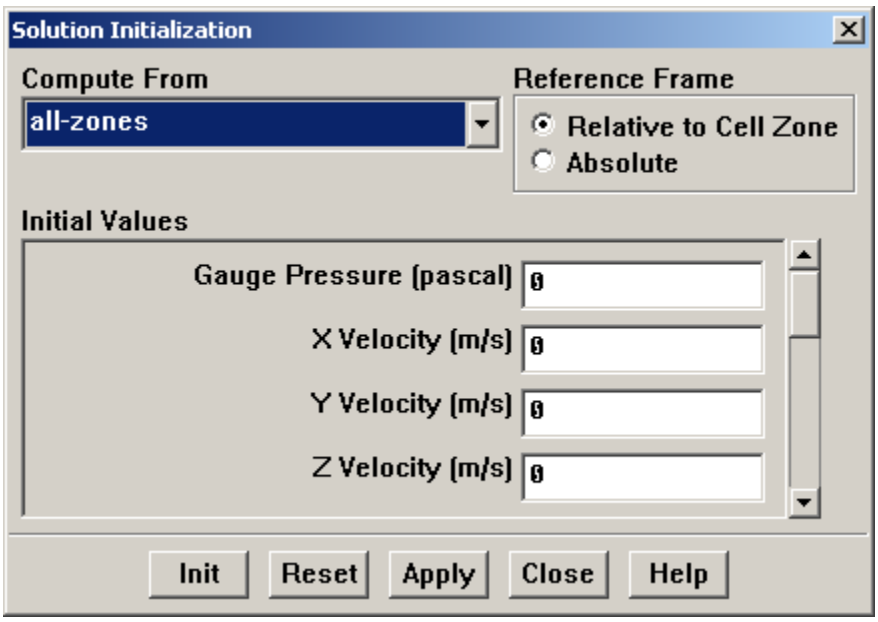
Solution Initialization
Compute From
all-zones
Reference Frame
Relative to Cell Zone
Absolute
Initial Values
Gauge Pressure (pascal)
0
X Velocity (m/s)
0
Y Velocity (m/s)
0
Z Velocity (m/s)
0
Init
Reset
Apply
Close
Help

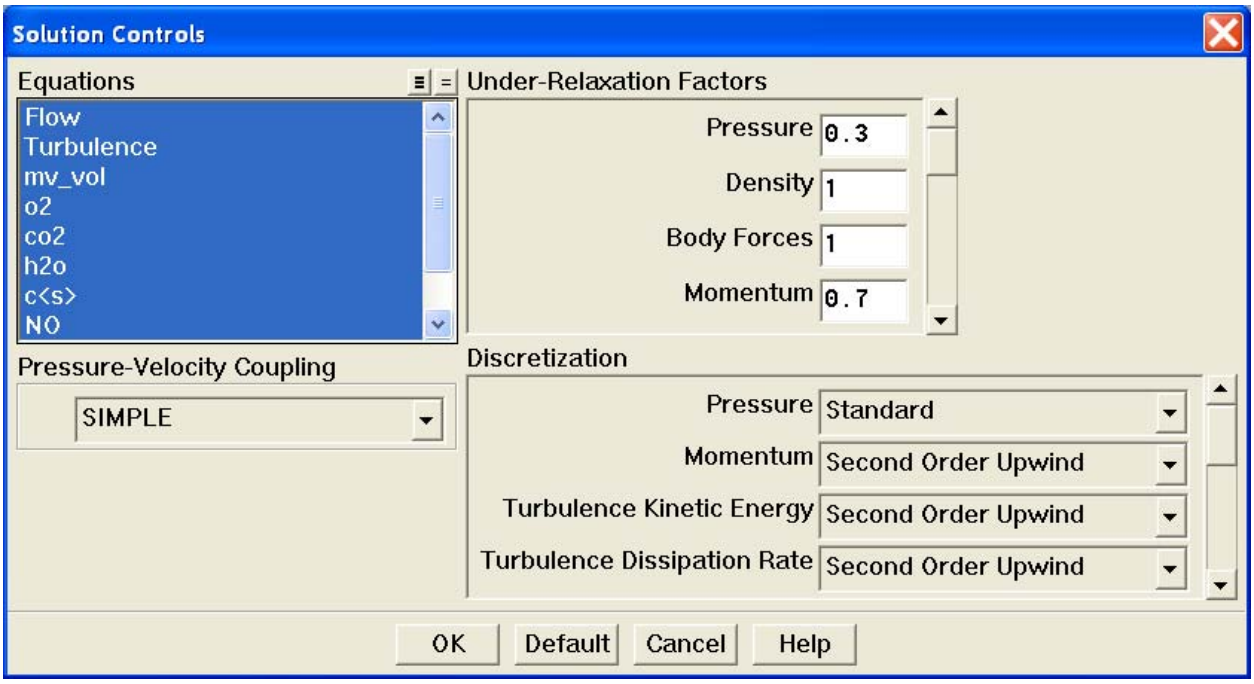
Solution Controls
Equations
Flow
Turbulence
mv_vol
o2
co2
h2o
c<s>
NO
Under-Relaxation Factors
Pressure
0.3
Density
1
Body Forces
1
Momentum
0.7
Pressure-Velocity Coupling
SIMPLE
Discretization
Pressure
Standard
Momentum
Second Order Upwind
Turbulence Kinetic Energy
Second Order Upwind
Turbulence Dissipation Rate
Second Order Upwind
OK
Default
Cancel
Help

3. Turn on residual plotting during calculation.

SOLVE → MONITORS → RESIDUAL

Under OPTIONS, check PLOT. Keep all default CONVERGENCE CRITERION.

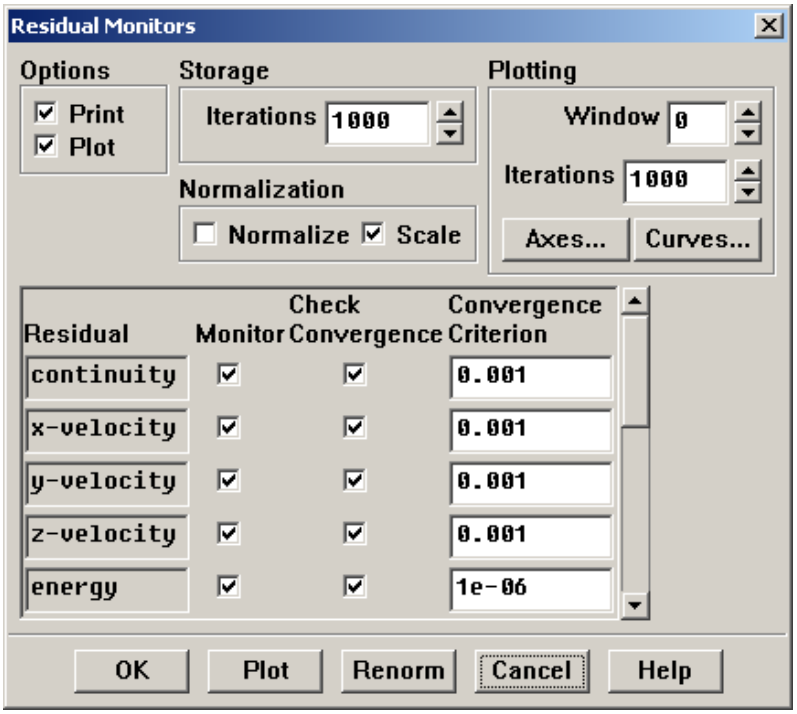

4. Start the calculation by requesting 5000 iterations.

SOLVE → ITERATE

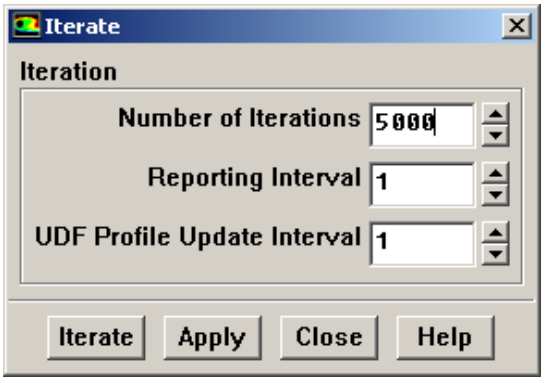

APPENDIX B

PRESSURE DRIVEN AIR FLOW VELOCITY ESTIMATE

Problem Description:

When the bottom doors of the pyroscrubber are open, outside air will be sucked in because the gases inside the pyroscrubber are at a much higher temperature than outside ambient air. Moreover, the density difference will induce a large pressure difference, which will create a naturally induced cold air draft rushing in through these doors. A schematic showing a section of the pyroscrubber and a door is shown in Fig. B-1. The following is used to calculate the air velocity, which will be compared with the numerical simulation results.

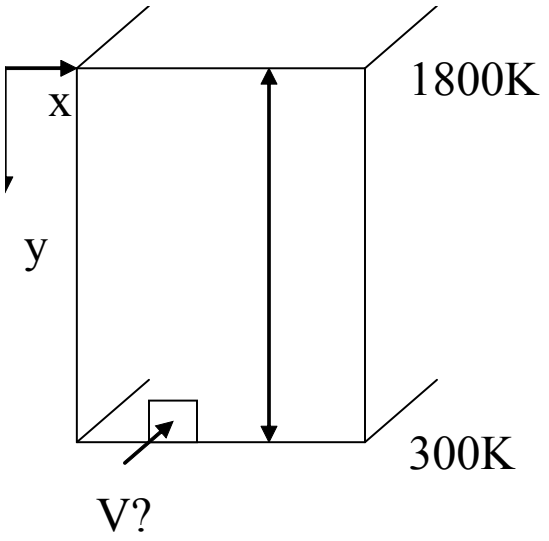

Figure B-1 A schematic showing a section of the pyroscrubber and a door

Assumptions:

1. The height from the center of the bottom door to the center of the pyroscrubber exhaust duct is 36.35ft (11.08m), as shown in Figure B1.
2. Ambient air condition: The ambient temperature is assumed constant at all elevations.

   $P = P_o = 1.01 \times 10^5$ Pa,

   T = 300K

   R = 0.287 kJ/kg*K (Air gas constant)
3. Inside the pyroscrubber:

   At exit, T_{top}= 1800K

   At bottom, T_{btm}= 300K

   Assume that the temperature increases linearly with respect to height from 300K to 1800K. Using the coordinate as shown in Figure B1

   T=1800 - (1500/11.08)* y (K)
4. For simplicity, assume the gas constant, R, of inside gases is the same as air:

   R=0.287 kJ/kg*K
5. All gases follow ideal gas assumption.

Calculation:

Inside the pyroscrubber, the pressure difference counting from the bottom to the exit is:

$$\Delta P=(P_{ref}-P)=\int_0^h \rho_o g dy - \int_0^h \frac{P}{RT} g dy = \rho_o g h - \int_0^h \frac{P_o}{R(1800-135.39y)} g dy$$

$$= \frac{1.01\text{x}10^5}{287 \cdot 300} \cdot 9.8 \cdot 11.08 - \int_0^h \frac{1.01\text{x}10^5 \cdot 9.8}{287 \cdot (1800-135.39y)} dy = 127.37 - 45.64 = 81.73 Pa$$

$$\Delta P = \frac{3}{2}\rho V^2$$

$$==> V = (\frac{81.73 \cdot 2}{3 \cdot 1.17})^{1/2} = 6.8 m/s$$

From CFD simulation results, V=6.0 m/s

The hand calculated result is quite close to the CFD results.

APPENDIX C

USER DEFINED FUNCTIONS (UDF)OF SPECIFYING THE SURFACE REACTION RATE OF A PARTICLE

In the particle combustion model, since Fluent user interface only accepts Arrhenius form of reaction rate as $k_{f,r} = A_r T^{\beta} e^{-E_r/RT}$, in order to appropriately model the particle surface reaction, a UDF program must be written and incorporated. The programming language used is C++. The code is shown below.

```
#include "udf.h"
DEFINE_PR_RATE (particle_rate, c, t, r, mw, pp, p, sf, dif_i, cat_i, rr)
{
/* Argument types
cell_t c
Thread *t
Reaction *r (reaction structure)
real *mw (species molecular weight)
real *pp (gas partial pressures)
Tracked_Particle *p (particle structure)
real *sf (current mass fractions of solid species in particle char mass)
int dif_i (index of diffusion controlled species)
int cat_i (index of catalyst species)
real *rr (rate of reaction kgmol/s)
```

```
*/
if (!strcmp(r->name, "reaction-1"))
{
   /* C + 0.5O2 -> CO */
   /* k = T(-0.067 + 5.26e-5 * T) */

   if (P_T(p) >= 1274)
      {
      real ash_mass =
      P_INIT_MASS(p)*(1.-DPM_CHAR_FRACTION(p)-DPM_VOLATILE_FRACTION(p));
       real one_minus_conv =
      MAX(0.,(P_MASS(p) -ash_mass) / P_INIT_MASS(p)/ DPM_CHAR_FRACTION(p));
      real rate = P_T(p)*(-0.067 + 5.26e-5*P_T(p));
      *rr=-rate*P_DIAM(p)*P_DIAM(p)*M_PI*sf[0]*one_minus_conv;
      }
   else
      {
      *rr = 0;
      }
if (!strcmp(r->name, "reaction-2"))
{
   /* C + CO2 -> 2CO */
   /* k = 4.4*exp(1.62x10^8/RT) */
```

```
    real ash_mass =
    P_INIT_MASS(p)*(1.-DPM_CHAR_FRACTION(p)-DPM_VOLATILE_FRACTION(p));
     real one_minus_conv =
    MAX(0.,(P_MASS(p) -ash_mass) / P_INIT_MASS(p)/ DPM_CHAR_FRACTION(p));
    real rate = 4.4*exp(-1.62e8/UNIVERSAL_GAS_CONSTANT/P_T(p));
    *rr=-rate*P_DIAM(p)*P_DIAM(p)*M_PI*sf[0]*one_minus_conv;
}
}
```

VITA

Lei Zhao was born in Yantai, Shan Dong Province, People's Republic of China. He came to the United States in 2006. He received his B.S. degree from the University of Science and Technology of China, Hefei, China in 2005 and joined the M.S. program in Mechanical Engineering at the University of New Orleans in Fall 2006.